Ph.D. Thesis

Study of the biomechanical behavior of the all ceramic dental crown

Michel FAGES DDS

2012

Ph.D. Thesis

Study of the biomechanical behavior of the all ceramic dental crown

Michel FAGES DDS

Supervisors: Prof. Dr. Frédéric Cuisinier, DDS., PhD.
and Dr. Kinga Turzó, PhD.

UFR Odontologie, Université Montpellier I and
Department of Oral Biology and Experimental Dental Research**,**
Faculty of Dentistry, University of Szeged

Graduate School of Clinical Science
Research in Dental Medicine

Szeged

2012

PUBLICATIONS RELATED TO THE THESIS

1. Slangen P, Corn S, Fages M, FJG Cuisnier / Fringe 2009 6TH International Workshop on Advanced Optical Metrology 1st Edition. «Prosthodontic crown mechanical integrity study using Speckle Interferometrie» 2009: 734-738.

2. Durand JC, Jacquot B, Salehi H, Fages M, Margerit J,Cuisinier FJG. « Confocal Raman microscopic analysis of the interface zirconia/feldspathic ceramic interface ». Dent Mater. 2012 Jun;28(6):661-71. Epub 2012 Mar 23.

3. Fages M, Slangen P, Raynal J, Corn S, Turzo K, Margerit J, Cuisinier FJG. « Comparative mechanical behavior of dentin-enamel and dentin ceramic junction assessed by Speckle Interferometry». Dent Mater. 2012 Jun 18. PMID: 22717295 [Epub ahead of print]

4. Fages M, Corn S, Ienny P, RaynalJ, Slangen P, Margerit J, Cuisinier FJG. « CAD/CAM: A new « tailor made » methodology for assessing mechanical behavior of full ceramic crowns ». *(Under review Journal of Prosthetic Dentistry)*

CONTENTS

1. Introduction

1.1. Restorations with dentin-bonded ceramic crowns

In 1965, McLean and Hughes developed a high-alumina reinforced porcelain prosthetic restoration as an alternative to metal-ceramic reconstructions. Because of the inadequate translucency of the aluminous porcelain core material, a veneer of feldspathic porcelain was required to achieve acceptable aesthetics. Therefore, this type of porcelain crown was only used for anterior restorations and had a reputation for being fragile. The "all ceramic" prosthetic restorations remained marginal for many years.

Recently, there has been development in the area of dental ceramic materials. Higher strength substructure materials have been used, and manufacturing methods have advanced considerably. Today, the popularity of all-ceramic materials as an alternative to metal-ceramic is increasing. However, not all of the problems have been solved

In 1995, Burke et al. asked the following question: Is “the dentin-bonded ceramic crown an ideal restoration?” (1). In this article, the authors stated that “the dentin-bonded all-ceramic crowns might exhibit many favorable characteristics, including those of good aesthetics, marginal blending with gingival tissues and the ability to be placed on conservative preparations, which may minimize the risk of pulpal damage.” The indications include cases in which conventional crowns require replacement, those in which minimal preparation techniques are appropriate and those in which there has been tooth surface loss. Finally, the authors concluded that the longevity of these restorations is, as yet, unknown in the absence of long-term clinical data (1).

Seventeen years later, all-ceramic systems have become suitable for a large range of indications in almost all areas of fixed restorative dentistry (2,3). Furthermore, these systems have evolved to produce metal-free restorations, due to the evolution of materials and technologies such as Computer Aided Design and Computer Aided Manufacturing (CAD/CAM). The term CAD/CAM is used in the context of a software tool that covers a number of engineering functions (Fig. 1).

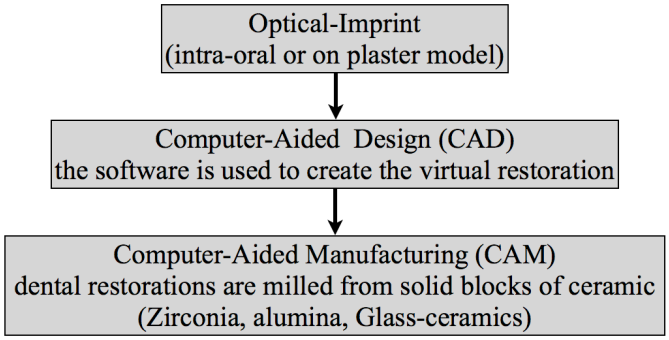

Fig. 1. The general principles of CAD/CAM in prosthetics

Today, dental ceramic materials are regarded as some of the best materials for dental restorations as they are biocompatible and inert, resistant to corrosion, and have a low temperature and electrical conductivity (4). Coupled with the aesthetic demands for dental restorations, these improved characteristics have resulted in increased use and have led to many efforts to improve their mechanical properties. Different types for different uses are available for frameworks or monolithic reconstructions; an overview that covers specific destinations and required technology is shown in Table I.

Ceramics	Nature	Destination		Technology		
		Framework	Monolithic	Pressed	Milled	Split-casting
Glass-ceramics	Feldspathic	No	Yes	Yes	Yes	No
	Lithium dissilicate	Yes	Yes	Yes	Yes	No
Alumina	Alumina	Yes	No	No	Yes	Yes
	Alumina-zirconia	Yes	No	No	Yes	No
	High-strengh alumina	Yes	No	No	Yes	No
Zirconia	Y-TZP, HIP	Yes	Yes	No	Yes	No

Table I. Ceramic materials available for frameworks or monolithic reconstructions.

Glass-ceramics are particularly suitable for fabricating monolithic restorations like inlays and crowns veneers because these materials provide good aesthetic results (5). High-strength ceramics like zirconia are indicated for bridges (6, 7, 8, 9). Zirconia is the reference element for making ceramic frameworks due to its favorable mechanical properties that are enhanced by aesthetic advantages. Because of the interesting properties of zirconia, alumina infrastructures have been progressively removed from use. Furthermore, the increased applications of zirconia are due to the development of CAD/CAM systems. The framework (Fig.2. A1) is milled in a zirconia block and then veneered with a feldspathic ceramic (Fig.2. A2). The glass ceramic single crowns (Fig.2B) are milled in blocks of glass ceramic. For those crowns, there is no framework.

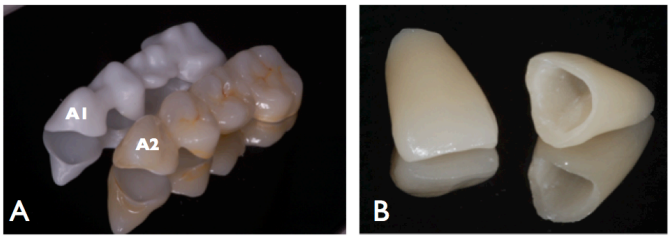

Fig. 2. Two all ceramic reconstructions: A) A1: zirconia framework to be veneered, A2: the same framework after veneering (courtesy Dr. B. Bennasar). B) monolithic glass ceramic crowns (own picture).

In Figure 3. the illustration of two clinical cases is shown.

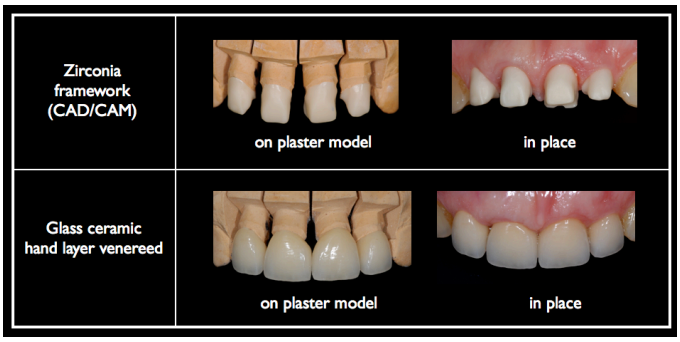

Fig. 3. Zirconia frameworks and glass ceramic hand layer frameworks.

Fig.3 shows zirconia frameworks on both a plaster model and teeth and zirconia frameworks hand layer veneered with glass-ceramic on both a plaster model and teeth. The framework is designed with a computer, and a block of zirconia is milled with a milling

machine. Then, the glass ceramic is hand-layer veneered to obtain an aesthetic result (picture supplied by author).

Fig. 4 shows a monolithic glass ceramic (without framework) milled with a CAD/CAM system. In this case, the monolithic glass ceramic is designed with a computer and milled in a ceramic bloc with a milling machine.

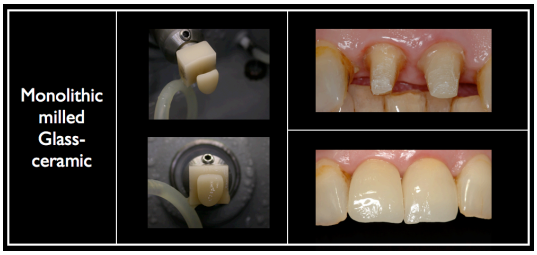

Fig. 4. Monolithic glass ceramic (without framework) milled with a CAD/CAM system. In this case, the monolithic glass ceramic or the lithium disilicate is designed with a computer and milled in a ceramic bloc with a milling machine (own pictures).

Monolithic glass-ceramic crowns have a reputation for fracturing during use, as the risk of fracture under occlusal force is high. This issue is described as one of the major problems of glass ceramic restorations, especially on posterior teeth (Fig. 5) (10, 11).

The problem appeared early with Dicor glass-ceramic crowns. These crowns were the first glass ceramic crowns produced in substantial numbers; so studying them is highly instructive (12, 13, 14, 15). The Dicor system was deemed too fragile and was progressively abandoned. Generally, we can say that the evolution of dental materials and the development of new restorative materials had generated new information about these materials. For the posterior area, restorations with frameworks (alumina or zirconia) veneered secondarily have been recommended.

Fig. 5. Ceramic fractures on a glass ceramic crown in the posterior area.

However, Pallis et al. in 2004 claimed there were no significant differences in fracture resistance between two all-ceramic restorative systems for posterior applications (veneered frameworks and monolithic ceramic crowns), but there was a significant difference in the causes of failure between the all-ceramic systems studied (16). In a recent study, the authors stated that dentists can use metal or zirconia frameworks successfully if the frameworks are designed properly; furthermore, the authors indicated the use of leucite-containing pressed ceramics to avoid veneer ceramic surface crumbling and to minimize chipping (17).

Guess et al. in 2010 showed that the application of CAD/CAM lithium disilicate ceramic in a monolithic/fully anatomical configuration results in fatigue-resistant crowns, whereas hand layer veneered zirconia crowns revealed a high susceptibility to mouth-motion cyclic loading with early veneer failures (18). Fatigue is a process (sequence of mechanisms) that a material undergoes. Under the action of stress, the local properties of a material will change, which can cause cracking and eventually structural failure. Failure in the layering ceramic takes the form of cone cracking, either cohesively within the veneering ceramic (chipping) or adhesively at the core veneer interface (delamination) (19-22). The location of the interface as the origin of failure has been reported previously (23), and this finding suggests that the bond strength between the veneering ceramic and the zirconia framework is a weak point in layered all-ceramic restorations (24, 25).

Zarhan et al., who were interested in CAD/CAM milled reinforced feldspathic ceramics, said that the performance of Vita mark II monolithic crowns was superior to Y-TZP Zirconia crowns in the fatigue tests (26). Baltzer reported the same findings in 2008, and he said that currently, crowns with veneered oxide ceramic copings do not offer any greater fracture resistance compared with Vita Mark II crowns as long as the minimum thickness requirements are met (27). Thus, sintered glass-ceramics are widely used as biomaterials for dental restoration, especially as inlays, onlays, veneers and crowns (28).

In accordance with the recent literature, glass ceramics seem to be indicated for fixed prosthetic reconstructions, but the role of complex prosthesis geometry and its interaction with other factors on damage initiation and propagation has yet to be well characterized (29).

If crown preparation is important to success, as Friedlander Doyle et al. (12, 13, 14) demonstrate, it is clear that crown material and thickness are also of primary importance for stress magnitude. Moreover, other variables like cement modulus and load position contribute

to the magnitude of stress, and the interactions between these variables can have an important influence (29). In 1999, Kelly (30) noted that validated tests should be developed to elucidate the role(s) that cement systems, bonding, occlusion, and even metal copings play in the success of fixed prostheses and to allow for meaningful comparisons among novel ceramic and metal substructures. Therefore, we see the complexity of the problem of evaluating the roles of the different agents and the difficulty in reproducing biomechanical patterns for testing purposes.

1.2. Biomechanical concept of tooth restoration

Success and longevity for prosthetic reconstructions demand a sound understanding of dental biomechanical principles and their possible applications to the prosthetic tooth.

Restorations that are all ceramic require proper adhesive bonding to dentin to achieve their required life expectancy. The strongest ceramics have a fracture toughness of at least 3.0 $MPa.m^{1/2}$ (31), which is relatively close to the enamel fracture toughness of 1.3 $MPa.m^{1/2}$, in a direction perpendicular to the enamel rods (32). Nevertheless, fractures of the ceramic part of all-ceramic crowns are difficult to prevent, and crack growth is a significant problem (33). This phenomenon can be explained in part by a mismanagement of the stress accommodation zone.

For natural tooth substances, the situation is different. The dentin-enamel junction (DEJ) in teeth is the zone between two distinct calcified tissues that have very different biomechanical properties: enamel and dentin (34). Enamel is hard and brittle and envelops the softer dentin (Fig. 6.).

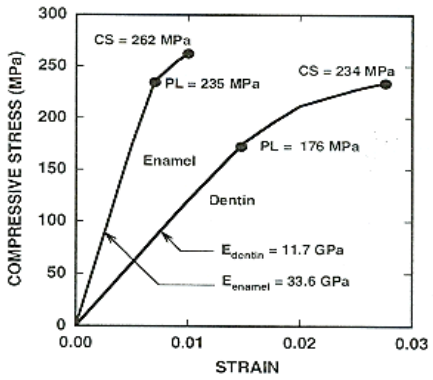

Fig. 6. Comparison of dentin and enamel subjected to compression (35).

Comparing dentin and enamel that have been subjected to compression, we can observe that dentin is capable of sustaining significant plastic deformation (ultimate compressive strength [CS] = 234 MPa) under compressive loading before it fractures. Therefore, dentin is more flexible and tougher than enamel. For enamel, the elastic modulus (E) is approximately three times greater than that of dentin. Enamel is a stiffer and more brittle material than dentin (35).

The enamel and dentin work together during the many load cycles experienced by the tooth over its lifetime. Generally, interfaces between materials with dissimilar elastic and mechanical properties represent "weak links" in a structure, but the DEJ acts successfully to transfer applied loads (e.g., masticatory or impact loads) from the enamel to the dentin and to inhibit enamel cracks from propagating into the dentin and causing tooth fracture (36,37), even in cases of bruxism.

In human enamel and dentin, fatigue damage is the end result of extreme loads and is frequently associated with pathology or extensive wear. The fracture-resistant properties of the DEJ are believed to originate from a gradual change in microstructure and in the properties of dentin and enamel rather than from the abrupt transition between the two dissimilar tissues (38, 39). Wang and Weiner suggested that the DEJ is one of the working sites of the tooth during mastication (40).

Imbeni et al. (34) propose that collagen fibrils perpendicular to the interface constitute the key reinforcing mechanism at the DEJ, thus explaining why so few cracking events cause delamination when they impinge on the DEJ. These researchers determined profiles of the Vickers hardness and indentation toughness taken normal to, and across, the DEJ from the enamel to the dentin in a human molar. Typical profiles of the Vickers hardness and indentation toughness taken normal to, and across, the DEJ from the enamel to the dentin in a human molar can be observed in Fig. 7. Hardness indentations were made with a load range between 3 and 5 N to minimize brittle fracture damage but to still form cracks around the indents to enable toughness measurements. Lines of indents were performed on three different teeth (each from a unique patient) with three series for each tooth. The indentation was determined from the indentation load (**P**), and the average crack lengths (**c**) emanating from the indent corners, according to $\mathbf{K_{ind,c} = \chi P/c^{3/2}}$ where χ is the residual indentation coefficient (taken as 0.076 for enamel). Such measurements could only be made in the enamel when

inelasticity in the dentin suppresses the formation of indent cracks. These profiles show that cracks in the enamel experience a region of decreasing hardness but increasing toughness as they approach the DEJ (34).

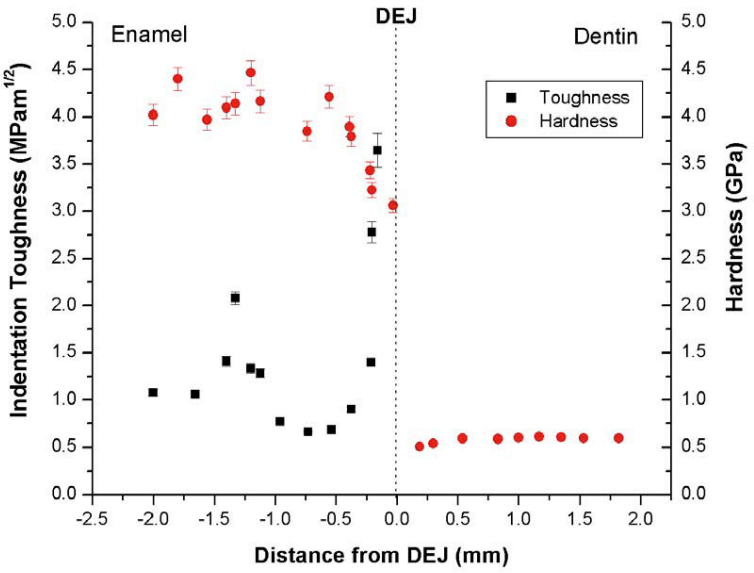

Fig. 7. Typical profiles of the Vickers hardness and indentation toughness taken normal to, and across, the DEJ from the enamel to the dentin in a human molar (34).

Paul Zaslansky et al. (41) highlighted the importance of the DEJ as the binding interface between enamel and dentin (Fig. 8.). These authors have shown that adjacent to the DEJ is a 200-300 mm-thick zone of dentin with a much lower stiffness (compression and elastic modulus) than the bulk of the dentin in the tooth. Using Speckle Interferometry (SI), this group found that a compressive load applied to the tip of the main cusp of a human premolar caused the entire enamel cap to move essentially as a stiff body, tilting towards the buccal surface. For the natural tooth, Zaslansky writes, *"the asymmetry in stiffness between the buccal and lingual sides may therefore have a profound significance in determining how exactly the enamel cap responds to load during mastication"*. This asymmetric nature of the structure may also contribute to the distribution of loads that are not applied along the long axis of the tooth. The possible asymmetry in stiffness between the buccal and lingual sides of the tooth points to a basic property of tooth function, presumably related to the precise manner in which stress is distributed during mastication.

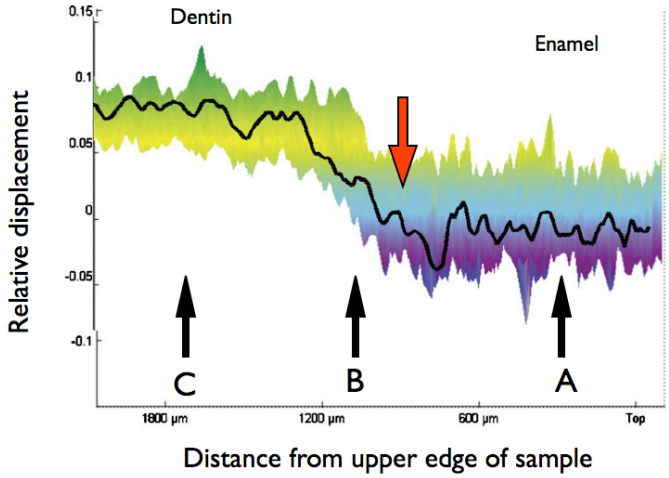

Fig. 8. Edge view (side profile) of displacements. A qualitative interpretation of the magnitudes and gradients in displacements can be observed along one sample.

A graph of the averaged displacements across the surface (Fig. 8.) determined for each row along the sample is superimposed on the displacement profile (black line), and three regions can be identified: (A) enamel, in which the displacements follow a plateau with no obvious gradient in displacements, (B) the sub-DEJ and sub-JED zones, where a marked gradient in displacements can be identified, and (C) the bulk dentin with a smaller gradient. The stiffness is inversely related to the gradient, and consequently, region (B) has the lowest stiffness. The red arrow points to the approximate location of the DEJ (41).

Chattah et al. showed that the enamel cap in a mini-pig animal model is capable of deforming and rotating at loads as low as 16 N (42).

Magne and Belser understood the interest in the DEJ and said: ”*The fascinating properties of the DEJ must be a reference for the development of new dentin bonding agents that must restore the biomechanical integrity of the crown restored”* (43).

Bonding agents must be selected very carefully because they determine not only the adhesion but also the ultimate strength of full-ceramic crowns (44, 45, 46); therefore, it is important to compare the mechanical behavior of natural teeth and of the all-ceramic crowns glued on dentin. Instead of “glue joint”, we will use the term dentin-ceramic junction (DCJ). After an understanding of the role of the DEJ is achieved, it is necessary to observe the behavior of the adhesive joint and assess whether it is possible to have the role of the DEJ. From there, we must find the balance between the natural tooth preparation, the material of

reconstruction, the fixation material and the nature of the load, what is known as the "biomechanical concept".

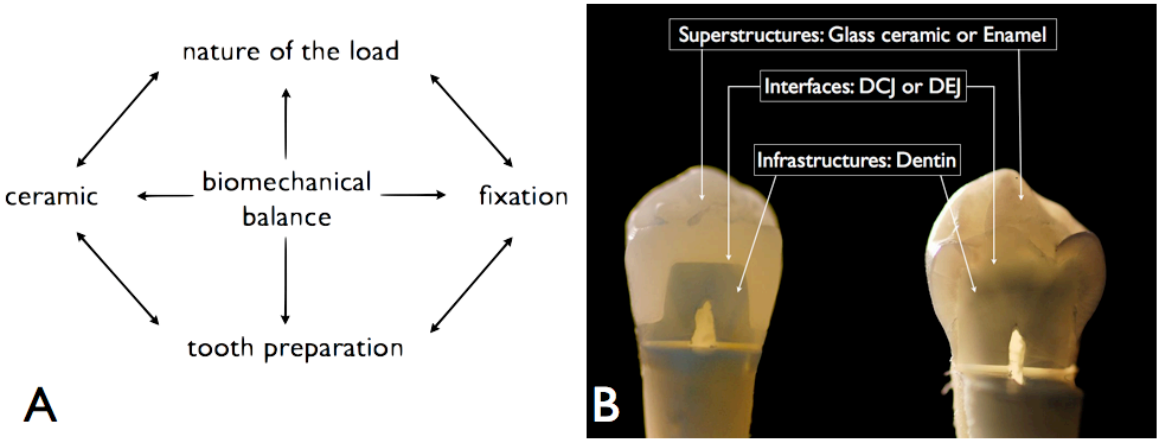

Fig. 9. A) the **biomechanical concept** of tooth restoration (own table). B) the ideal biomechanical postulate is to have reduced interfaces and for the materials for a prosthetic reconstruction to obtain the same behavior as the natural tooth. In this case, the ceramic replaces enamel, and the DCJ replaces the DEJ (Photographs courtesy of Dr. J. Raynal).

It is essential to find a methodology for analyzing the behavior of the prosthetic tooth to apply the principles of biomechanics, which allows achieving the best shape for tooth preparation in accordance with the principle of the biomechanical concept.

1.3. Mechanical behavior of glass-ceramic materials/restorations

A systematic review has indicated that there is an urgent need to develop a comprehensive classification system for clinical ceramic prosthesis failure, technical complications and biologic complications (47). Dynamic loading of all-ceramic materials is indispensable to assess the clinical performance of all-ceramic molar crowns (48).

Traditional testing of ceramic crowns creates stress states and damage modes that differ greatly from the clinical reality, and there is a need to develop new *in vitro* testing protocols (49, 50). While advances in material formulations and clinical techniques promise a benefit to patient care, various confounding variables affect the success of a dental restoration. These factors can be difficult to simulate in a laboratory environment that does not accurately match the clinical environment (51). Mechanical failure tests of materials are useful only if

the results are accurate, reproducible and in accordance with the clinical situation. Fig. 10. shows a typical instrument for mechanical testing of restorative materials

Fig. 10. Instrumentation for mechanical testing of restorative ceramic reconstruction.

In current times, it is possible to develop a method for assessing the mechanical behavior of full-ceramic peripheral crowns based on the use of industrial and dental CAD/CAM systems (52, 53). CAD/CAM enables the manufacturing of a series of samples and sample-holders perfectly adapted to dental prosthetic tests. In fixed prosthetics, the sample must consist of two parts: one **infrastructure** that represents the tooth after a standardized preparation and a **superstructure** that represents the prosthetic element. For glass ceramic reconstructions, the two elements are assembled by an adhesive system (54). In the literature, these reconstructions are defined as Resin Bonded All Ceramic crowns (RBCs) (55).

To create the infrastructure, several methods can be employed. It is possible to prepare human teeth manually or to use parts of animal teeth (bovine) (56). It is also possible to prepare a natural or synthetic dental crown and then, using epoxy resin, make several replications of the prepared tooth (57). Studies with natural hydrated teeth resemble real teeth, but it seems impossible to manually obtain a series of completely identical and calibrated samples (57). Furthermore, the results of those studies can be distorted because the various manual procedures are too “operator dependent”. The potential of CAD/CAM to improve reproducibility, to reduce experimental variation and to develop a method for making samples is the most efficient. This method could be applied for every type of dental preparation and restorative material. CAD is initially used to model the infrastructure (Fig. 11.). The software

permits the conception of a very precise model in 3D in accordance with clinical requirements (58, 59, 60,61,62). For example, it is possible for a program to design a standardized preparation, including the dimensions and angulations of the axial walls and the size and form of the shoulder. It is also possible to modify some geometric parameters to study their influence on the mechanical properties of the prosthesis.

After the design process, the infrastructure items are milled by an automated industrial machining system during the CAM stage.

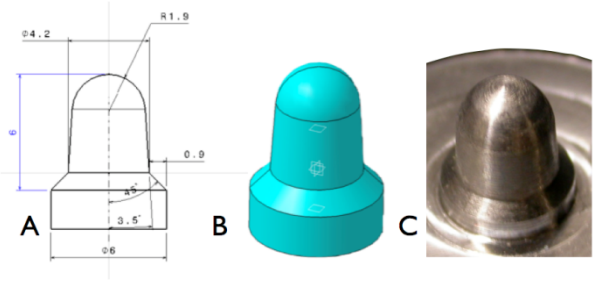

Fig. 11. A shape made by CAD/CAM can be perfectly calibrated and reproduced. A) the projection, B) the 3D shape design, C) the machined shape.

The superstructure, a monolithic ceramic cap, is then created with dental CAD/CAM technology from an optical print of the infrastructure (61, 62) and milled from a ceramic block (63, 64). All the superstructures with identical external geometries are adhesively luted onto the infrastructure.

The whole specimen (infrastructure plus superstructure) can be created by CAD/CAM systems, which assures perfect precision and reproducibility (65).

With this method, it is possible to subject different samples (series) made by CAD/CAM to compressive loading until fracture and to record and analyze the mechanical responses. This method also allows for experimental variations within and between series to be tested. This approach has two main advantages: it allows the behavior of materials to be tested but also allows supports that are well suited to the clinical reality to be shaped naturally, rather than using strictly geometrical shapes that are never experienced in clinical circumstances.

The form of prepared teeth and the amount of the tooth structure that is removed are important contributors to the mechanical success of the overlying crown. It seems necessary to determine the effect of geometric features on the mechanical response and to identify the role played by several geometric factors. The essential principles for preparing a tooth to

receive a complete monolithic glass ceramic crown must be defined. For that situation, it is necessary to understand the general behavior of ceramics subjected to stress as a function of the geometry of its support.

Between 1955 and 1961, scientific studies began to analyze tooth preparations and to identify features that were essential for success (66, 67). In 1980, Shillingburg et al. published the basic book “Fundamentals of fixed prosthodontics” (68). In recent years, CAD/CAM and current technologies in dental ceramics have greatly improved, allowing for constant production of new materials for the restoration of single or multiple teeth.

It is interesting to note that in 1990, Friedlander, Doyle and colleagues describe in three articles the effects of tooth preparation design on the breaking strength of Dicor crowns (12, 13, 14). These authors have noted that the preparation was an important component to ensure success. Bernal et al. were interested in the effect of the finish line form and the luting agent on the breaking strength of glass ceramic crowns (15). More recently, studies have shown that monolithic glass-ceramic layers are vulnerable to both occlusal surface damage and internal cementation surface fracture (69). The influence of the different preparation elements on the resistance of the ceramic reconstruction under loading has never been clearly analyzed. It appears that the various studies of the influence of preparation design on the resistance of ceramics were based on old principles of Shillinburg et al. (68), Goodacreet et al. (59), Mizrahi (70), and the failure studies of the Dicor system.

The problem has always been approached from this direction rather than starting with the materials or their support structures or even the behavior of the natural tooth.

Therefore, it appears that the natural tooth and its particular behavior were never really taken into account in considering the implementation of fixed prostheses, and that the distinctions between the mechanics of materials and the biomechanics of the natural or prosthetic tooth have not been regularly made.

1.4. Aims of the study

The first aim of my study was to compare the mechanical behavior of dentin enamel and dentin ceramic junctions by Speckle Interferometry (SI) and to investigate the properties of monolithic glass ceramic crowns, which are the most biomimetic prosthetic fixed reconstructions. The properties of these crowns are related to the preparation method.

Therefore, the first part of my study was an optical study by means of Speckle Interferometry, targeting the comparison of the mechanical behavior of the dentin enamel junction (DEJ) and the dentin ceramic junction (DCJ). In this part, the behavior of a natural tooth and a monolithic glass ceramic reconstruction under loading was observed. SI has been used by Zaslansky et col. to observe the movements of the tooth enamel at the nanoscale level (32, 41). To the best of our knowledge, our study is the first to investigate the behavior of the enamel-dentin junction under duress in comparison with the bonded joint dento-prosthetic, ceramic-dentin junction.

The second aim of my thesis was to determine the effect of geometric features on the mechanical response of monolithic glass ceramic peripheral crowns manufactured by the CAD/CAM system and to identify the role played by several geometric factors.

The goal was to prepare a shape in accordance with the principles of biomechanics and of the accommodation constraints of the DEJ. For this aim, we developed an original method for assessing the mechanical behavior of full-ceramic peripheral crowns. This method was based on the use of industrial and dental Computer Assisted Design (CAD) and Computerized Assisted Manufactured (CAM) systems. CAD/CAM enables the manufacturing of a series of samples and sample-holders that are perfectly identical, reproducible and adapted to dental prosthetic tests.

All the characteristics of tooth preparation have an influence on the behavior of the ceramic crown under loading stress. Taking this general principle into consideration, we can propose the best shape for a prepared tooth receiving a monolithic ceramic crown manufactured and adhesively luted with biomechanical concepts.

2. Statement of the problem

2.1. Statement of the optical study

The material properties of enamel and dentin and the interface between them have been studied extensively, and these components are described as non-homogeneous, graded and anisotropic (34, 70-76). The tooth organ itself is attached to the alveolar bone socket (77) via the periodontal ligament (PDL), a soft, highly vascularized, specialized connective tissue whose fibers extend into the bone on one side and into the cementum and root dentin on the other (70, 78). Little is known about the manner in which a whole tooth works under loads and even less about a whole tooth while still embedded in the jaw.

The mechanical behavior of whole teeth has been experimentally measured using strain gauges/extensometers to measure local displacements and strains (79-81).

However, these localized measurements do not reflect the complexity of the whole tooth structure. An alternative approach is to use numerical simulations, such as finite element modeling (FEM), and to compare the results to experiments (81-84). The inherent limitation of FEM is the difficulty of correctly representing the mechanical properties of graded biological materials such as enamel and dentin. Optical metrology methods, such as photoelasticity and Moiré interferometry, have been used with considerable success for studying teeth and their supporting structures (85-91). More recently, Speckle Interferometry (SI) has been adapted to the study of whole tooth mechanical behavior under loads (32). SI is a non-contact, non-destructive method that is capable of mapping three-dimensional, nanometric-scale whole surface displacements on an irregular object. SI is an optical technique that measures the micrometer scale movements or deformations of almost all types of surfaces and materials.

Today, SI is one of the most advanced techniques of analysis to perform measurements, such as displacement, roughness, deformations, and vibration, without contact with the work piece. The SI method is able to detect deformation and rotation but is insensitive to whole body translation (32, 41, 92). Zaslansky et al. used SI to map displacement patterns of human premolar crowns when loaded on the buccal cusp (32). The results showed that the enamel cap basically behaves as a stiff body that is capable of deforming and rotating only under loads**.**

In this thesis, we compared for the first time the mechanical behavior of the natural tooth and a prosthetic crown manufactured with a CAD-CAM system using SI.

We developed a complete apparatus that enabled the study of the compressive mechanical behavior of the concerned teeth by SI.

Although the mechanical and optical set up was classic, this study was the first time that the CAD/CAM was used to make the samples and that the sample holder was made individually with a prosthetic method.

To obtain reliable and reproducible measurements, we considered the half-cut crowns because this approach allows for the observation of the behavior of the DEJ and the DCJ in the observation plane either far away or very close to the loading zone. This approach has major advantages and represents another originality of this study. Zaslansky worked with parallelepiped cuts from premolars (41), while Chattah et al. (42) studied whole teeth. We used lower left and right premolars extracted from the same person for orthodontics reasons.

2.2 Statement of the mechanical study

Once behavior of the tooth under stress has been described, and the specificity that promotes its durability is understood, it is necessary to determine the ideal form of preparation that is able to employ the concept of biomimicry.

Replacing the enamel by a ceramic and the DEJ by a bonded joint may seem problematic. Moreover, all-ceramic crowns are reputed to fracture during function, especially in the posterior area. This may be because the relationship between the physical properties of these materials and the geometry of the support has not been adequately studied. In this chapter various parameters that can improve the strength of monolithic ceramic reconstructions are analyzed, which constitutes a new approach in this field.

All the characteristics of tooth preparation influence the behavior of the ceramic crown under loading. In 2011, Goodacre (59) described nine scientific principles developed for ensuring mechanical, biologic, and esthetic success for tooth preparation of complete coverage restorations for metal and ceramic materials. In 2004 he proposed a design of tooth preparations for optimal success (93). The purpose of this study is to outline the role of the three main geometric features and their effects on the mechanical response for biomimetic ceramic crowns. The selected features are: the **total occlusal convergence** (**TOC**), the

curvature of the occlusal face (**COF**), and the form of the finish line, represented by the **shoulder angulation** (**SA**).

For the validity of the study we produced different samples with specific characteristics using CAD/CAM systems only. CAD was first used to model an infrastructure that represented the tooth preparation. The CAD software allows the 3D design of a model with high precision and in accordance with clinical requirements (59, 60, 68). We determined a basic preparation, for which the value of the three factors varied due to the CAD system. Using a mechanical press, samples were submitted to a compressive loading until rupture. Mechanical tests were monitored, graphs were produced, and the rupture force values were collected. The results were established to determine the strongest design and to analyze the corresponding favorable parameters.

3. Materials and Methods

3.1. Materials and Methods for the optical study

3.1.1. Principle of the Speckle Interferometry (SI)

When a laser beam illuminates a surface that is not highly polished, an image (interference pattern) related to the structure of the surface itself, the speckle, is produced as a result. The speckle from the object then interferes on the optical sensor with a reference beam (object speckle or smooth beam) to detect the phase of the light relative to the position and shape of the object, which then creates specklegrams (Fig. 12.). The subtraction of two specklegrams at different loads enables an analysis of the changes in the surface (by deformation example) from interference fringes that appear.

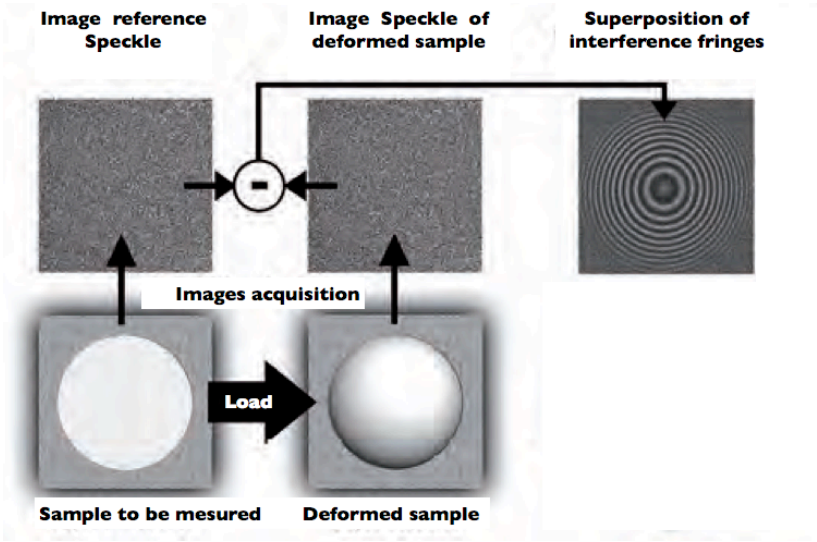

Fig. 12. The process of SI.

Fig. 13. shows on a dental plaster model the difference between white lights, the image reference speckle and the image speckle of the sample under strength. The B image is grainy but the sample is clearly visible. On the C image, there are different alternating levels of gray and fringes. The fringes correspond to gray levels between 0 and 255 with a coding similar to the fringe of altitude. When the deformation is greater than the sensitivity of the interferometer, it creates an additional fringe as a new level.

The gray levels obtained will be automatically converted into displacement values that account for the sensitivity of the interferometer.

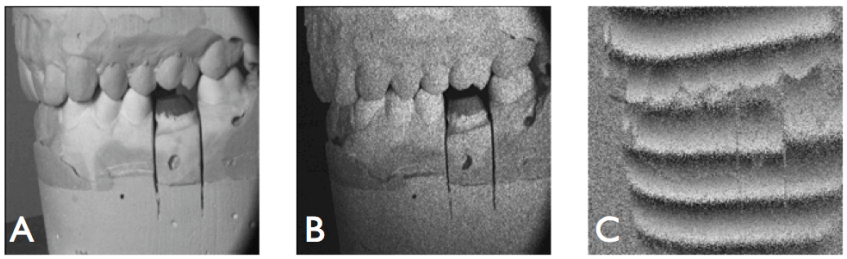

Fig. 13. Example for speckle images on a plaster model: A) white light image; B) reference speckle image; C) speckle image model under load in which the fringes correspond to the deformation of the plaster model.

3.1.2. Mechanical set-up

The compression test device fulfils the high sensitivity of SI and also handles the rigid body motions of the whole system. The sample tooth must be placed in a dedicated mold in the lower jaw while the force transducer holder (Model 31® mid-range precision miniature load cell) is slowly translated vertically by the stepping motor (DC-Mike Actuators: M-235®). The system can generate a force-driven displacement (DC motor controller: C-8622M Mercury), or just a user's displacement. The compression set-up is connected to the computer through NI USB-6251 "High-performance M series multifunction" (National Instruments, Austin, TX, USA) and interfaced with LabVIEW programming created by the author. The whole mechanical system is screwed on the holographic table-top (Newport ©, Irvine CA, USA). Very small displacement steps up to 1.6 nm can theoretically be achieved. The force can be applied to the tooth directly with the force transducer or using a relay rod. The force is always applied on the same part of the tooth surface for all the samples, which requires some degrees of adjustment to place the lower jaw properly.

Fig .14. shows the set-up diagram and Fig. 15. depicts the mechanical set-up.

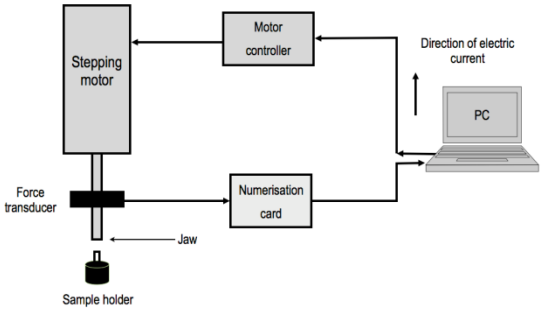

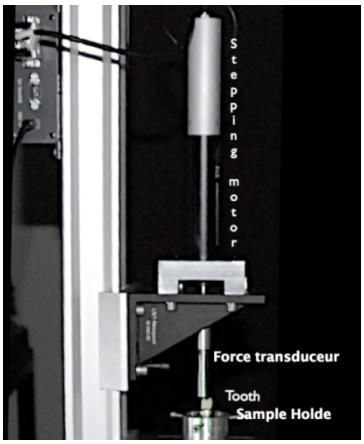

Fig. 14. Mechanical set-up diagram

Fig. 15. Mechanical set-up

3.1.3. SI set-up

For this study, we used the frequency-doubled YAG laser emitting 50 mW continuous waves at a wavelength of 532 nm in the green light region. The laser beam is then injected into a COTS (commercially off the shelf) system (Canadian Instruments) that offers injection, variable intensity coupling in the output fibers, and also phase shifting. There are two input fibers, one for injection and one for detection of the reflected signal at the output interfaces. Parts of the output fibers are bare and wrapped around piezoelectric transducers (PZT).

The optical set-up is presented in Figs.16. and 17.

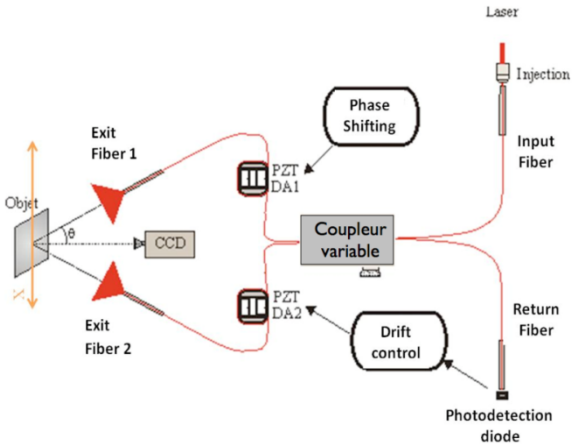

Fig. 16. SI set-up diagram.

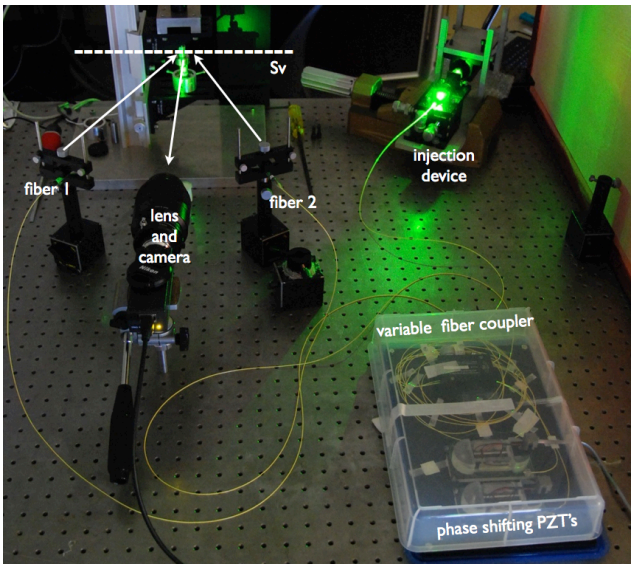

Fig. 17. This figure shows the plane speckle interferometer with the observation and illumination beams (solid lines), sensitivity vector Sv (dashed line), variable fiber coupler, and the phase shifting and injection devices.

The phase shift was applied on either or both of the two output fibers. The system was protected from thermal and mechanical effects by a plastic box and was easily breadboard able. Phase shifts were calibrated using common procedures (94).

The results of calibration for the two piezoelectric transducers da1 and da2 are presented in Fig. 18. It was also possible to calibrate the system using the back reflections on the output fibers, producing fringes at the exit of the second input fiber (Fig. 19.) and detected by a pin diode.

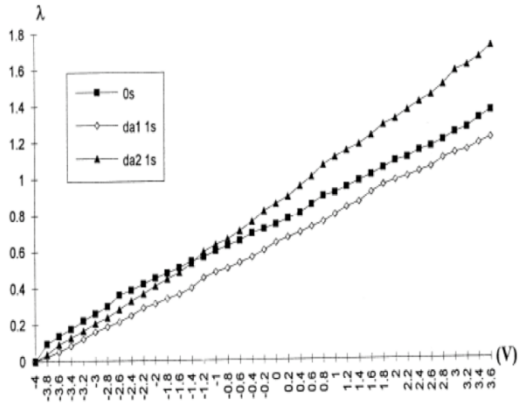

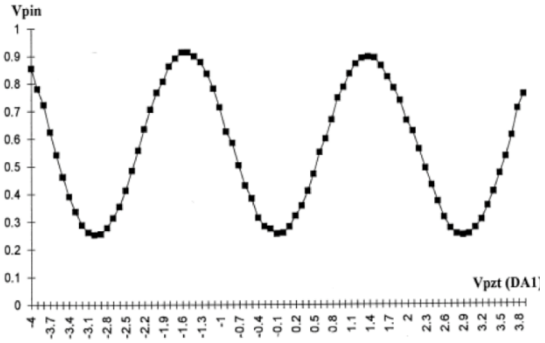

Fig. 18. Calibration curves of the PZT.

Fig. 19. Back reflected intensity modulation

Because in-plane displacements are of great interest for dental measurements, an

optical fiber in-plane sensitive interferometer has been designed. The sensitivity vector (Sv) is shown in Fig. 17. and horizontal sensitivity was achieved. A“4-bucket” phase shifting algorithm led to phase variations during the compression test. Live fringes were determined by subtracting the reference state from the current load state. From minimal to maximal loading, different phase maps were recorded and stored in the computer. Moreover, the reference state was also refreshed because for some load steps, the number of fringes can be very high and the noise is too great to allow for a good interpretation of the resulting fringes.

3.1.4. Displacement calculations

Different operation modes of SI are commonly used, such as the subtraction-mode, time-averaged SI, and double-pulsed SI (95). In this work, we focus on subtraction-mode SI, or more specifically, on phase-shifting SI, which is mainly used for static deformation measurements.

Combining the primary interference pattern phase changes between the recordings yielded new secondary interference fringes (also called correlation fringes). Considering the two states of the object (state 1 - initial / state 2 - excited), the two primary interference patterns I_1 and I_2 were determined by the following equations:

$$\begin{aligned} I_1 &= I_r + I_{o,1} + 2\sqrt{I_r I_{o,1}}cos(\varphi_s) \\ I_2 &= I_r + I_{o,2} + 2\sqrt{I_r I_{o,2}}cos(\varphi_s - \Delta\varphi) \end{aligned}$$

The spatial dependency of the variables I = I(x, y) and φ = φ(x, y) was omitted for readability reasons. The variable φ_s denotes the start phase (also called speckle phase) at the initial state of the object. The variable Δφ represents the phase change between state 1 and state 2.

These speckle interferograms can be subtracted to give the following equation for the secondary interference fringe pattern, assuming perfect spatial correlation between the two primary speckle patterns:

$$I_1 - I_2 = 2\sqrt{I_r I_o}(cos(\varphi_s + \Delta\varphi) - cos(\varphi_s))$$

It is apparent that the self-interference terms disappear, and only the modulation of the interference term remains. However, because of the large variation in the object intensity (I_o), this interferogram contained a large amount of speckle noise, which decreased the accuracy of the measurements.

Currently, noise limits the accuracy of intensity subtraction SI to approximately 15 nm.

Regarding the in-plane sensitivity of the setup, the angle of the impinging beam θ is approximately 30° and determines the correspondence between the phase gray level variation and the in-plane displacement (u_x).

In our interferometer, the wavelength of the laser was 532 nm, and its relationship with the in-plane displacement is given by the following equation:

$$u_x = \frac{\lambda}{4\pi \sin\theta} \varphi_x$$

The resulting variation of one grey level of phase u_x is approximately 2.08 nanometers.

3.1.5. Samples

For each experience, intact premolars free of caries were stored in physiological serum after being extracted as part of routine orthodontic treatment of young healthy adolescent patients (aged < 18 years). Right and left premolars from the same patient were used. Therefore, several sets of two samples (a natural tooth and a prosthetic tooth) were created. One set was kept intact, and the opposite set was prepared to receive the prosthetic crown.

The samples were first created with whole teeth. Then, a longitudinal cut oriented in the vestibular-lingual direction was performed, and one of the two parts was removed using a diamond disc. Longitudinal cuttings were used to allow for planar object observation and for an appreciation of the differential behaviors “inside” the tooth at the natural DEJ and DCJ interfaces.

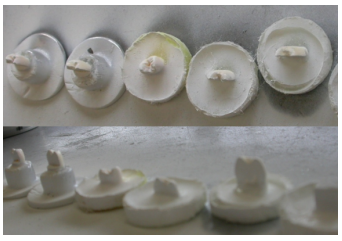

Fig. 20. Preliminary tests: different samples and different sample holders.

3.1.6. Manufacturing the prosthetic samples

The prosthetic crowns were manufactured with a prosthodontic chairside CAD-CAM system from an optical print. The software allowed for a perfect clone of the reference sample to be created. The necessary space for the glue was also entered with ideal values. This duplication process yields two samples with identical anatomy for further processing. The glue joint thickness can also be modified, if required.

A Cerec 3D (Sirona Dental System, Bensheim, Germany) unit was used to manufacture the prosthetic crowns as a clone of the opposite tooth using the reproduction of the Cerec software V2.80 (94). The software was set to provide a dento-prosthetic spacing of 100 µm and peripheral joint of 40 µm for a thickness of 800 µm.

The quality of the machining has been validated by electron microscopy observations.

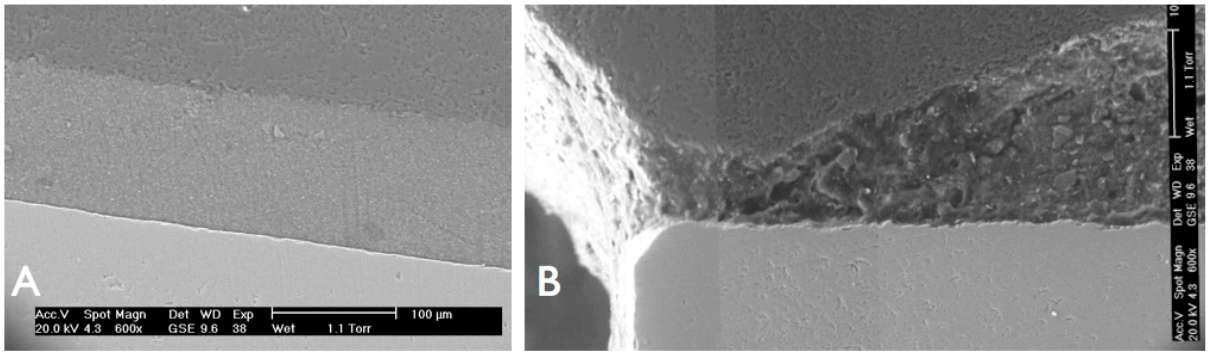

Fig. 21. A) dento-prosthetic spacing, B) peripheral joint spacing (pictures supplied by author).

Optical imprints of the prepared tooth and of the opposite tooth were recorded, and the Cerec MC® machine milled the prosthetic crowns (96). The cloning process is presented in Fig. 22.

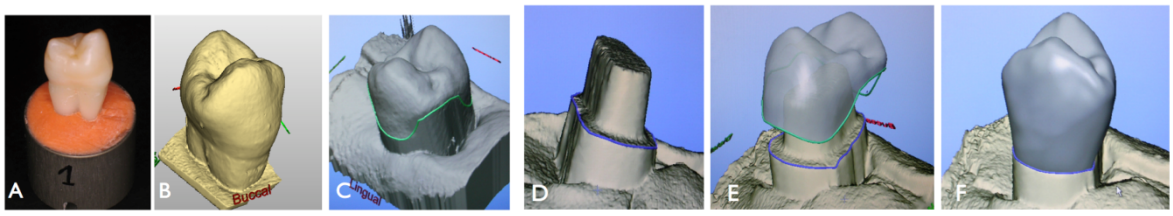

Fig. 22. Cloning process: A) intact natural crown sample, B) optical print, C) shaping, D) optical print of the second tooth prepared to receive the prosthetic, E) adaptation of the shaping on the prepared tooth, F) CAD finished, CAM ready.

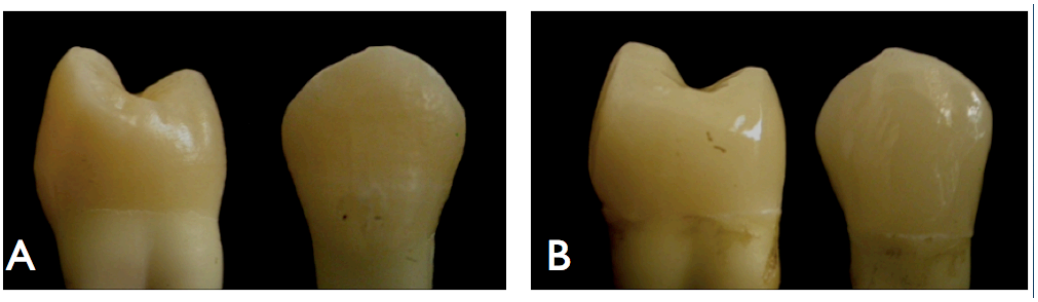

Fig. 23. A) natural tooth, B) prosthetic clone.

The Vita MarkII (Vita Zahnfabrik, Bad Säckingen, Switzerland) ceramic blocks from albite enriched feldspathic ceramic were used. The abrasive coefficient was close to that of dental enamel. After milling, the extrados were glazed (Azkent®, Vita Zahnfabrik, Bad Säckingen, Switzerland). Crowns were then glued onto the prepared tooth using Relyx Unicem® adhesive cement (3M Espe Dental Division, St. Paul, MN, USA) following the classical clinical protocol by illumination of each side of the crown for 4 s at 3000 mW/cm^2 with a Swissmaster Light® lamp (E.M.S. Nyons, Switzerland) (Fig. 24.).

Fig. 24. Materials used to create the prosthetic clone: Cerec 3D, Vita MarkII ceramic, Relyx-Unicem luting cement, SwissMaster lamp.

3.1.7. Sample holders

The first sample holders were made in epoxy resin, but the SI experiments showed the instability of the sample holders and some deformation of the epoxy resin. Therefore, the sample holders were cast in chromium cobalt using the imprint of a root and the lost wax technique. As a result, each sample holder was perfectly adapted to the tooth being studied.

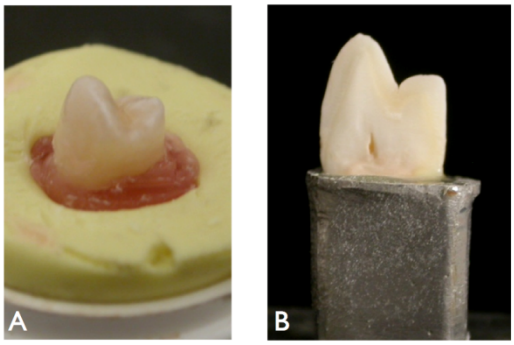

Fig. 25. The lost wax technique for the realization of the sample holder from a root imprint: A) print of roots in the wax, B) the chromium cobalt sample holder and the sample after a vertical cut.

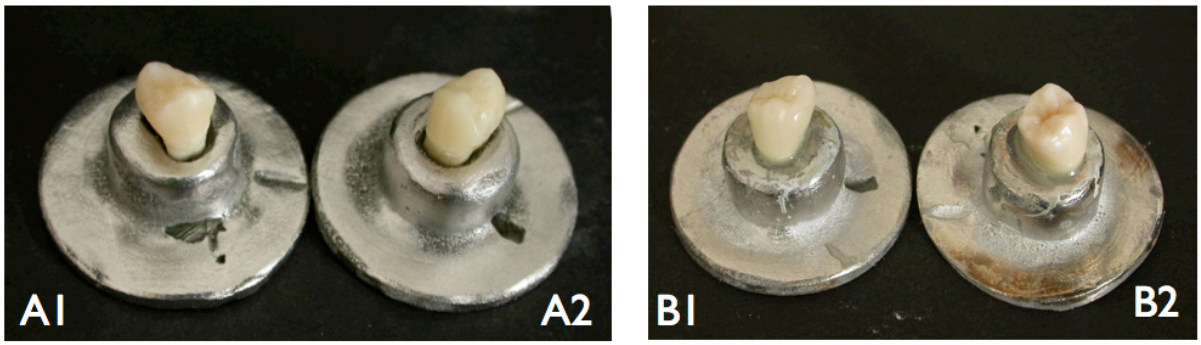

Fig. 26. Examples of samples and sample holders (chromium cobalt): A) first upper premolar A1 natural tooth, A2 prosthetic clone, B) B1 prosthetic clone, B2 natural tooth.

The samples were glued into the sample holder with a layer of Araldite (Hunstman Advanced Materials, The Woodlands, Texas, USA).

3.1.8. Typical experiments

Specimens were white powdered using Eutest 3 Developer Castolin Eutectic powder (Castolin, Lausanne, Switzerland) to generate a uniform diffusing surface and to avoid different modulations between the dentin and enamel or the ceramic and dentin. For the first tests, the compression test consisted of an initial increase in the load until the whole set-up was well established at approximately 120 N. Then, the force was decreased to the minimum contact and was slightly enhanced to generate live fringe maps. For the final testings with cuting samples, we applied successive loads starting from 0 N.

The same loads were applied to the natural tooth and to the prosthetic crown samples to enable comparisons of their respective compressive behaviors.

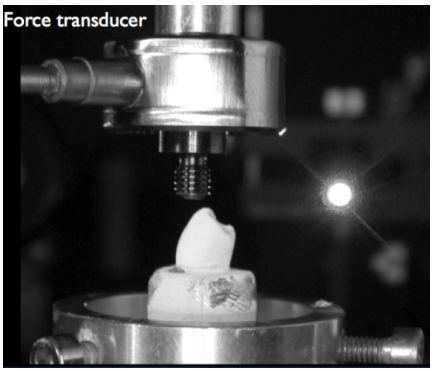

Fig. 27. Sample powdered (whole tooth) in place before loading.

The starting load was approximately 0 N. The compression was performed stepwise using discrete displacements of the transducer tip (one step was approximately 1.6 nm of Y-displacement). Therefore, a greater number of steps equal a higher compression. There was a simple relationship between compression, the displacement of the tip and the loading force. The sample can be loaded or unloaded. In the case of loading, the load will always slightly decrease after the required load application. The loading range applied to the different samples was between 5 N and 120 N. The CCD camera recorded the interferences of the two illumination beams coming from the two output illuminating optical fibers at the sample surface. Live fringes were displayed between a reference state and the current experimental load state. Between minimal and maximal loading, different phase maps were recorded and stored in the computer memory. The mechanical deformations were computed from the displacement maps generated from the phase difference maps.

SI is a relative displacement measurement. The maximum range between two successive measurements is approximately 20 μm. In our experiments, we needed to record smaller steps because of the appearance of some mechanical noise. Therefore, new displacement references (zero displacement reset) were recorded during the test.

3.2. Materials and methods for the mechanical study

3.2.1. Infrastructure

3.2.1.1 CAD

CAD: Catia V5 software (Dassault Systems, Vélizy-Villacoublay, France) was used to design the infrastructures. It designed a geometric form based on fixed prosthetic principles (58, 68) using the following seven parameters:

D1: total diameter.

D2: preparation diameter.

HI: occluso-cervical dimension.

LI: width of the shoulder.

TOC: total occlusal convergence.

SA: shoulder angulation.

COF: curvature of the occlusal face

Six different specimens were constructed based on the above parameters, with variations in the following critical parameters: TOC, SA, COF.

TOC: 7° or 21°.

SA: 45° or 90°.

COF: 1.9 mm, 13 mm, 0 mm (0 mm corresponds to a flat occlusal face, 13 mm and 19 mm to a rounded occlusal face)

The specimens were named according to their characteristics:

S1: $21^{\mathrm{TOC}}45^{\mathrm{SA}}1.3^{\mathrm{COF}}$

S2: $7^{\mathrm{TOC}}45^{\mathrm{SA}}1.9^{\mathrm{COF}}$

S3: $21^{\mathrm{TOC}}90^{\mathrm{SA}}1.3^{\mathrm{COF}}$

S4:$7^{\mathrm{TOC}}90^{\mathrm{SA}}1.9^{\mathrm{COF}}$

S5:$7^{\mathrm{TOC}}90^{\mathrm{SA}}0^{\mathrm{COF}}$

S6: $7^{\mathrm{TOC}}45^{\mathrm{SA}}0^{\mathrm{COF}}$

The six different infrastructure characteristics are shown in Table II.

Series		S1	S2	S3	S4	S5	S6
							
Fixed values	D1 (mm)	6	6	6	6	6	6
	D2 (mm)	4.2	4.2	4.2	4.2	4.2	4.2
	H1 (mm)	9	9	9	9	9	9
	L1 (mm)	0.9	0.9	0.9	0.9	0.9	0.9
Variable values	TOC (°)	21	7	7	21	7	7
	COF (°)	1.3	1.9	1.9	1.2	0	0
	SA (°)	45	45	90	90	90	45

Table II. The six different infrastructure characteristics.

The goal was not to reproduce an identically prepared tooth, but to individualize the features of the preparation that significantly affect the mechanical response of the ceramics. The height and diameter of the infrastructure were determined to obtain volumes close to the clinical reality (in this case a lower premolar), and the width of the cervical limit was set in accordance with the literature (900 µm). They do not reflect a strict clinical reality but resulted from different measures allowed for a discussion about the proposed method.

3.2.1.2. CAM

During this study a 5-axis DMU40 milling machine (Deckel Maho Gildemeister, Bielefeld, Germany) was used ensuring an accuracy of 2 µm.

The infrastructure was milled from aluminum barrels (Al 6060). The dimensional reproducibility was enhanced with 6060 aluminum milling. However, to obtain samples with a limited set of controllable design parameters, the modulus of elasticity of the dentin and the periodontal-ligament was deliberately omitted. The infrastructure is not composed from a material that has the same modulus of elasticity as dentin (97). Therefore, the nature of the

study is strictly to compare materials that are subject to certain constraints on media and not specific physiological responses of the dental organ.

For each shape, 5 identical samples were milled. This is an acceptable number of samples for operating results to establish statistically significant values**.** The bars were 2 cm in diameter and 1.5 cm in height. The infrastructure exhibited a height of 9 mm, and the part of the barrel that was not milled was used as a sample holder (Fig.39).

Fig. 39. The aluminum-milled infrastructures.

3.2.2. Superstructure

Superstructures were produced with the Cerec AC CAD/CAM system (Sirona Dental System, Bensheim, Germany).

3.2.2.1. CAD

Optical imprints of each of the infrastructures were recorded with the “blue cam” intraoral camera. Models of the superstructures were created with the 3.60 CAD/CAM software. The software was set to yield a dental-prosthetic spacing of 100 µm and a peripheral joint of 40 µm for a total thickness of 900 µm. The maximum thickness on the occlusal face was 2 mm, resulting in a flat surface of 4 mm^2.

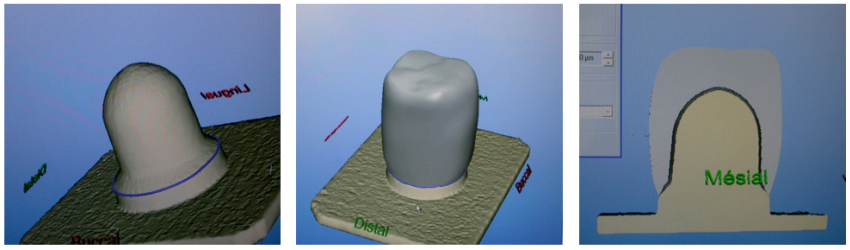

Fig. 40. CAD : the optical print, modeling, verification with vertical cut.

3.2.2.2. CAM

Superstructures were manufactured using the MC-XL milling unit (Sirona Dental System, Bensheim, Germany).

The caps were milled from Vita MarkII ceramic blocks (Vita Zahnfabrik, Bad Sackingen, Germany). One optical imprint was taken for each shape. Five superstructures were milled from the same optical print. A total of 30ceramic caps were milled (5 samples for 6 series). There was no significant difference between the dimensions of the superstructures. For this study, the resulting samples were not glazed or polished.

3.2.3. Preparation of the complete specimen (superstructure + infrastructure)

To increase the area of the ceramic surface, the superstructures were etched on their internal surface with 5% hydrofluoric acid gel for 1 min. They were then cemented to the infrastructure with Relyx-Unicem cement (3M ESPE Dental Division, St. Paul, Minn., USA) and subsequently cured using a Swiss Master Light curing unit ((E.M.S., Nyons, Switzerland) following the standard clinical protocol of illumination (4 s at 3000 mW/cm^2 per face). Each series was numbered, and each sample within the series was numbered individually.

Fig. 41. Specimen preparation: the superstructures (ceramic caps) are adhesively glued on the aluminum-milled infrastructure.

3.2.4. Mechanical testing systems

Compression tests were performed with the Dartec mechanical testing system (Test Ressources Inc., Shakopee, Minn., USA), which was driven by the Tematest software (Tema

Concept, Chanteloup les Vignes, France) using regulated loading speeds. We used a 500-daN load cell TC4 transducer (Nordic Transducer, Hadsund, Denmark), coupled with a 1 mm range LVDT (Linear Variable Differential Transformer) displacement sensor (L10R transducer, RDP Electrosense, Pottstown, Pa, USA).

3.2.5. Mechanical measurements

The samples were positioned between the jaws of the mechanical press (Fig. 42.). A 10 N preload was applied to the sample prior to the test. Then, sequential loading was performed to measure specific mechanical values (stiffness, strength). Thus, successive loading (+300 N) and unloading (-100 N) cycles were performed, while the LVDT sensor monitored the compressive displacement response of the sample. As soon as rupture occurred, the press was stopped. During the test, the force and displacement were continuously recorded and the rupture force values were noted.

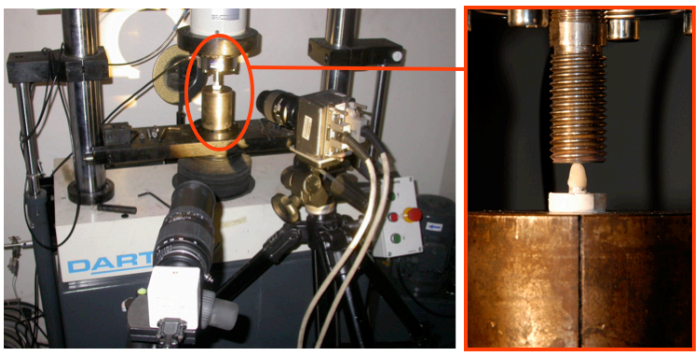

Fig. 42. Mechanical testing system and **s**pecimen between jaws.

3.2.6. Statistical analysis

The Kruskal–Wallis analysis of variance by ranks was used to determine if the three factors appear significant and if the combination of the three factors was significant.

4. Results

4.1 Results of the optical study

4.1.1. Results obtained on whole teeth

The first results were obtained on uncut samples, and the main objective was to validate the experiment. Displacement measurements were not performed.

The obtained images allowed the determination of the following parameters:

- the stiffness of the mechanical set-up
- the efficiency of the sample-holders
- the movement of all the natural crown and all the prosthetic clones

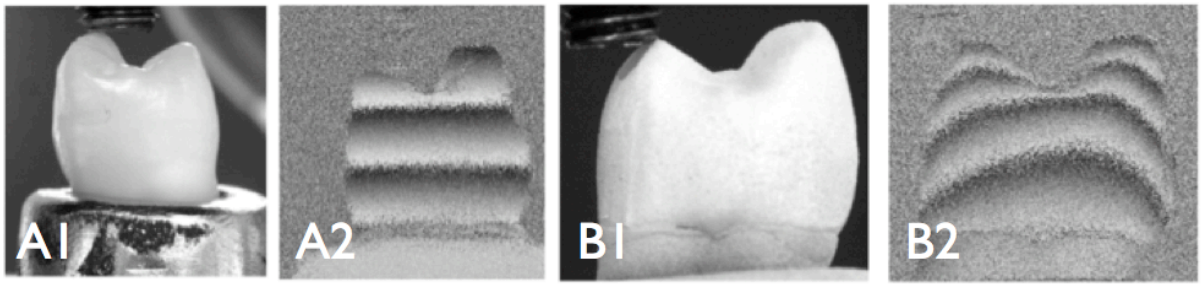

Fig. 43. Whole samples under loading: A) natural whole tooth, B) prosthetic clone under white light and speckle picture under loading. The fringes show the movement of the crowns under a load. The root and the sample holder were stable, and only the enamel cap and the ceramic cap were moving. There is no fringe on the sample holder (A2) and at the beginning of the roots (B2).

4.1.2. Results obtained on half cut teeth

On SI images, the interfaces appear distinctly along their entire lengths, thus showing the complete loading (from 35.5 N for the DEJ on the natural tooth and from 36 N for the prosthetic crown).

Fig. 44. Natural tooth and clone before and after the vertical cut.

Table III. indicates the range of forces in which the photos were taken, the number of new references (displacement reset) and the numbers of the pictures taken.

	Force (N)	New-ref	Pictures	Pictures with measurements
Natural tooth	0-96.5	3	24	12
Prosthetic tooth	0-117.74	7	39	13

Table III. This table shows the range of forces in which the photos were taken, the number of new references (displacement resets) and the numbers of pictures.

In this chapter, we have selected typical photos and results to avoid overloading this section. We worked in relative motion. It was necessary to work by intervals corresponding to displacement solicitations consistent with the measurement capability of the interferometer. If the movement of the sample becomes too large, it exceeds the measurement range of the interferometer.

Therefore, with the natural tooth presented in Fig. 45, we have a white light image (A) and SI images (B, C, D). Fig. 45 B starts at 0 N and the image was taken at 35.5 N. The start reference is 0 N (New ref: 0) and the strength was 35.5 N, so the ΔF was 35.5 N. For Fig.45 C, the image was taken with a variation of 0.16 N (ΔF: 0.16 N) between the total force applied (40.39N) and the new reference value of 40.23 N.

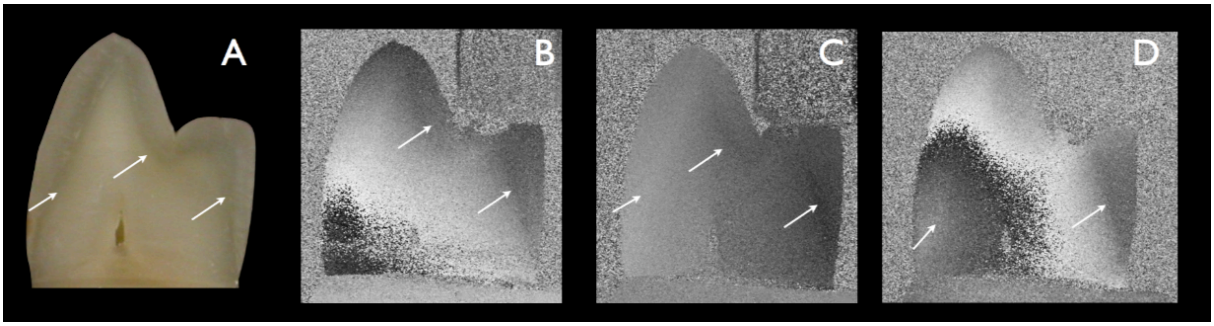

Fig. 45. White light and SI images for natural tooth sample; A)White light image, B) Screenshot N° 04: Force: 35.5 N, ΔF: 35.5 N (New ref: 0); C) Screenshot N° 13: Force: 40.39 N, ΔF: 0.16 N (New ref: 40.23); D) Screenshot N° 24: Force: 82.54 N, ΔF: 13.96 N (New ref: 96.5).

Fig. 45 A displays the sample under white light before painting. Figs. 45 B, 45C, and 45 D are SI images recorded at different compression levels and present typical fringes.

Fringes occur when the displacement induces an optical phase of 360° to 0°. The displacement in the X direction was computed from the optical phase. In Figs. 45 B, 45 C, and 45 D, different continuous gray lines demarcate the DEJ (white arrows) corresponding to the image taken in white light (A). The DEJ was clearly visible when the applied force reached 35.5 N. The DEJ was always more visible in front of the loading point.

Images of a prosthetic crown are presented in Fig. 46.

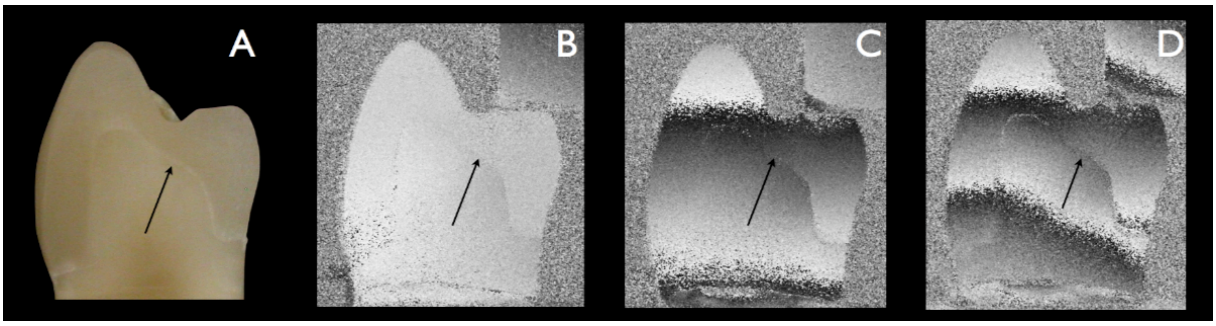

Fig. 46. White light and SI images for prosthetic crown sample; A) White light images; B) Screenshot N° 08: Force 36.78 N, ΔF: 2.57 N (New ref: 41.01 N); C) Screenshot N° 15: Force 77.56 N, ΔF: 5.29 N (New ref: 82.85 N); D) Screenshot N° 33: Force 64.09 N, ΔF: 18.7 6N (New ref: 41.01 N).

Fig. 46 A displays the sample under white light before painting, and Figs. 46 B, 46 C, and 46 D were recorded at different compression levels and present typical fringes at different loads. The DCJ appeared from 38 N and is clearly visible in figures 46 B, 46 C, and 46 D (black arrows). For the natural crowns, the DCJ appeared as a continuous gray line corresponding to the image taken in white light (Fig. 46 A).

The SI images displayed in Figs. 45 B, 45 C, and 45 D show that the natural enamel cap moved independently from the dentin. This difference is clearly delimited by a line corresponding to the anatomical location of the dentin-enamel junction (DEJ). For the prosthetic crown, the same type of shift occurred at the glue junction of the ceramic crown with the dentin in the SI images (46 B, 46 C, and 46 D). The DEJ was less well marked than the DCJ due to the smaller associated displacements.

The highest loading values enabling the distinction of the interface zone were 117.4 N for the prosthetic crown and 82.5 N for the natural tooth. Beyond 120 N, all samples behaved

like rigid bodies. Approximately at 200 N, some samples were destroyed due to brittleness of the materials.

From all of the screenshots, different images were chosen for use in computing the displacement maps. We have selected five screenshots that are presented below.

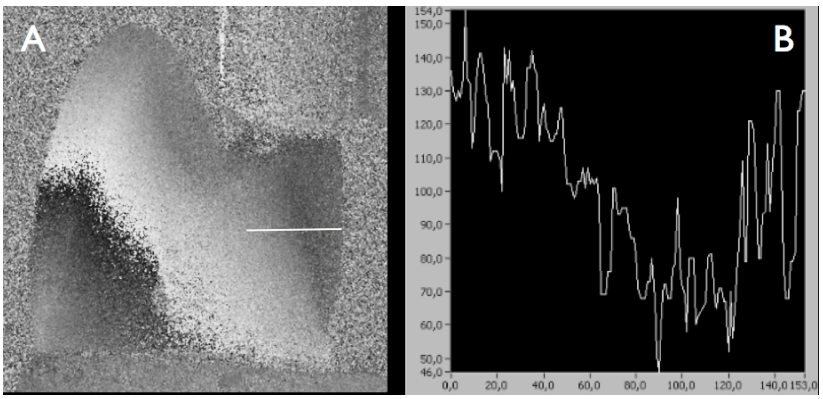

Fig. 47. ***Screenshot 1:*** Natural tooth behavior at a load of 38.65 N, ΔF =1.74 N, N ref: 40.39 N. A) SI image: the single white line corresponds to the region of interest (ROI) used for the calculation of displacement. B) displacement curve along the white line. Displacements are shown in nm versus the position in pixels.

In Fig. 47 A, from left to right, we denote the transition between light gray to dark gray corresponding to the region between the dentin and the enamel. One white line has been defined as the region of interest (ROI). In Fig. 47 B, the curve represents the displacement change in nanometers versus the position along the white straight line shown in Fig. 47 A. The relative displacement between the dentin and the enamel was 52 nm for loads between 38.6 N and 40.4 N (ΔF = 1.8 N)

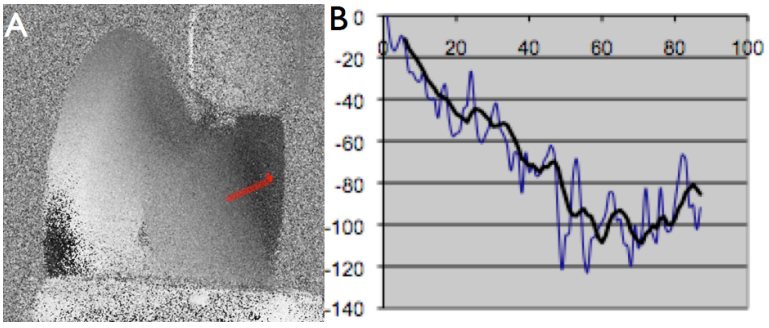

Fig. 48. ***Screenshot 2:*** Natural tooth behavior at a load of 39.21 N, ΔF = 1.18 N, N ref: 40.39 N. A) SI

image: six red equal parallel lines were defined across the DEJ. B) Displacement curves: Blue curve displacement values along one of the 6 red lines. The black curve is the mean value fitting of the 6 blue curves.

In Fig. 48 A, in front of the cusp subjected to the load, the delineation made by the DEJ is visible, and the gray levels differ because of a different accommodation.

To calculate the displacement value, six red equal parallel lines were defined across the DEJ. The displacement was calculated as the average value of the six-stacked profiles. In Fig. 48 B, the black curve is the mean value fitting of the blue curve values along the six paths, and the blue curve is one of the six displacement curves. The mean relative displacement between the dentin and the enamel was approximately 20 nm for loads between 39.21 N and 40.39 N (ΔF = 1.18 N).

The same analytical process was applied for the prosthetic crowns (Figs. 49, 50, 51).

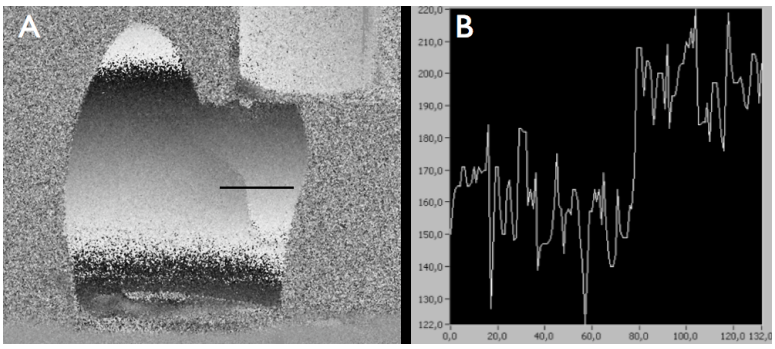

Fig. 49. ***Screenshot 3:*** Prosthetic crown behavior at a load of 76.34 N, ΔF = 6.51 N, N ref: 82.85 N. A) SI image: a single black line corresponds to the region of interest (ROI) used for the displacement calculation. B) The displacement curve along the white line; in this case, the step was approximately 43 nm.

In Fig. 49 A, one red line was defined as the region of interest, as the technical noise was less prominent than for the natural tooth. The area of interest was located in a fringe in front of the stress zone from left to right. We denote the transition between light gray to dark gray corresponding to the region between the dentin and the ceramic cap. In Fig. 49 B, the curve represents the displacement change in nanometers versus the position along the red straight line shown in figure 49 A. The relative displacement between the dentin and the ceramic cap was 43 nm for loads between 82.8 N and 76.3 N (ΔF = 6.5 N)

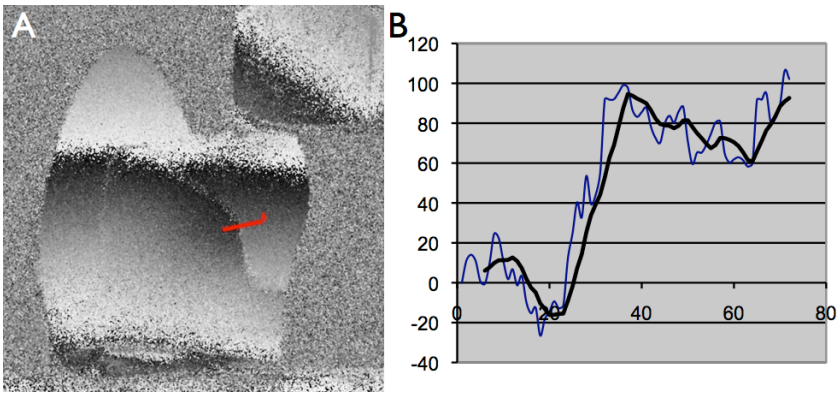

Fig. 50. ***Screenshot 4:*** **Prosthetic** crown behavior under a load of 72.85 N, ΔF = 10 N, N ref: 82.85 N. A) SI image: six red equal parallel lines are defined across the DEJ. B) Displacement curves: The blue curve represents displacement values along one of the six red lines. The black curve is the mean value fitting of the 6 blue curves. The displacement was approximately 95 nm.

In Fig. 50, to evaluate the displacement values, six equal parallel straight paths were defined in the region of interest across the DCJ in the palatine zone in front of the loading point (Fig. 50 A). In Fig. 50 B, the displacement is displayed as the average value of the six-stacked profiles. The black curve is the median value fitting of the blue curve values. In this case, the relative displacement was approximately 95 nm for loads between 82.8 N and 72.8 N (ΔF = 10 N).

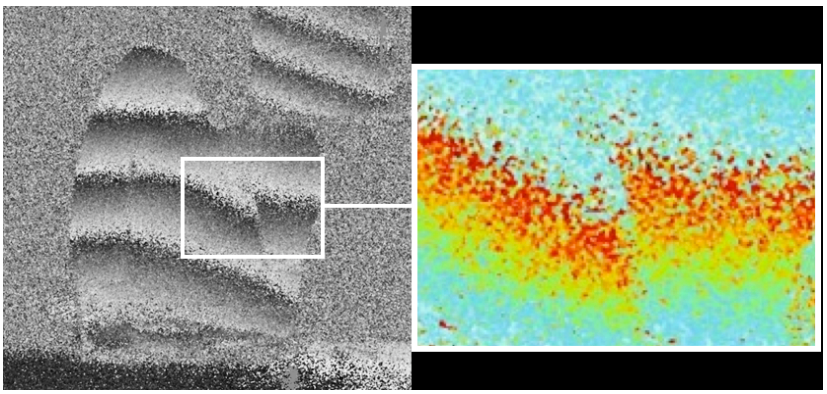

Fig. 51. ***Screenshot 5:*** SI image sample "prosthetic crown" and displacements shown in a contour colored map. The behavior for a load of 52.78 N, ΔF = 30.07 N, N ref: 82.85 N.

The SI image in Fig. 51 was selected to represent the characteristic isodisplacements map of the discontinuity zone located in front of the loading point for a ceramic crown. A

colored and zoomed image is also presented. The fringe shift in the region of interest clearly delineates a mechanical interface between the ceramic and the dentin layers, which were separated by the glue.

However, the results show differences in the behavior of the different samples (natural and prosthetic) at the same load value.

Fig. 52 shows the natural tooth with the same load as the prosthetic tooth (Fig. 51) and allows for a comparison of the DEJ and DCJ. For identical loads, the images of the fringes are completely different.

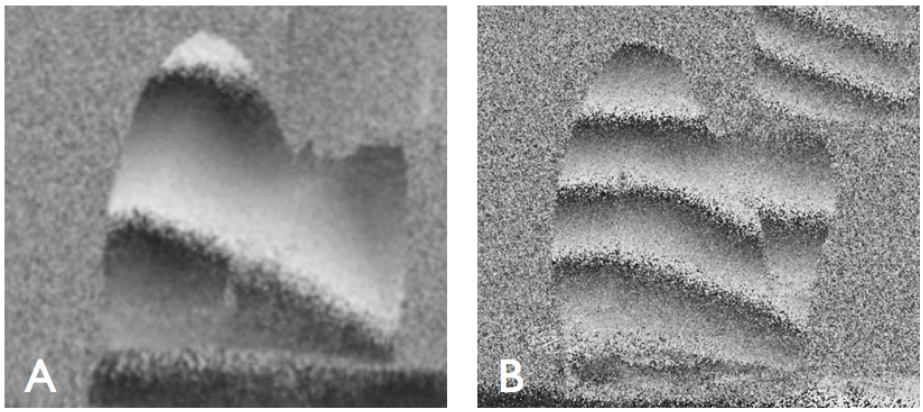

Fig. 52. Natural tooth (A) and prosthetic sample (B) under the same load (53.7 N)

4.2. Results of the mechanical study

The results of the mechanical study are presented in Tables IV., V., VI. and in the bar graphs of Figures 53, 54, 55. All the experimental results were used for the analysis.

4.2.1. Evaluation of the rupture force for each specimen

Values of the rupture force for each specimen are shown in Table IV:

Rupture force	Series 1 (S1)	Series 2 (S2)	Series 3 (S3)	Series 4 (S4)	Series 5 (S5)	Series 6 (S6)
Sample 1	1.094	1.304	1.259	2.017	1.597	1.967
Sample 2	0.923	1.297	1.304	1.889	2.033	1,568
Sample 3	0.970	1.175	1.466	1.436	2.146	1.720
Sample 4	1.166	1.217	1.214	1.214	1.440	2.104
Sample 5	1.088	1.286	1.196	1.869	2.206	2.155

Table IV. Values of the ultimate loading force for each sample of each series.

4.2.2. Statistical results for the rupture forces

Means, standard deviations and dispersions obtained for the rupture forces are shown in Table V. and Figure 53.

Series	**S1**	**S2**	**S3**	**S4**	**S5**	**S6**
						
Mean rupture (kN)	1.048	1.255	1.314	1.744	1.884	1.902
SD	0.057	0.099	0.150	0.256	0.344	0.252
Dispersion (%)	4	9	11	14	18	13

Table V. Mean values of the ultimate force, standard deviation (SD) and dispersion for each series.

The dispersion is the ratio of the standard deviation and the mean, expressed in percentage (%).

The lowest mean rupture force was 1.048 kN (Series 1:$21^{TOC}45^{SA}13^{COF}$) and the highest was 1.902 kN (Series 7: $7^{TOC}45^{SA}0^{COF)}$.

The ultimate force values were used to distinguish two groups of results: (1.04-1.3 kN) for series $7^{TOC}45^{SA}19^{COF}$, $21^{TOC}45^{SA}13^{COF}$,$7^{TOC}90^{SA}19^{COF}$ and (1.7-1.9 kN) for series $21^{TOC}90^{SA}13^{COF}$, $7^{TOC}90^{SA}0^{COF}$, $7^{TOC}45^{SA}0^{COF}$. Each group was associated with geometric features.

Series $21^{TOC}90^{SA}13^{COF}$, $7^{TOC}90^{SA}0^{COF}$, $7^{TOC}45^{SA}0^{COF}$ had a higher dispersion than series

$7^{TOC}45^{SA}19^{COF}$, $21^{TOC}45^{SA}13^{COF}$,$7^{TOC}90^{SA}19^{COF}$.

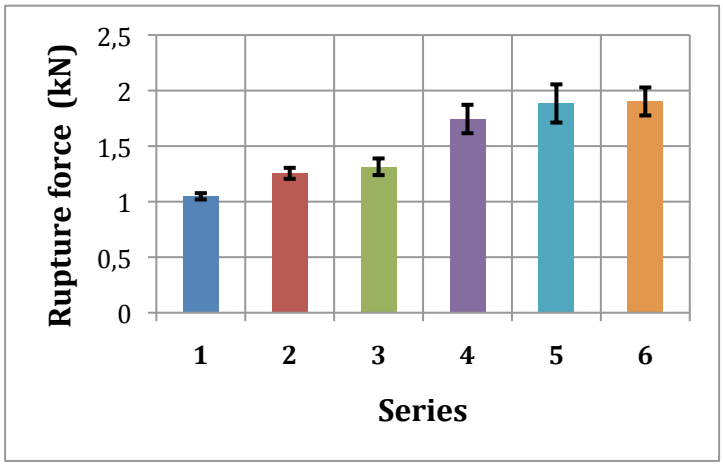

Fig. 53. Rupture forces for each series.

4.2.3. Comparison of the strength values between series

Results in Table VI. are given in percentage to enable a better comparison between series.

Series	S1	S2	S3	S4	S5	S6
S1	-	19.05	24.8	66.7	80	80
S2	19.05	-	4.8	40	51.2	52
S3	24.8	4.8	-	33	44	45
S4	66.7	40	33	-	8	25
S5	80	51.2	44	8	-	0.5
S6	80	52	45	25	0.5	-

Table VI. Differences in rupture forces between the series in percentage (%).

4.2.4. Statistical analysis of the strength values

The statistical analysis (Table VII.) highlights the significant design parameters including the general shape and the first radius of curvature of the occlusal surface.

Specimen characteristics	TOC	SA	COF	G. Shape
p	p=0,98	p=0,056	p=0,0001	p=0,0002

Table VII. Results of the **s**tatistical analysis.

4.2.5. Mechanical response of the specimens

4.2.5.1. Force-displacements curves

Although the results show different values at break for all samples with a variation between the two extremes of approximately 80% (1.048 kN and 1.902 kN), the force-displacement curves show slopes and behavior quite similar between sets, as shown in Fig. 54. For each figure (1 to 6) the 5 curves corresponding to the five samples are shown. Force-displacement curves exhibit the mechanical response of the samples. The force increased with displacement until rupture of the samples occurred.

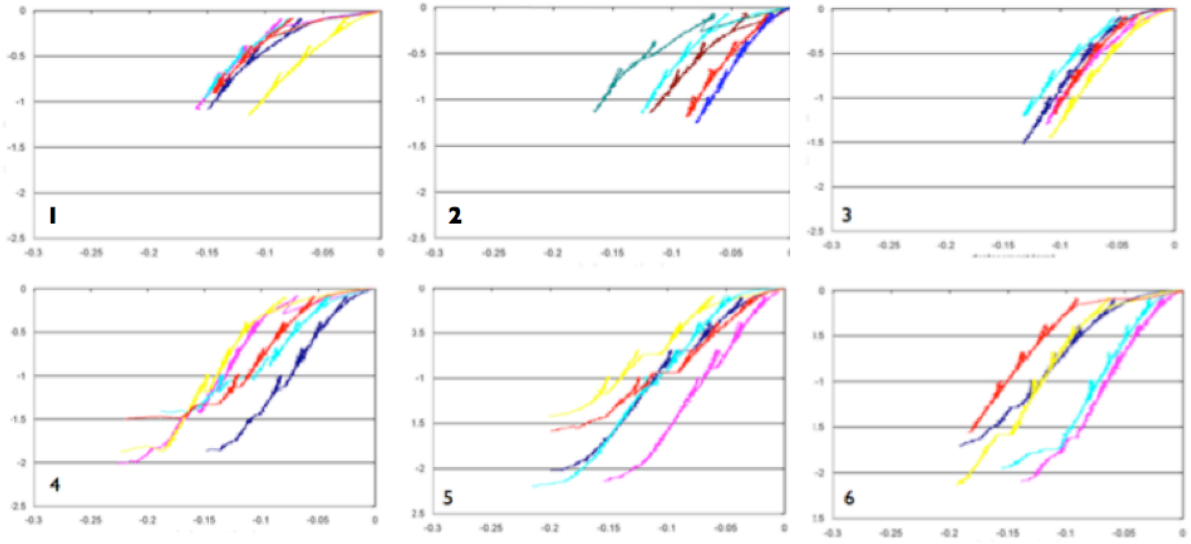

Fig. 54. Force-displacement curves for each series.

For each series, the measured curves showed a similar shape for all the samples within the series. Series 1, 2 and 3 ($7^{TOC}45^{SA}19^{COF}$, $21^{TOC}45^{SA}13^{COF}$, 7TOC90SA19COF) exhibited sudden brittle fracture. On the contrary, series 4, 5 and 6 ($21^{TOC}90^{SA}13^{COF}$, $7^{TOC}90^{SA}0^{COF}$ and $7^{TOC}45^{SA}0^{COF}$) exhibited a change of slope at high force levels, which could be related to the ductility of the adhesive due to its progressive plasticization of during testing and the progressive positioning of the tooth on its support before rupture occurred. Consequently, the curves for series 4, 5, 6 ($21^{TOC}90^{SA}13^{COF}$, $7^{TOC}90^{SA}0^{COF}$,$7^{TOC}45^{SA}0^{COF}$) show higher rupture forces as well as a higher dispersion than the curves for series 1,2,3 ($7^{TOC}45^{SA}19^{COF}$, $21^{TOC}45^{SA}13^{COF}$,$7^{TOC}90^{SA}19^{COF}$).

4.2.5.2. Apparent stiffness of ceramic

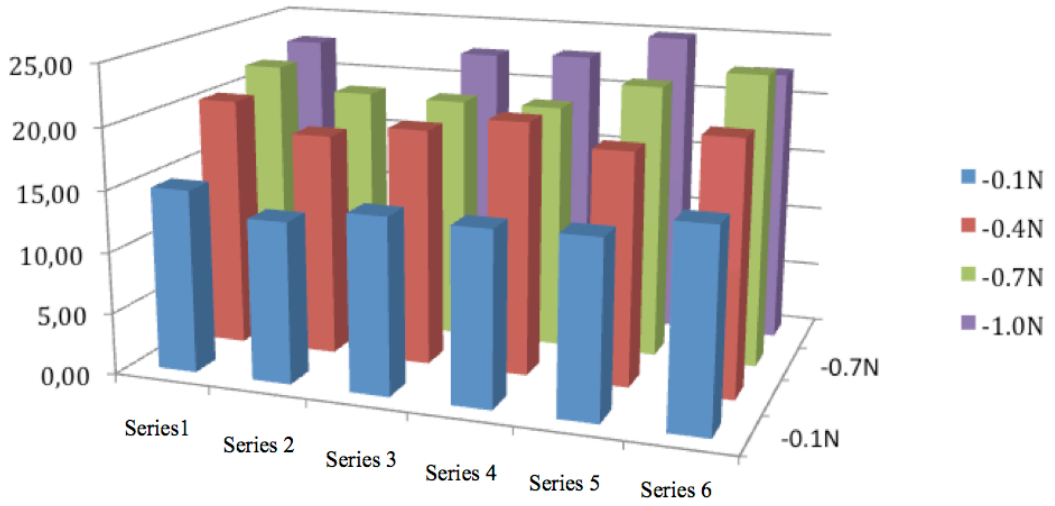

Fig. 55. Responses to stress exhibited by the samples; the evolution of apparent stiffness (kN/mm) for different loading force levels was calculated.

The apparent stiffness increased with increasing loading force. All samples showed an increase in stiffness by approximately 50%. In all the series, a similar degree of stiffness evolved in the same way (Fig. 55.) for the different load levels. For series $21^{TOC}45^{SA}13^{COF}$ rupture occurred before 1 kN was reached.

5. Discussion

5.1 Discussion of the optical study

The importance of the DEJ as an interface binding the enamel and dentin surfaces has long been recognized (Tylman, 1928 (98). Our understanding of the role and the location of the DEJ have evolved with ongoing research. The unique mechanical properties of this zone were first recognized from micro-hardness profiles (Craig et al., 1959 (99, 100). Wang and Weiner (1998) (40, 85) measured the strain across this zone when a compressive load was applied and suggested that this zone is an important working part of the tooth during mastication. An asymmetry between enamel and dentin was noted previously (Wood et al., 2003 (101) but was not quantified. Bechtle et al. explained the phenomenon of crack arrest at the DEJ using the elastic modulus mismatch between the dentin and the enamel (102).

It was found (Zaslansky 2005 (92**)** using SI that a compressive load applied to the tip of the main cusp of a human premolar caused the entire enamel cap to move essentially as a stiff body, tilting towards the buccal surface.

Recently, Barak et al. (103) highlighted the importance of enamel in a whole-tooth demonstration through a finite element model study and validated their findings by a metrology method. Chattah et al. (42) showed that the enamel cap in a mini-pig animal model was capable of deforming and rotating at loads as low as 16 N. Conversely, Zaslansky et al. (41) showed that the enamel cap of an isolated human premolar did not deform or rotate at loads lower than 80 N. Human enamel is stiffer than that of the mini-pig, and the cusps do not deform or crack until high loads are reached. However, in both cases, the aim was to preserve the functionality of the grinding surfaces over long periods of time. The use of these opposing strategies to achieve the same end has been attributed to phylogenetic differences in masticatory function (104, 105). The mini-pig molar is capable of deforming and rotating at low loads, and the intrinsic reaction of the crown to eccentric loading is complemented and even enhanced by the structures supporting the tooth (42).

On SI images, the interfaces appeared distinctly along their entire lengths, thus showing their complete loading (from 35.5 N for the DEJ on the natural tooth and from 36 N for the prosthetic crown). The first interpretation confirms that the enamel bulk and the ceramic cap will move slightly under loading as rigid bodies. However, the mechanical response was

different for the same applied loading force, and the displacement was greater for ceramic than for enamel. Thus in Fig. 51, at a load of 53.7 N, the SI image clearly shows an isodisplacement between enamel and dentin. In Fig. 52, at a similar load (52.3 N), the image identifies the DEJ and the differing behaviors of the enamel and dentin. However, this image does not show an iso-displacement as was shown in Fig. 51.

This iso-displacement is confirmed in SI pictures in Figs. 49 and 50, with values of 43 nm and 95 nm, respectively. This behavior demonstrates the accommodation strength of the DCJ and confirms its protective role for the ceramic caps.

Moreover, we emphasize that the displacement of the crown, whether enamel or ceramic, is different if the measurement area is far from or close to the loading zone. In each case, the most important displacements were located opposite to the load. The gray levels also showed a displacement of the opposite cuspid but of a smaller magnitude.

For the natural tooth, Zaslansky said that the asymmetric nature of the structure between the buccal and lingual sides might also contribute to the distribution of loads that are not applied along the long axis of the tooth. The possible asymmetry in stiffness between the buccal and lingual sides of the tooth points to a basic property of tooth function, presumably related to the precise manner in which stress is distributed during mastication.

Conversely, for the prosthetic crown, the glue joint thickness will be the same everywhere (100 μm) except in the zone of the cervical joint, where it is approximately 40 μm. The displacement of the ceramic cap will be a function of the thickness of the glue and its elastic modulus (106). The behavior of the samples appeared rational. Above a certain load (82.6 N for the natural tooth and 117.4 N for the prosthetic crown), the SI images showed that the DEJ and the DCJ could not be clearly observed (Fig. 56).

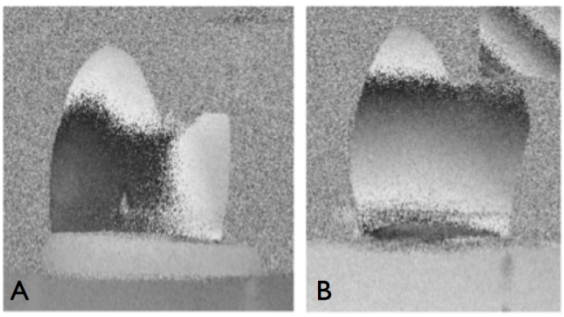

Fig. 56. On the natural tooth (A) and the prosthetic sample (B) the DEJ and the DCJ cannot clearly be observed.

When the interfaces in both settings could no longer accommodate the loading stress, the teeth began to act as whole rigid objects, and continuous increases in loading forces generated cracks and fractures of the samples.

This work tends to confirm both Zaslansky's and Weiner's studies, as it proves the importance of the DEJ zone in the tooth structure. Moreover, we have demonstrated a similar behavior for the DCJ. We believe these zones are crucial for the stress resistance of the crown structure, whether natural or prosthetic. For mono-bloc vitreous ceramic prosthetic crowns, load resistance is a result of the gluing process (107, 108).

In reality, the soft DCJ or DEJ interfaces are graded structures, and much remains to be understood about the manner in which the whole tooth behaves under load.

An astute use of dento-prosthetic spacing will be to select the glue joint thickness based upon the glue elastic modulus. This approach will refine attempts to mimic the physiological behavior of the natural tooth. Reconstruction ceramics have wear coefficients close to those of natural enamel and are assembled with adhesives having a modulus of elasticity similar to natural DEJ; therefore, we can expect the construction of real biomimetic prosthetic teeth in the near future.

5.2. Discussion of the mechanical study

We have evaluated the efficiency of this original method, and the effect of the three variables, TOC, COF, SA, separately and then together.

5.2.1. Evaluation of the efficiency of the method

5.2.1.1. Low dispersion of strength results

The standard deviation of the rupture force was 0.057 for S1 ($21^{TOC}45^{SA}19^{COF}$) and 0.099 for S2 ($7^{TOC}45^{SA}13^{COF}$). The dispersions were 4% and 9%, respectively, which were satisfactory for the fracture mechanics results. It is interesting to note that several studies used 10 samples and obtained results with much higher standard deviations and dispersions. Our results are satisfactory when considering that some important studies (45) commonly propose results with dispersion of more than 30% and all our results have dispersion lower than 20%.

5.2.1.2. Reproducibility of the samples stiffness

There is a relationship between the dispersion and the load level as indicated by the increase in the stiffness with increasing loading force, as shown in Fig. 55.

All series showed an evolution in stiffness regardless of the shape of the sample. The increase in the stiffness could be due to glue compaction or an increase in the contact area between the ceramic and the aluminum infrastructures during the loading cycles. As a result, the stack of elements (infrastructure/glue/superstructure) must be considered to be a laminated composite. The difference between 15 kN/mm and 25 kN/mm (the most extreme distance from the results) corresponds to a difference of approximately 27 µm in the compressive displacement. This value of compaction may correspond to the progressive plasticization of the adhesive during testing and the progressive positioning of the tooth on its support. This phenomenon is intrinsic to the composite effect of our assembly and could explain the similar evolution of the apparent stiffness of the entire series.

5.2.1.3. Efficiency of the CAD/CAM method

The results presented in this study highlight the importance of the CAD/CAM construction and confirm that this method is efficient for creating all types of models to obtain results with a minimum dispersion, which is due to the reduction of operator-dependent steps and the suppression of the material dependence of the conventional prosthetic chain. The infrastructures may be created manually (109), with a milling machine (110) or from a prefabricated standard wax model. The use of CAD has several advantages. First the measurements are very accurate making it possible to create a model with a geometric shape or clinical shape depending on the study. Most importantly, it is possible to individually vary the geometrical parameters to evaluate their effects on mechanical properties. The results exhibit differences because of different geometries. CAM allows for the precise production of as many samples as necessary. Furthermore, the optical imprint used to produce the ceramic cups is devoid of all the inconveniences of the traditional prints (111). An added benefit is that the infrastructures and the sample holders were milled as one unit. Previous studies used natural teeth or a model glued to a metal or resin sample holder as a sample (112, 113) however, the interface and its behavior may have affected the results.

5.2.2. Effect of the three variables

5.2.2.1. Total Occlusal Convergence (TOC)

Goodacre et al noted that the TOC was one of the first aspects of tooth preparations for complete crowns to receive specific numeric recommendations (93). Jorgenson (114) tested the retention of crowns at various TOC angles by applying a tensile force to a cemented crown. Maximal tensile retentive values were recorded at 5° TOC, supporting earlier recommendations of 2 to 5°. In 1994 Wilson and Chan (115) reported that maximal tensile retention occurred between 6 and 12° TOC. Studies by Ohm E et al (116), and other authors (117) reported mean TOC angles that ranged from 12.2 to 27°. Other authors reported that 20° of TOC and chamfer margin could be used for CAD/CAM all-ceramic crown in clinical application (118). However, it is important to note that those values were essentially derived from retention/stabilization problems and not for biomechanical considerations. So, for this study and in reference to the literature, two TOCs were determined for the infrastructures: 7° (series 1, 3, 5 and 6) and 21° (series 2 and 4).

It is interesting to note that in three articles in 1990 Friedlander and Doyle et al describe (119,13,14) the effect of tooth preparation design on the breaking strength of Dicor crowns. They reported that tooth preparation with a 1.2-mm shoulder finish line, sharp axio gingival line angle, and 10° of TOC produced the strongest Dicor crowns. Moreover, three groups of restorations fabricated for preparations with 5° of occlusal convergence were significantly weaker than those made for preparations with 15° of convergence**.** For them a total occlusal convergence angle of 10° provided the best combination of restoration strength and remaining dentin thickness.

The results obtained in our study tend to confirm the hypothesis that a more pronounced convergence results, in a sooner fracture.

According to Table IV and V the weakest series are those of S1 with a TOC of 21°, a rounded occlusal surface and a SA at 45°. This is the most “conical” shape. Series 2 exhibited the second worst result with a TOC of 7° and a global conical shape (45° and 19° SA COF).

The TOC appears to be the factor that decreases the strength of the ceramic. In our study, the TOC decreased the rupture force of the ceramic by 19% (S1/S2) to 40% (S2/S4).

Our explanation of this result is that a high TOC value may favor the “opening” of the ceramic during the application of the load (13), leading to tensile stresses into its internal area**.**

Fracture may start from the inside of the crown and propagate to its outside (120). The weakening induced by tensile stressed areas increased with high TOC angles.

5.2.2.2. Curvature of the Occlusal Face (COF)

The occlusal reduction determines the occlusal ceramic thickness. One essential factor is the available space for the restoration, which requires a certain occlusal thickness (121). In 2001 Sutton and Cord said that 86% of practitioners had been underprepared occlusally (122). Malament and Socransky (6) investigated the effect of ceramic thickness on the strength of all-ceramic crowns but were unable to correlate failure of restorations with thickness when the crowns were bonded to prepared teeth with resinous cement. They found no significant differences in the probability of survival after 11.7 years (3430 cumulative monitoring years) between bonded crowns that were less than 1 mm thick and those greater than 1 mm thick. The midaxial thickness of crowns in this study averaged approximately 1.5 mm. Therefore, if the crown is bonded with resinous cement, the reduction should be based on the ceramic thickness required to achieve desirable color and contour. It is proposed that incisal/occlusal surfaces be reduced 2 mm because that depth permits the development of normal morphology and has been identified as a safe and reasonable amount to remove from teeth. In a cusp-replacing ceramic premolar restoration Chang et al concluded that the reduction of the buccal cusp by at least 1.5 mm could reduce stress (123). For Sornsuwan et al, cusp angle is a key factor that controls the stress generated at the crown fissure (124) and the effects of notch radius on the failure load are still inconclusive due to the relatively complex shape of occlusal surfaces. He proposed that occlusal geometry is an important issue that affects the degree of stress concentration and should be understood by both technician and clinician for appropriate design and material selection for all-ceramic crowns (125).

For this study, 2 mm thickness for ceramic was set for the top of the cup. This reduction was in accordance with the occluso-cervical dimension. The occluso-cervical dimension of mandibular second premolar and first molar measured with periodontal, authors determine whether 4 mm minimal dimension for molars had been satisfied (126,127).

In this study the occlusal face was flat (0°) or rounded (19 or 13°). The aim was to observe the difference with a flat or rounded occlusal surface oriented perpendicularly to the load. For Hmaidouch et al (128), copings with flat occlusal reduction and luting space settings

of 100 µm exhibit a better internal and marginal fit compared with copings with anatomic occlusal reduction and luting space settings of 50 µm, regardless of the cement used. On the other hand Rekow et al stated that geometry profoundly influences the stress concentration and fracture initiation and that the propagation and the magnitude of the stress concentration at the margin is directly related to the amount of variation in axial wall height around the periphery of the crown (129). Thompson and Rekow the thickness of the luting cement and its modulus elasticity is so to take in account (129). In this study the space for the adhesive cement is measured at 100 µm.

There are 4 series with curved occlusal face (S1, S2, S3, S4) and 2 with flat occlusal face (S5, S6). The best results were for S5 and S6.

The two best performances were recorded for infrastructures with a flat occlusal surface (0° COF). This "efficiency" was confirmed by the large difference in results between S2 and S6 (52%) in which only the COF was different. The difference was very low between S5 and S6 highlighting its role in load distribution. For preparations with a flat occlusal face, the loading force is more evenly distributed, lowering contact stress and leading to higher rupture force values. The stress distribution is harmonious and significant and decreases load transfer on axial walls.

In addition, regarding the mechanical behavior, preparations with curved occlusal face must present exactly the same curvature on the inside of the ceramic tooth. If not, stress concentration may occur.

The statistical analysis showed that the factor "COF" is considered to be individually significant ($p = 0.0001$). Furthermore the results showed that the combination with other factors plays a very important role. It therefore seems necessary to not consider the various factors individually, but in combination.

5.2.2.3. Shoulder Angulation (SA)

The finish line is often studied to evaluate the best marginal cervical gap. In some studies it appears that the marginal gaps were greater for the chamfer finish line specimens than in the shoulder finish line specimens. However, the fracture strength of the chamfer finish line specimens was greater than that of the shoulder finish line specimens (130). For Jalalian et al a chamfer margin could improve the biomechanical performance of posterior

single crown alumina restorations (131). For the veneered zirconia crowns the finish line design did not influence the fatigue or the fracture resistance. The selection of any of the finish line designs should be based on the clinical condition of the restored tooth (132).In some studies about monolithic ceramic reconstructions data indicated that occlusal thicknesses in excess of 0.66 mm are the optimal design for ceramic crowns on mandibular first molars from biomechanical point of view (133). Other authors recommended finish line depths for all-ceramic crowns that ranged from 0.5 to 1.0 mm (58, 134). Moreover it has not been advantageous to increase all-ceramic crown finish line depth beyond 1 mm with the use of a semi translucent all-ceramic material. In our study the thickness was always 0.9 mm, and the shoulder angulations' were an important element. Giannetopoulos et al (135) fabricated three brass models prepared with different marginal finish lines: a 0° bevel (or 90° shoulder), a 30° bevel and a 60° bevel. The results of this study indicated that the introduction of a marginal angle of the restoration increased the potential for marginal chipping. The best results were obtained with 0° and the worst with 60°. Furthermore, it was noted that stronger glass ceramic restorations were reported when the shoulder finish line had a sharp axio-gingival line angle, possessed minimal cervical inclination, and was located as close as possible to the same occluso-cervical level on all four axial surfaces (14).

In our study there were two angulation shoulders: 45° and 90°.

Its influence is evident by comparing S1/S3 series and S2/S4. This is less significant for series S5 and S6 because of the role of the COF at 0°. There is only 1% of difference between those two shapes, and the only difference is the SA. However this does not mean that the SA has no influence. Indeed, if we compare S1 and S3 the only difference is the SA and the difference of rupture is 24.8%. If the clausal surface is rounded and/or the walls are more convergent the role of SA appears. SA is an important factor in accommodation of compressive stresses, which are more favorable for the strength of ceramics than oblique shear stresses. A 90° cervical shoulder acts as a "lock" at the opening of the ceramic and increases its tensile strength by 25% (S1/S3) to 40% (S3/S4).

5.2.2.4 Parameter combinations of the three variables

The results and the statistical analysis (p= 0.0002) confirm various mechanical principles and demonstrate the influence of the geometry of the preparation on the material reconstruction. This can be illustrated comparing S2/S4 and S5/S6

Series	S2	S4	S5	S6
				
Rupture difference	40%		0.5%	

Table VIII. Comparison between S2/S4 and S4/5.

For S4/S5 the only difference was the SA and the difference in resistance to rupture was only 0.5%. According to this result it seems that SA has no influence.

For S2/S4 the only difference was the SA and the difference in resistance to rupture was 40%.

The TOC was the same for S2, S4, S5, and S6 but between S2/S4 and S5/S6 the difference was the COF. It is possible to conclude that if the COF was 0° SA had no influence but if the COF was rounded SA have an important influence

If we compare S1/S3 and S2/S4:

Series	S1	S3	S2	S4
				
Rupture difference	19.05%		40%	

Table IX. Comparison between S1/S3 and S2/S4.

For S1/S3 the only difference was the SA and the difference in resistance to rupture was 24.8%. For S2/S4 the only difference was the SA and the difference in resistance to rupture was40%.

Results between groups and within groups were significantly different, highlighting the influence of the combination of TOC with SA. It is thus possible to multiply examples.

The best shape to receive a bonded all-ceramic reconstruction, in agreement with the biomimetic concept seems to be: $7^{TOC}90^{SA}0^{COF}$.

Therefore, it is clear that preparing the tooth geometry should no longer be considered as a trivial act but fulfills precise mechanical requirements, which allow the practitioner to improve its practices on the basis of clinical cases in order to reach optimum results.

6. Conclusions

Several conclusions can be drawn from this study:

1. The strain accommodation capacity of the tooth is derived from the differential displacement between different tissues. The Speckle Interferometry study shows that the enamel tooth cap moves as a rigid body under loading. This adaptability due to the DEJ (Dentin Enamel Junction) should serve as an example for our prosthetic reconstructions. The dentin-enamel junction acts as an interface until a certain maximal loading is achieved. Beyond this threshold, the loading accommodation property disappears, and the entire tooth then behaves as a rigid body. Physiological behavior and the biomechanical comportment of the natural tooth must serve as a model for our prosthetic reconstructions.

2. The results of this study demonstrate a similar behavior for the prosthetic crown and tooth according to biomimetic concepts. In this case, the ceramic crown replaces the enamel cap and the glue (dentin ceramic junction) replaces the dentin-enamel junction. Displacement of the ceramic crown also occurs like a rigid solid; however the amount of movement is different from that of enamel. This is due to the histological irregular structure of the DEJ and that the DCJ is of constant thickness. However these behaviors indicate the interface role of the DEJ and the DCJ in the capacity of enamel and ceramic to adapt the stresses of the physiological functions or even of parafunctions.

3. This study also demonstrates the prime importance of CAD / CAM systems. With these methods it is possible to represent and manufacture serial samples with perfectly well defined dimensions and shapes. It is the first study that used only the CAD / CAM systems to produce reference samples and clones of the references samples. This method allows for relevant comparative studies. The ability to set different thicknesses and volume materials such as ceramic or glue will allow for comparative studies of identical samples with different natures or assembled in different ways. For example, it will be possible to vary the volume of the dento-prosthetic tooth space to evaluate the behavior of a bonded joint according to its thickness or its elastic modulus. This will make possible to determine the optimal characteristics of materials for perfectly prosthetic bio integrated reconstructions.

4. Our results demonstrated that it is still necessary to know the geometric shapes that are most favorable for bonded ceramic crown on all prepared teeth. It is also the first time that we have individualized different geometrical factors that affect the strength of the ceramic, this again thanks to CAD/ CAM. These results show that the three factors TOC, SA and COF, individually exert an influence on the strength of ceramics and more accurately their combination.

5. This study permitted the individualization of some notions that the practitioner must take into account in shaping its clinical action; however this process must be completed. Knowing the role of each element of the preparation and the biomechanical behavior of the tooth, allows the practitioner to make a reasoned act adapted to the clinic and to materials. Complementary shapes (S7: $21^{TOC}45^{SA}0°^{COF}$, S8: $21^{TOC}90^{SA}$ $0°^{COF}$) allow for the refinement of our understanding of the role of each parameter of the tooth preparation. Finite element studies and fatigue tests would provide further insight.

In general, dental preparations should no longer be considered as simple geometric shapes optimizing the "retention-stabilization." They must be understood as architectural constructions favorably distributing load transfers, in line with new materials for reconstruction and fixing bio-mimetic vocation.

Although the behavior of ceramic materials has been widely studied in mechanics, it appears that the liaison agent plays a key role in the accommodation constraints. Its role is part of a developing mechanical field of study which will also be our next line of work and research.

7. Acknowledgements

My first acknowledgements go for Prof.Nagy Katalin, Dean of the Department of Dentistry and Oral Surgery at University of Szeged, and Prof. Zoltan Rakonczay (University of Szeged, Department of Dentistry and Oral Surgery) who accepted that I defend my thesis in the Dental School of Szeged.

Foremost I would like to thank to the two co-directors of my thesis: Dr. Kinga Turzó (University of Szeged, Department of Dentistry and Oral Surgery) for her constant help support, and her wise advices and to Prof. Frederic Cuisinier (Université Montpellier I, UFR Odontologie, EA 4203) for having always supported me, and trusted in my works.

I would like to thank Prof. Csilla Gergely (Université Montpellier II, Laboratoire Charles Coulomb), and Prof. Jacques Margerit (Université Montpellier I, UFR Odontologie, Prosthetic Department) for their support throughout my work.

I am grateful to Pierre Slangen, Stéphane Corn, Patrick Ienny and all the whole team of Mechanics Laboratory of the “Ecole des Mînes d’Alès” for their friendly involvement in my work.

I also thank to my wife Ketsila and my children Anoussone and Guillaume to their patience and their support.

8. References

1.Burke FJ, Qualtrough AJ, Hale RW. The dentin-bonded ceramic crown: an ideal restoration? *Br Dent J*. 1995 Jul 22; 179(2): 58-63.

2.Keough BE, Kay HB, Sager RD, Keen E. Clinical performance of scientifically designed, hot isostatic-pressed (HIP'd) zirconia cores in a bilayered all-ceramic system. *Compend Cont in Educ Dent*. 2011 Jul-Aug; 32(6): 58-68.

3.El-Mowafy O, Brochu JF. Longevity and clinical performance of IPS-Empress ceramic restorations--a literature review. *J Can Dent Assoc*. 2002 Apr; 68(4): 233-7.

4.Anusavice KJ. Recent developments in restorative dental ceramics. *J Am Dent Assoc.* 1993 Feb; 124(2):72-4, 76-8, 80-4.

5.Herrguth M, Wichmann M, Reich S.The aesthetics of all-ceramic veneered and monolithic CAD/CAM crowns. *J Oral Rehabil.* 2005 Oct;32(10):747-52.

6.Malament KA, Socransky SS, Thompson V, RekowD.Survival of glass-ceramic materials and involved clinical risk: variables affecting long-term survival. *Pract Proced Aesthet Dent.* 2003;Suppl:5-11.

7. Höland W, Schweiger M, Watzke R, Peschke A, KappertH.Ceramics as biomaterials for dental restoration.*Expert Rev Med Devices*. 2008 Nov;5(6):729-45.

8.Kelly JR, BenettiP.Ceramic materials in dentistry: historical evolution and current practice.*Aust Dent J.* 2011 Jun;56 Suppl 1:84-96.

9.Kelly JR.Dental ceramics: current thinking and trends. *Dent Clin North Am.* 2004 Apr; 48(2), 513-30.

10.Magne P, Dietschi D, Holz J. Esthetic restorations for posterior teeth: practical and clinical considerations.*Int J Periodontics Restorative Dent.* 1996 Apr; 16(2): 104-19.

11.Heintze SD, Cavalleri A, Zellweger G, Büchler A, Zappini G. Fracture frequency of all-ceramic crowns during dynamic loading in a chewing simulator using different loading and luting protocols.*Dent Mater.* 2008 Oct; 24(10): 1352-61.

12.Friedlander LD, Munoz CA, Goodacre CJ, Doyle MG, Moore BK. The effect of tooth preparation design on the breaking strength of Dicor crowns: Part 1.*Int J Prosthodont*. 1990 Mar-Apr;3(2):159-68.

13.Doyle MG, Munoz CA, Goodacre CJ, Friedlander LD, Moore BK.The effect of tooth preparation design on the breaking strength of Dicor crowns: 2. *Int J Prosthodont.* 1990 May-Jun; 3(3): 241-8.

14.Doyle MG, Goodacre CJ, Munoz CA, Andres CJ.The effect of tooth preparation design on

the breaking strength of Dicor crowns: 3.*Int J Prosthodont.* 1990 Jul-Aug;3(4):327-40.

15.Bernal G, Jones RM, Brown DT, Munoz CA, GoodacreCJ.The effect of finish line form and luting agent on the breaking strength of Dicor crowns. *Int J Prosthodont.* 1993 May-Jun;6(3):286-90.

16.Pallis K, Griggs JA, Woody RD, Guillen GE, Miller AW. Fracture resistance of three all-ceramic restorative systems for posterior applications. *J Prosthet Dent.* 2004 Jun; 91(6): 561-9.

17.Christensen RP, Ploeger BJ. A clinical comparison of zirconia, metal and alumina fixed-prosthesis frameworks veneered with layered or pressed ceramic: a three-year report. *J Am Dent Assoc.* 2010 Nov; 141(11): 1317-29.

18.Guess PC, Zavanelli RA, Silva NR, Bonfante EA, Coelho PG, Thompson VP.Monolithic CAD/CAM lithium disilicate versus veneered Y-TZP crowns: comparison of failure modes and reliability after fatigue. *Int J. Prosthodont.* 2010 Sep-Oct; 23(5): 434-42.

19.Özkurt Z, Kazazoglu E, Ünal A. In vitro evaluation of shear bond strength of veneering ceramics to zirconia. *Dent Mater J*. 2010; 29:138-46.

20.Aboushelib MN, de Jager N, Kleverlaan CJ, Feilzer AJ.Effect of loading method on thefracture mechanics of two layered all-ceramic restorative systems. *Dent Mater*. 2007; 23:952-59.

21.Studart AR, Filser F, Kocher P, Lü thy H, Gauckler LJ. Mechanical and fracture behaviourof veneer-framework composites for all-ceramic dental bridges. *Dent Mater*. 2007; 23:115-23.

22.Taskonak B, Yan J, MecholskyJr JJ, Sertgöz A, Koçak A. Fractographic analyses of zirconia-based fixed partial dentures. *Dent Mater.* 2008; 24:1077-82

23.Aboushelib MN, Kleverlaan CJ, Feilzer AJ. Microtensile bond strength of different components of core veneered all-ceramic restorations. Part II: Zirconia veneering ceramics. *Dent Mater*. 2006; 22:857-63.

24.Aboushelib NM, Kleverlaan CJ, Feilzer AJ. Effect of zirconia type on its bond strength with different veneer ceramics. *J of Prosthodont*. 2008; 17:401-08.

25.Fahmy NZ. Bond strength, microhardness, and core/veneer interface quality of an allceramicsystem. *J of Prosthodont.* 2010; 19:95-102.

26.Zahran M, El-Mowafy O, Tam L, Watson PA, Finer Y.Fracture strength and fatigue resistance of all-ceramic molar crowns manufactured with CAD/CAM technology. *J Prosthodont.* 2008 Jul;17(5):370-7.

27.Baltzer A. All-ceramic single-tooth restorations: choosing the material to match the

preparation-preparing the tooth to match the material. *Int,J Comput Dent.* 2008;11(3-4):241-56.

28.Rekow D, Thompson VP.Engineering long term clinical success of advanced ceramic prostheses. *J Mater Sci Mater Med.* 2007 Jan;18(1):47-56.

29.Rekow ED, Harsono M, Janal M, Thompson VP, Zhang G.Factorial analysis of variables influencing stress in all-ceramic crowns.*Dent Mater.* 2006 Feb;22(2):125-32.

30.Kelly JR Clinically relevant approaches to failure testing of all-ceramic restorations. *J Prosthet Dent.* 1999; 81:652-61.

31.Bieniek KW, Marx R. The mechanical loading capacity of new all-ceramic crown and bridge materials, *Schweiz Monatsschr Zahnmed*. 1994; 104 (3): 284-9.

32.Zaslansky P, Shahar R, Barak MM, Friesem A and Weiner S, Tooth and bone deformation:structure and material properties by ESPI, *Proc. SPIE2006*. vol.6341.

33. Gonzaga CC, Cesar PF, Miranda WG Jr, Yoshimura HN. Slow crack growth and reliability of dental ceramics. *Dent Mater*. 2011 Apr; 27(4):394-406.

34.Imbeni V, Kruzic J.J, Marshall G.W, Marshall S.J. and Ritchie R. O. The dentin–enamel junction and the fracture of human teeth.*Nature Materials.* 2005; 4, 229-232.

35.Anusavice K.J. Mechanical properties of dental materials, In*: Phillips' Science of Dental Materials*,(Ed.), 49-74, W.B. Saunders Company, Tenth Edition, ISBN 0-7216-5741-9, Philadelphia, Pennsylvania, USA

36.Foung H, Sarikaya M, White SN, Snead Ml. Nano mechanical properties profiles across dentin-enamel junction of human incisor teeth. Materials Sciences and Engineering. 2000;119-128.

37.Habelitz S, Marshall SJ, Marshall GW and Balooch M. The functional width of the dentino enamel junction determined by AFM-based nanoscratching. *J. Struct Biol.* 2001; 135:244-301

38.Meyer JM, Bodier-Houlle P., Cuisinier F.J.G, Lesot H. and Ruch J.V. Initial aspects of mineralization at the dentino-enamel junction in embryonic mouse incisor in vivo and in vitro: a TEM comparative study. *In Vitro Cell Dev Biol Anim.* Mar 1999; 35 (3): 159-68.

39.Marshall GW, Balooch M, Gallagher RR, Gansky SA and Marshall SJ. Mechanical properties of the dentin-enamel junction: AFM studies of nano hardness, elastic modulus andfracture. *J Biomed Mater Res.* 2001; 54:87-95.

40.Wang R, Weiner, S. Strain–structure relations in human teeth using Moire fringes. *J.Biomech.* 1998, 31,135–141.

41.Zaslansky P, Friesem AA and Weiner S. Structure and mechanical properties of the soft

zone separating bulk dentin and enamel in crowns of human teeth: insight into tooth function. *JStruct Biol*. 2006 Feb; 153(2): 188-99.

42.Chattah LT, Shahar R and Weiner S. Design strategy of minipig molars using electronic speckle interferometry : comparison of deformation under load between the tooth mandible complex and isolated tooth. *Advanced Materials.* 2009; 21, 413-418.

43.Magne P, Belser U. *Bonded Porcelain Restorations in the Anterior Dentition: A Biomimetic Approach. Quintessence* Publishing Co, Inc 2003.

44.Addison O, Sodhi A and Fleming GJ. Seating load parameters impact on dental ceramic reinforcement conferred by cementation with resin-cements. *Dent Mater.* 2010 Sep; 26(9): 915-21.

45.Attia A, Kern M.Influence of cyclic loading and luting agents on the fracture load of twoall-ceramic crown systems. *J Prosthet Dent*. 2004 Dec; 92(6): 551-6.

46.Guarda GB, Gonçalves LS, Correr AB, Moraes RR, Sinhoreti MA and Correr-Sobrinho L. Luting glass ceramic restorations using self-adhesive resin cement under different dentinconditions. *J Appl Oral Sci*. 2010 Jun; 18(3): 244-8.

47.Anusavice KJ, Kakar K, FerreeN.Which mechanical and physical testing methods are relevant for predicting the clinical performance of ceramic-based dental prostheses? *Clin Oral Implants Res*. 2008 Mar; 19(3): 326-8.

48.Heintze SD, Cavalleri A, Zellweger G, Büchler A, Zappini G. Fracture frequency of all-ceramic crowns during dynamic loading in a chewing simulator using different loading and luting protocols. *Dent Mater*. 2008 Oct; 24(10): 1352-61.

49.Kelly JR.Clinically relevant approach to failure testing of all-ceramic restorations.*J Prosthet Dent*. 1999 Jun; 81(6): 652-61.

50.Kelly JR, Rungruanganunt P, Hunter B, VailatiF.Development of a clinically validated bulk failure test for ceramic crowns.*J Prosthet Dent.* 2010 Oct;104(4):228-38.

51.Donnelly TJ, Burke FJ.In vitro failure of crowns produced by two CAD/CAM systems.Eur *J Prosthodont Restor Dent.* 2011 Sep;19(3):111-6.

52.Miyazaki T, Hotta Y.CAD/CAM systemsavailable for the fabrication of crown and bridge restorations.dental cad cam system. *Aust Dent J.* 2011 Jun;56 Suppl 1:97-106.

53.McLaren EA, Terry DACAD/CAM systems, materials, and clinical guidelines for all-ceramic crowns and fixed partial dentures. *Compend Contin Educ Dent*. 2002 Jul; 23(7):637-41, 644, 646.

54.Burke FJ, Fleming GJ, Nathanson D, Marquis PM.Areadhesive technologies needed to

support ceramics? An assessment of the current evidence. *J Adhes Dent.* 2002 Spring;4(1):7-22.

55.Sutton AF, McCord JF.Variations in tooth preparations for resin-bonded all-ceramic crowns in general dental practice.*Br Dent J.* 2001 Dec 22; 191(12): 677-81.

56.Abdelaziz KM, Freitag S, Kern M ; Fracture load of composite resin and feldspathic all-ceramic CAD/CAM crowns..*J Prosthet Dent.* 2006 Feb; 95(2):Attia117-23A,

57.Borges GA, Caldas D, Taskonak B, Yan J, Sobrinho LC, de Oliveira WJ. Fracture loads of all-ceramic crowns under wet and dry fatigue conditions. *J Prosthodont*. 2009 Dec;18(8):649-55.

58.Schilinburg HT, Hobo S, Whitsett LD, Jacobi R, Brackett SE. *Fundamentals of Fixed Prosthodontics.Quintessence Books. Chicago, 1997; 11-72.*

59.Goodacre CJ, DDS, MSD, aWayne V. Campagni, DMD,band Steven A. Aquilino, DDS.Tooth preparations for complete crowns: An art form based on scientific principles. *The Journal of Prosthetic Dentistry*.Avril 2011. Vol 85 N°4, 363-376

60.Lorenzoni FC, Martins LM, Silva NR, Coelho PG, Guess PC, Bonfante EA, Thompson VP, Bonfante G. Fatigue life and failure modes of crowns systems with a modified framework design. *J Dent.* 2010 Aug; 38(8): 626-34.

61.Mehl A, Ender A, MoremannW,ThAttin : Accuracy testing of a new intra-oral Camera. *Intl J of Comput Dent.* 2009; vol 12, N°1,11-28.

62.Christensen GJ, Child PL Jr. Fixed prosthodontics: time to change the status quo? *Dent Today*. 2011 Sep;30(9):66, 68, 70-3.

63.Schneider W.No compromises the new CEREC MC XL and inLab MC XL milling machines. *Int J Comput Dent*. 2007 Jan;10(1):119-26.

64.Conrad HJ, Seong WJ, PesunIJ.Current ceramic materials and systems with clinical recommendations: a systematic review. *J Prosthet Dent.* 2007 Nov;98(5):389-404.

65.Syrek A, Reich G, Ranftl D, Klein C, Cerny B, BrodesserJClinical evaluation of all-ceramic crowns fabricated from intraoral digital impressions based on the principle of active wavefront sampling. *J Dent.* 2010 Jul;38(7):553-9.

66.Jorgensen KD. The relationship between retention and convergenceangle in cemented veneer crowns. *Acta Odontol Scand.* 1955; 13:35-40.

67.Nuttall EB. Factors influencing success of porcelain jacket restorations. *J Prosthet Dent* 1961; 11:743-8.

68.Shillingburg HT, Hobo S, Whitsett LD. *Fundamental of fixed prosthodontics*. Chicago, IL: Quintessence Publishing Co; 1981. p. 79.

69.Zhang Y, Kim JW, Bhowmick S, Thompson VP, RekowED.Competition of fracture mechanisms in monolithic dental ceramics: flat model systems. *J Biomed Mater Res B Appl Biomater.* 2009 Feb; 88(2): 402-11.

70.Mizrahi B.All-ceramic silica/glass-based crowns--clinical protocols.*Br Dent J.* 2011 Sep 23; 211(6): 257-62.

70.Nanci A, Ten Cate, A.R , Ten Cate's Oral Histology*: Development, Structure, and Function.* Mosby, St. Louis 2003.

71.Spears IR, van Noort R, Crompton RH, Cardew GE, Howard IC. The effects of enamel anisotropy on the distribution of stress in a tooth. *J Dent Res.* 1993 Nov;72(11):1526-31.

72.Habelitz S, Marshall SJ, Marshall GW Jr, Balooch M. Mechanical properties of human dental enamel on the nanometre scale. *Arch Oral Biol*. 2001 Feb;46(2):173-83.

73 .Habelitz S, Marshall SJ, Marshall GW Jr, Balooch M.The functional width of the dentino-enamel junction determined by AFM-based nanoscratching. *J Struct Biol.* 2001 Sep;135(3):294-301.

74.Kinney JH, Balooch M, Marshall SJ, Marshall GW Jr, Weihs TP.Hardness and Young's modulus of human peritubular and intertubular dentine. *Arch Oral Biol.* 1996 Jan; 41(1):9-13.

75.Kinney JH, Marshall SJ, Marshall GW.The mechanical properties of human dentin: a critical review and re-evaluation of the dental literature. *Crit Rev Oral Biol Med.* 2003;14 (1):13-29.

76.Tesch W, Eidelman N, Roschger P, Goldenberg F, Klaushofer K, Fratzl P.
Graded microstructure and mechanical properties of human crown dentin.*Calcif Tissue Int.* 2001 Sep;69(3):147-57.

77.Saffar JL, Lasfargues JJ, Cherruau M.Alveolar bone and the alveolar process: the socket that is never stable. *Periodontol* 2000. 1997 Feb;13:76-90.

78.Ho SP, Marshall SJ, Ryder MI, Marshall GW.The tooth attachment mechanism defined by structure, chemical composition and mechanical properties of collagen fibers in the periodontium.*Biomaterials.* 2007 Dec;28(35):5238-45.

79.Jantarat J, Palamara JE, Messer HH.An investigation of cuspal deformation and delayed recovery after occlusal loading.*J Dent.* 2001 Jul;29(5):363-70.

80.Jantarat J, Panitvisai P, Palamara JE, Messer HH.Comparison of methods for measuring cuspal deformation in teeth. *J Dent.* 2001 Jan;29(1):75-82.

81.Popowics TE, Rensberger JM, Herring SW.Enamel microstructure and microstrain in the fracture of human and pig molar cusps.*Arch Oral Biol.* 2004 Aug;49(8):595-605.

82.Spears IR, Macho GA.Biomechanical behaviour of modern human molars: implications for interpreting the fossil record. *Am J Phys Anthropol.* 1998 Aug;106(4):467-82.

83 Palamara D, Palamara JE, Tyas MJ, Messer HH.Strain patterns in cervical enamel of teeth subjected to occlusal loading. *Dent Mater.* 2000 Nov;16(6):412-9.

84.Palamara JE, Palamara D, Messer HH.Strains in the marginal ridge during occlusal loading.*Aust Dent J.* 2002 Sep;47(3):218-22

85.Wang RZ, Weiner S.Strain-structure relations in human teeth using Moire fringes. *J Biomech.* 1998 Feb;31(2):135-41.

86.Wood JD, Wang R, Weiner S, Pashley DH.Mapping of tooth deformation caused by moisture change using moiré interferometry. *Dent Mater.* 2003 May;19(3):159-66.

87.Kishen A, Tan KB, Asundi A.Digital moiré interferometric investigations on the deformation gradients of enamel and dentine: an insight into non-carious cervical lesions. *J Dent.* 2006 Jan;34(1):12-8.

88.Asundi A, Kishen A..Stress distribution in the dento-alveolar system using digital photoelasticity. *Proc Inst Mech Eng H.* 2000;214(6):659-67.

89.Asundi A, Kishen A.A strain gauge and photoelastic analysis of in vivo strain and in vitro stress distribution in human dental supporting structures. *Arch Oral Biol.* 2000 Jul;45(7):543-50.

90.Asundi A, Kishen A.Advanced digital photoelastic investigations on the tooth-bone interface. *J Biomed Opt.* 2001 Apr;6(2):224-30.

91.Shahar R, Weiner, S, *Journal of Materials Science*. 2007, 42, 8919.

92.Zaslansky P, Currey JD, Friesem AA, Weiner S.Phase shifting speckle interferometry for determination of strain and Young's modulus of mineralized biological materials: a study of tooth dentin compression in water.*J Biomed Opt*. 2005 Mar-Apr;10(2):024020.

93. Goodacre CJ. Designing tooth preparations for optimal success.*Dent Clin North Am*. 2004 Apr; 48(2):v, 359-85.

94.Slangen P, De Veuster C, Renotte Y, Berwart L and Lion Y. “Computer-aided interferometric measurements of drift and phase shifter calibration for DSPI (Digital Speckle Pattern Interferometry)”, *Opt.Eng*. 1995; Vol.34, n°12, pp 3526-3530.

95.Creath, K. Phase-measurement interferometry techniques, *Progress in Optics XXVI, Elsevier Science Publisher B.V*. 1988, Chapt.5, 349-393.

96.Fasbinder DJ, « The Cerec system: 25 years of chairside CAD/CAM Dentistry.*J.Am Dent Assoc.*Jun 2010; 141 Suppl 2: 3S-4S.

97.Kelly JR, Rungruanganunt P, Hunter B, Vailati F.Development of a clinically validated bulk failure test for ceramic crowns.*J Prosthet Dent*. 2010 Oct; 104(4): 228-38.

98.Tylman SD.The dentino-enamel junction. *Journal of dental Research*. 1928; 615-22

99.Craig.R, Peyton F.A. .The micro-hardness of enamel and dentin. *J.Dent.Res.*1958; 37. 661-668.

100.Craig.R., Gehring.P. , et al. Relation of structure to the microhardness of human dentin. *J.Dent.Res*.1959. 38, 624-630.

101.Wood.JD, Wang.R.Z. et al. Mapping of tooth déformation caused by moisture change using Moiré Interferometry. *Dent.Mater*. 2003,19, 159-166.

102.Bechtle S, Fett T, Rizzi G, Habelitz S and Klocke A, Schneider GA.Crack arrest within teeth at the dentinoenamel junction caused by elastic modulus mismatch.*Biomaterials*. 2010 May; 31(14):4238-47.

103.Barak MM, Geiger S, Chattah NLT,Shahar R and Weiner S. Enamel dictates whole tooth déformation : a finite élément model study validated by a metrology method. *Jour of Struct.Biology*.2009; 168, 511-520.

104.Strait DS, Richmond BG, Spencer MA, Ross CF, Dechow PC and Wood BA. Masticatory biomechanics and its relevance to early hominid phylogeny: an examination of palatal thickness using finité-elements analysis. *J Hum Evol.* 2007 May; 52(5): 585-99.

105.Chattah NL,Kupcik K, Shahar R, Hublin JJ and Weiner S. Structure-function relation of primate lower incisor : a study of the déformation of Macaca dentition using electronic speckle pattern interferometry (ESPI). *J.Anat.* 2011; 218 (1): 87-95.

106.Nakamura T, Wakabayashi K, Kinuta S, Nishida H, Miyamae M, Yatani H.Mechanical properties of new self-adhesive resin-based cement. *J Prosthodont Res.* 2010 Apr;54(2):59-64. Epub 2009 Oct 30.

107.Attia A, Abdelaziz KM, Freitag S and Kern M. Fracture load of composite and feldspathic all ceramic CAD/CAM crowns. *J.Prosthet.Dent* Feb 2006. 95(2): 117-123.

108.Attia A, Kern M. Fracture strength of all ceramic crowns luted using two bonding methods.*J.Prosthet Dent.* Mar 2004; 91(3): 247-252.

109.Abdelaziz KM, Freitag S, Kern M ; Fracture load of composite resin and feldspathic all-ceramic CAD/CAM crowns.. *J Prosthet Dent.* 2006 Feb; 95(2): Attia 117-23A,

110. Magne P, Schlichting LH, Maia HP, Baratieri LN.In vitro fatigue resistance of CAD/CAM composite resin and ceramic posterior occlusal veneers. *J Prosthet Dent.* 2010 Sep; 104(3): 149-57

111.Mehl A, Ender A, Moremann W,Th Attin : Accuracy testing of a new intra-oral Camera. *Int J of Comput Dent*. 2009; vol 12, N°1,11-28.

112.Kelly JR, Hunter B, Brenyo MR, et al; Simulating clinicalfailure duringin vitro-testing of all ceramic crowns. *J Dent Res.* 1998; 77 (Special Issue B): 778 (Abstract 1175)

113.Soares PV, Santos-Filho PC, Gomide HA, Araujo CA, Martins LR, Soares CJ.Influence of restorative technique on the biomechanical behavior of endodontically treated maxillary premolars. Part II: strain measurement and stress distribution.*J Prosthet Dent.* 2008 Feb; 99(2): 114-22.

114.Jorgensen KD. The relationship between retention and convergence angle in cemented veneer crowns. *Acta Odontol Scand.* 1955; 13:35-40.

115.Wilson AH Jr, Chan DC. The relationship between preparation convergence and retention of extracoronal retainers. *J Prosthodont.* 1994; 3:74-

116.Ohm E, Silness J. The convergence angle in teeth prepared for artificial crowns. *J Oral Rehabil.* 1978; 5:371-5.

117.Annerstedt AL, Engström U, Hansson A, Jansson T, Karlsson S, Liljihagen H, et al. Axial wall convergence of full veneer crown preparations. Documented for dental students and general practitioners. *Acta Odontol Scand.* 1996; 54:109-12.

118.Zhao YF, Wang HR, Li Y. The effect of tooth preparation design on the CAD/CAM all-ceramic coping crown's fitness.*Zhonghua Kou Qiang Yi Xue Za Zhi.* 2003 Sep; 38(5):330-2.

119. Friedlander LD, Munoz CA, Goodacre CJ, Doyle MG, Moore BK. The effect of tooth preparation design on the breaking strength of Dicor crowns: Part 1.*Int J Prosthodont.* 1990 Mar-Apr; 3(2):159-68.

120.Thompson VP, Rekow DE.Dental ceramics and the molar crown testing ground. *J Appl Oral Sci*. 2004;12(spe):26-36.

121.Baltzer A.All-ceramic single-tooth restorations: choosing the material to match the preparation--preparing the tooth to match the material.*Int J Comput Dent.* 2008; 11(3-4): 241-56.

122.Sutton AF, McCord JF.Variations in tooth preparations for resin-bonded all-ceramic

crowns in general dental practice.*Br Dent J.* 2001 Dec 22; 191(12): 677-81.

123.Chang YH, Lin WH, Kuo WC, Chang CY, Lin CL.Mechanical interactions of cuspal-coverage designs and cement thickness in a cusp-replacing ceramic premolar restoration: a finite element study.*Med Biol Eng Comput.* 2009 Apr; 47(4): 367-74

124.Sornsuwan T, Swain MV.Influence of occlusal geometry on ceramic crown fracture; role of cusp angle and fissure radius.*J Mech Behav Biomed Mater*. 2011 Oct;4(7):1057-66. Epub 2011 Mar 21.

125.Sornsuwan T, Ellakwa A, Swain MV.Occlusal geometrical considerations in all-ceramic pre-molar crown failure testing.*Dent Mater.* 2011 Nov; 27(11): 1127-

126. Maxwell AW, Blank LW, Pelleu GB Jr. Effect of crown preparationheight on the retention and resistance of gold castings. *Gen Dent.*1990; 38:200-2.

127.Weed RM, Baez RJ. A method for determining adequate resistance formof complete cast crown preparations. *J Prosthet Dent.* 1984; 52:330-4.

128.Hmaidouch R, Neumann P, Mueller WD. Influence of preparation form, luting space setting and cement type on the marginal and internal fit of CAD/CAM crown copings. *Int J Comput Dent.* 2011; 14 (3): 219-26.

129.Rekow ED, Zhang G, Thompson V, Kim JW, Coehlo P, Zhang Y.Effects of geometry on fracture initiation and propagation in all-ceramic crowns.*J Biomed Mater Res B Appl Biomater*. 2009 Feb; 88(2): 436-46.

130.Cho L, Choi J, Yi YJ, Park CJEffect of finish line variants on marginal accuracy and fracture strength of ceramic optimized polymer/fiber-reinforced composite crowns. *J Prosthet Dent.* 2004 Jun; 91(6):554-60

131.Jalalian E, Aletaha NS.The effect of two marginal designs (chamfer and shoulder) on the fracture resistance of all ceramic restorations, Inceram: an in vitro study.*J Prosthodont Res.* 2011 Apr; 55(2):121-5. Epub 2010 Oct 23.

132.Aboushelib MN. Fatigue and Fracture Resistance of Zirconia Crowns Prepared with Different Finish Line Designs.*J Prosthodont.* 2011 Oct 31

133.Wang WG, Zhang SF, Chen JJ, Li Y.Selection of optimal occlusal thickness and shoulder thickness in mandibular first molar all-ceramic crown: a three-dimensional finite element analysis.*Zhonghua Kou Qiang Yi Xue Za Zhi.* 2011 Apr; 46 (4): 205-9.

134.Chiche GJ, Pinault A. Esthetics of anterior fixed prosthodontics.Chicago,IL: *Quintessence Publishing Co*. 1994. p. 86, 91, 102-3.

135.Giannetopoulos S, van Noort R, Tsitrou E.Evaluation of the marginal integrity of ceramic copings with different marginal angles using two different CAD/CAM systems. *J Dent.* 2010 Dec; 38(12): 980-6.

Prosthetic Clone and Natural Human Tooth Comparison by Speckle Interferometry

Pierre Slangen [a], Stephane Corn [a], Michel Fages [b], Jacques Raynal [b], Frederic J.G. Cuisinier [b]

[a]ISR, LGEI, Ecole des Mines d'Alès, 6 Avenue de Clavieres F-30319 Ales Cedex France
[b]Université Montpellier Sud de France, EA 4203545 Avenue Prof. Viala, F-34193 Montpellier Cedex5 France

ABSTRACT

New trends in dental prosthodontic interventions tend to preserve the maximum of "body" structure. With the evolution of CAD-CAM techniques, it is now possible to measure "in mouth" the remaining dental tissues. The prosthetic crown is then designed using this shape on which it will be glued on, and also by taking into account the contact surface of the opposite jaw tooth.
Several theories discuss on the glue thickness and formulation, but also on the way to evolve to a more biocompatible crown and also new biomechanical concepts. In order to validate these new concepts and materials, and to study the mechanical properties and mechanical integrity of the prosthesis, high resolution optical measurements of the deformations of the glue and the crown are needed. Samples are two intact premolars extracted for orthodontics reasons. The reference sample has no modifications on the tooth while the second sample tooth is shaped to receive a feldspathic ceramic monoblock crown which will be glued.
This crown was manufactured with a chairside CAD-CAM system from an intra-oral optical print. The software allows to realize a nearly perfect clone of the reference sample. The necessary space for the glue is also entered with ideal values. This duplication process yields to obtain two samples with identical anatomy for further processing. The glue joint thickness can also be modified if required.
The purpose is to compare the behaviour of a natural tooth and its prosthetic clone manufactured with « bio-mechanical » concepts. Vertical cut samples have been used to deal with planar object observation, and also to look "inside" the tooth.
We have developed a complete apparatus enabling the study of the compressive mechanical behaviour of the concerned tooth by speckle interferometry.
Because in plane displacements are of great interest for orthodontic measurements[1], an optical fiber in-plane sensitive interferometer has been designed. The fibers are wrapped around piezoelectric transducers to perform " 4-buckets" phase shifting leading to phase variations during the compression test.
In-plane displacement fields from speckle interferometry already showed very interesting data concerning the mechanical behaviour of teeth : the dentine-enamel junction (DEJ) and the glue junction have been shown including their interfacing function. Mechanical action of the tooth surrounding medium will also be discussed.

Keywords: CAD-CAD clone, speckle interferometry, dentine enamel joint, prosthetic tooth crown

1. INTRODUCTION

New trends in dental prosthodontic interventions tend to reach biomimetic behaviour. Evolutions of CAD-CAM techniques enable to build ceramic prosthetic crowns and, above all, to set the cement joint thickness that links crown and remaining dental tissues. CAD is based on "in-mouth" optical print (i.e. shape on which the clone is glued and contact surface of the opposite jaw tooth). Prosthetic crown is then manufactured, using these parameters, from a feldspathic ceramic rod. In this study, the cloning process gives two samples with identical shape for further use: clone and tooth compression response are measured by speckle interferometry.

2. DESIGN AND GOALS

Several theories[1] discuss the glue thickness and its formulation, acting as a crucial interface that accommodates the different stresses applied to the prosthetic tooth. Moreover this biomechanical analysis tries to reproduce the natural behaviour of the dentine-enamel joint (DEJ). In order to validate these new concepts and materials, and to study the mechanical properties and the mechanical integrity of the prosthesis, high resolution optical measurements of the deformations of glue and crown are required[2]. In our case, samples are two intact premolars extracted for orthodontic reasons from the same patient. The reference sample is preserved while the second sample tooth is shaped to receive a feldspathic ceramic monoblock crown (Vita MarkII, Vita), clone of the reference tooth.

The crown has been made by prosthetic CAD-CAD system from optical prints directly realized in-mouth. The associated software enables the realization of the perfect clone of the tooth. The system is a "dentist" chairside system from Sirona: CEREC 3D.

The best spacing required to realize the glue joint between the crown and the tooth is also computed. In our case 100µm are left between the tooth and the crown and solely 40µm in the cervical junction zone. The copy process yields to two identical samples with the same crown anatomy: the natural tooth and the crown clone realized by CAD-CAM technique.

It is then possible to charge with the same loads two teeth with similar morphology but with different structures (natural and prosthetic) and so to compare their compressive behaviour.

Vertical cuttings have also been used to allow planar object observation, and also to appreciate the differential behaviours "inside" the tooth: the crown-glue-dentine joint for the clone and the DEJ for natural tooth (Fig.1). Recent works also consider the whole natural tooth but do not allow the visualization of the internal parts of the tooth[3]. For this study, a tooth compression test device and an optical fibers in-plane sensitive speckle interferometer have been developed. Samples are white powdered to diffuse laser light.

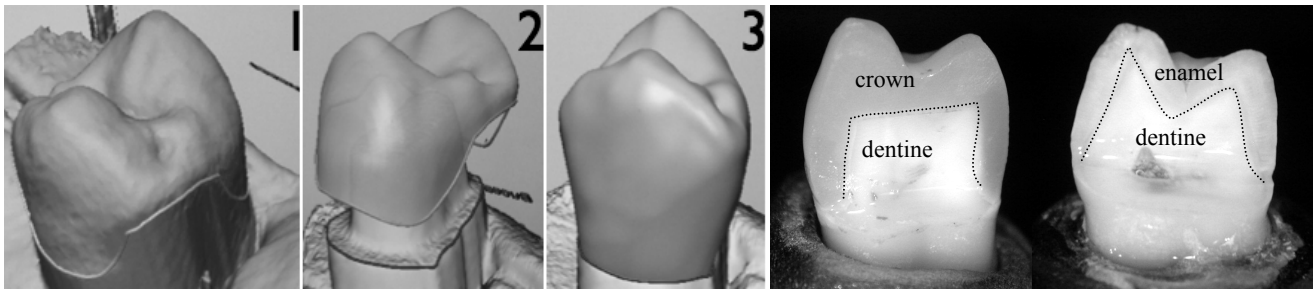

Fig. 1: CAD-CAM Cloning process in copy mode (1 ref optical print, 2 shaping, 3 CAM ready), clone and master cuts

2.1 Mechanical set-up

The mechanical set-up is presented in Fig.2. The compression test device fulfills the high sensitivity of speckle interferometry and also copes with the rigid body motions of the whole system. The sample tooth is placed in a dedicated mold in the lower jaw while the force transducer holder is slowly translated vertically by the stepping motor. The system can generate a „force-driven" displacement, or just a „user" displacement. The whole mechanical system is screwed on the holographic table top. Very small displacement steps, up to 1,6nm can theoretically be achieved.

The force can be applied to the tooth directly with the force transducer or using a relay rod (shorter than shown Fig.2). We can point out that the force is always applied on the same part of the tooth surface for all the samples. This requires some degrees of adjustment to place the lower jaw properly. Samples have got molded jaw or have just been cemented.

The teeth are affixed to the lower jaw from the root by using a dedicated molded base.

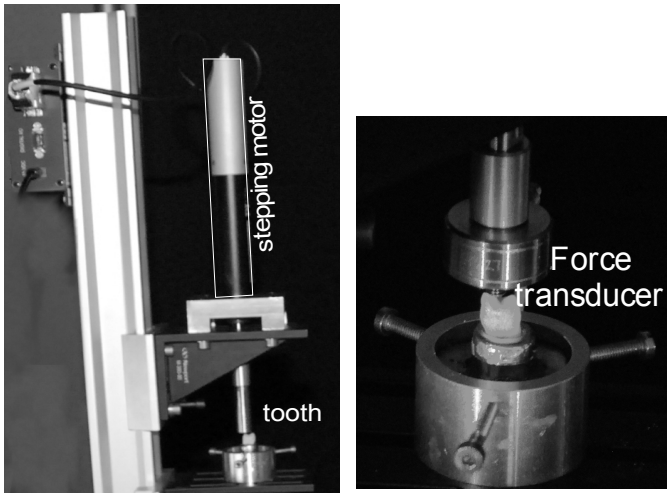

Fig. 2: Compression test mechanical set-up and dedicated molded lower jaw

2.2 Optical set-up

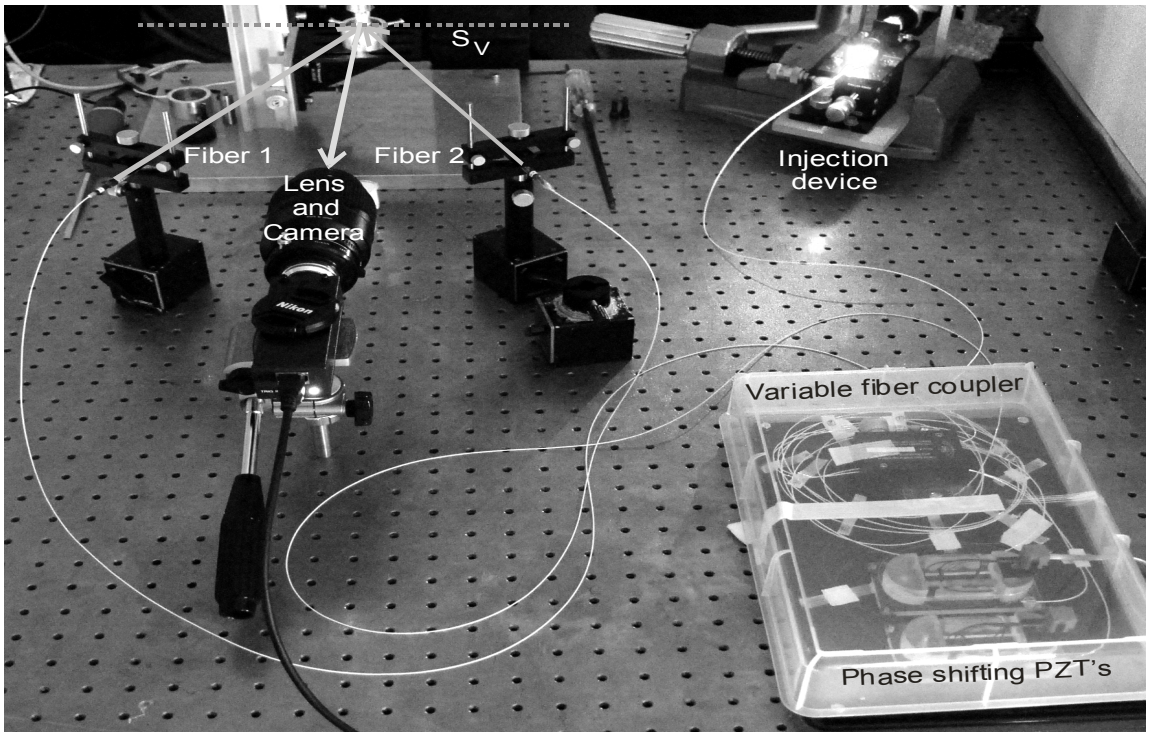

Fig. 3: In plane speckle interferometer, showing observation and illumination beams (full), sensitivity vector S_V (dashed), variable fiber coupler, phase shifting and injection devices.

The optical set-up is presented in Fig.3. This COTS system (Canadian Instruments) offers injection, variable intensity coupling in the output fibers, and also phase shifting. There is two input fibres, one for injection and one for detection of the reflected signal at the output interfaces. Parts of the output fibers are bared and wrapped around piezoelectric transducers. The phase shift is applied on any or both of the two output fibers. The system is protected from thermal and mechanical effects by a plastic box and is easily breadboard able. Phase shifts have been calibrated using common procedures[4].

The results of calibration for the two piezoelectric transducers *da1* and *da2* are presented in table 1. It is also possible to calibrate the system using the back reflections on the output fibres, producing fringes at the exit of the second input fibre (Table 2) and detected by a pin diode.

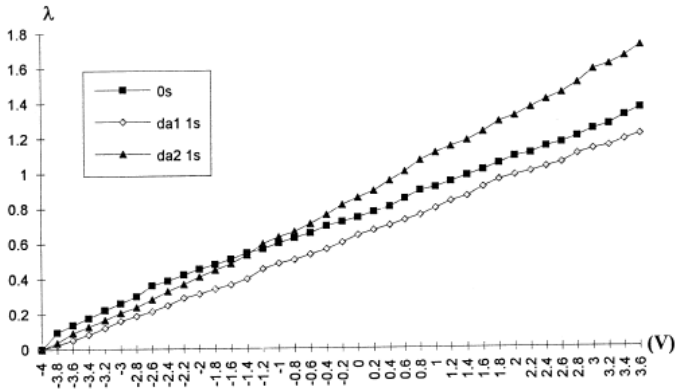

Table 1: Calibration curves of the PZT

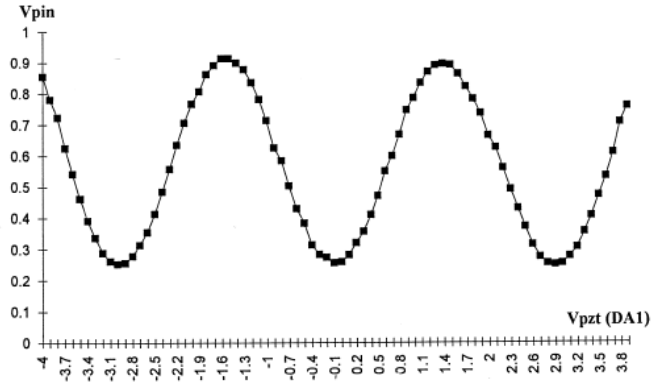

Table 2: Back reflected Intensity modulation

Because in-plane displacements are of great interest for orthodontic measurements, an optical fibers in-plane sensitive interferometer has been designed. The sensitivity vector, S_v, is showed at figure 3. Horizontal sensitivity is achieved. A "4-buckets" phase shifting algorithm[5] leads to phase variations during the compression test. The compression test consists of firstly increase the load until the whole set-up is well in place at about 120N. Then the force is decreased to the minimum contact and is finally slightly enhanced to generate live fringe maps. This is allowed thanks to the small increments of the step motor. Live fringes are displayed between a reference state and the current load state. Between minimal and maximal loading, different phase maps are recorded and stored in memory. Moreover the reference state is also refreshed as for some load steps the number of fringes can be very high and so the noise is too important to lead to good interpretation of the resulting fringes.

3. RESULTS AND DISCUSSION

First results have been obtained with samples cemented with araldite and for different loads (Fig.4). In-plane displacement fields from speckle interferometry already showed interesting data concerning the mechanical behaviour of the different tooth parts. The particular behaviour of the interface joining them histologically is very important for dental aspects.

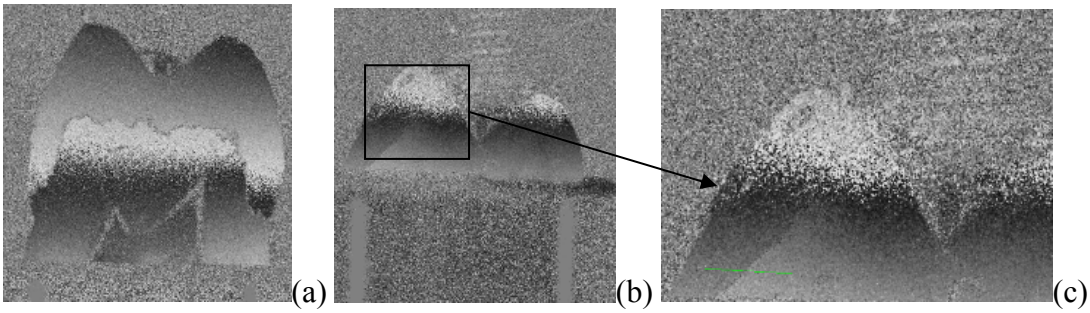

Fig. 4: Clone (a) and natural tooth (b) in-plane displacements, and (c) DEJ detection zoom

As the stabilization ramp has been applied, this shows off the samples have to be molded in the lower jaw by bulking it into chromium-cobalt mold obtained from lost wax technique. This ensures to cancel the effects of the glue between the tooth root and the lower jaw.

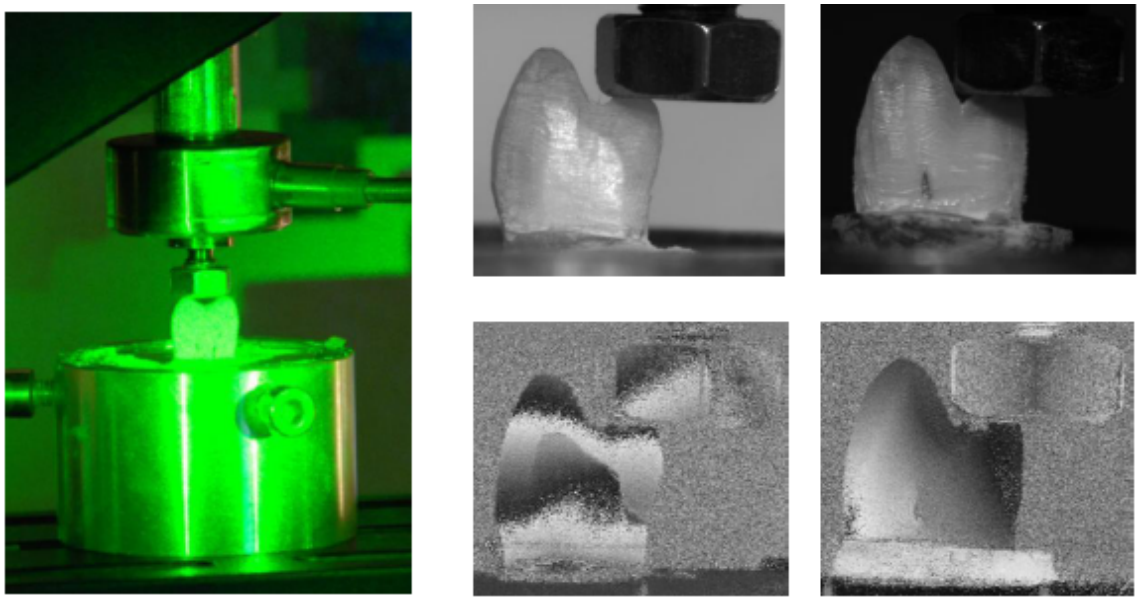
Fig. 5: Laser and white light images (before powdering) and PSDSPI fringes (left, clone; right, natural tooth)

With the new molds, and so avoiding the surrounding glue effect, the realized tests clearly show the enamel crown part is moving differently from the dentine (Fig.5). This difference is clearly delimited by a curve perfectly fitting the dentine-enamel junction (DEJ), as showed on the white light pictures. For the ceramic crown clone, the same kind of shift occurs at the cement junction between the ceramic crown and the dentine[6].

The loading range applied to the different samples is between 5 N and 120 N. Clone crown and natural tooth showed differential displacements: about 60nm for DEJ and about 100nm for the glue joint at the applied loads (20N and 40N). Each sample behaves as single solid beyond 120N.

Around 200N some samples have been destroyed due to fragile brittle fracture. This has been confirmed by compression test performed on different testing machine. We used high speed imaging to record this behaviour and also to reach the compression limits of the glue used to fix the samples on the lower jaw.

These measurements show that the natural enamel crown moves independently from dentine. This difference is clearly delimited by a line corresponding to the anatomical location of the dentine-enamel junction (DEJ). For the ceramic clone the same kind of shift occurs at the glue junction of the ceramic crown with the dentine[6].

Quantitative displacements along the sensitivity vector in the X direction are represented in figure 6. The results are presenting two different cases of load. Profiles have been investigated at locations showing differential behaviours. The displacement step is about 50 to 80nm for the presented samples. This strengthens the DEJ action as a critical zone

accommodating the deformation between dentine and enamel. For the clone, the same behaviour and accommodation effect also occurs but for the glue space between the crown clone and the dentine.

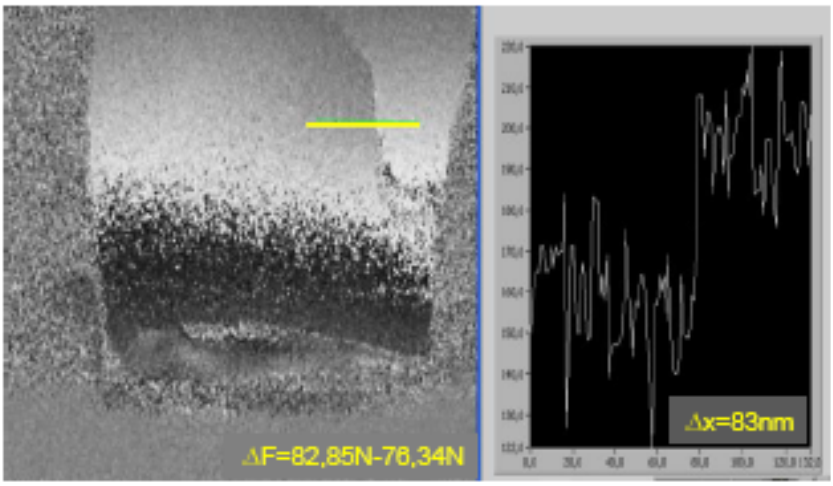

Fig. 6: Displacement map and profile for the clone tooth

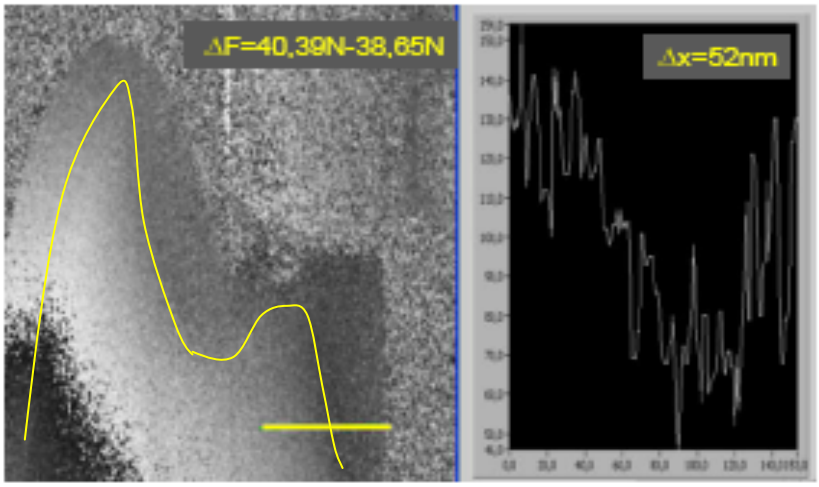

Fig. 7: Displacement map and profile for the natural tooth

4. CONCLUSION

This paper deals with the application of phase shifting speckle interferometry to mechanical compression test of tooth. Samples have been realized through CAD-CAM shape duplication to get identical samples. The displacement maps obtained for different loads have shown differential behaviour zones in the X direction. For the natural tooth it is located in the dentine enamel junction whereas for the ceramic crown clone it is located in the cement junction. Both samples present differential displacement of about 50 to 80 nm for loads around 70N.

The results are really interesting for people from dental research and provide a new way of investigation and of qualification in ceramic crown development.

In further processing, optical displacements will be compared to finite elements analyses of the tooth. Mechanical sensitivity of the tooth surrounding medium will also be examined.

A full 3D measurement will also be done by changing the interferometer sensitivity vectors during the test.

REFERENCES

[1] Xu, H H, Smith, D T, Jahanmir, S, Romberg, E, Kelly, J R, Thompson, V P, Rekow, E D, "Indentation damage and mechanical properties of human enamel and dentin", J.Dent.Res., **77**,3:472-480, (Mar 1998)

[2] Zaslansky, P, Shahar, P, Barak, M M, Friesem, A A, Weiner, S, "Tooth and bone deformation: structure and material properties by ESPI", Proc. SPIE, **6341**:6341091-6341096, (2006)

[3] Barak, M.M. et al., "Enamel dictates whole tooth deformation: A finite element model study validated by a metrology method", J. Struct. Biol., 2009, in press

[4] Slangen, P, De Veuster, C, Renotte, Y, Berwart, L, Lion, Y, "Computer-aided interferometric measurements of drift and phase shifter calibration for DSPI (Digital Speckle Pattern Interferometry)", Opt.Eng., **34**,12:3526-3530, (1995)

[5] Creath, K, Phase-measurement interferometry techniques, Progress in Optics XXVI, Elsevier Science Publisher B.V., Chapt.5, 349-393, (1988)

[6] Fages, M, Cloitre, T, Slangen, P, Corn, S, Cuisinier, F J G, "Speckle Interferometry of Natural and ceramic crown under loading", Joint Meeting IADR, Barcelona, July 2010

DENTAL MATERIALS XXX (2012) XXX–XXX

Available online at www.sciencedirect.com

SciVerse ScienceDirect

journal homepage: www.intl.elsevierhealth.com/journals/dema

Confocal Raman microscopic analysis of the zirconia/feldspathic ceramic interface

Jean-Cédric Durand, Bruno Jacquot, Hamideh Salehi, Michel Fages, Jacques Margerit, Frédéric J.G. Cuisinier*

Laboratoire de BIOlogie santé et NANOscience, EA 4203, UFR d'Odontologie, Université Montpellier 1, Montpellier, France

ARTICLE INFO

Article history:
Received 7 July 2011
Received in revised form
11 December 2011
Accepted 29 February 2012
Available online xxx

Keywords:
Confocal Raman microscopy
Interface
Zirconia
Y-TZP
Veneering ceramic

ABSTRACT

Objectives. Esthetic demands and biocompatibility have prompted the development of all-ceramic dental crowns. Yttria tetragonal zirconia polycrystalline (Y-TZP) framework material has the best mechanical properties compared to other all-ceramic systems, but the interface is the weakest component of core veneered restorations. Confocal Raman microscopy possibilities are used to ensure the understanding of the zirconia-feldspathic ceramic relationship, which is not well known.

Methods. Bilayered zirconia (Vita In-Ceram® YZ) veneer (Vita VM®9) blocks were manufactured. Raman analyses were performed using two protocols: (1) single spectra, line scans and images on a sectioned and polished specimen and (2) in depth line scans on unprepared specimen. Single spectra, images and line scans provide information about the crystalline phases, their distribution and the existence of a possible diffusion at the Y-TZP/VM®9 interface, respectively. The elemental distribution of zirconium (Zr) and silicon (Si) around this interface were investigated using energy dispersive X-ray spectroscopy (EDS).

Results. Raman single spectra embodied a unique spectrum (crystalline) on Y-TZP and two spectra (crystalline and amorphous) on VM®9; these spectra were clearly distinguished. Raman line scans showed a series of transition spectra across the interface from VM®9 to Y-TZP. It emphasized an interdiffusion zone, which was estimated at a maximum of 2 microns, found on 2d Raman images and confirmed by EDS. The elemental distribution with EDS showed a mutual diffusion of Zr and Si and was mainly dominated by Si diffusion in Y-TZP.

Significance. Confocal Raman microscopy highlights an interdiffusion zone at the zirconia-feldspathic ceramic interface. The elemental transition layer is estimated and is supported by EDS analysis as a coupling technique.

1. Introduction

The alloys of zirconium dioxide (ZrO_2) have become one of the essential materials in both industrial and medical fields over the last 40 years because of their low thermal diffusion and excellent mechanical and biological properties [1]. Improvements of its properties, such as the stabilization of the tetragonal phase at room temperature [2], combined with computer-aided design/manufacturing (CAD/CAM)

* *Corresponding author at:* Laboratoire BioNano, EA 4203, UFR d'Odontologie, Université Montpellier 1, 545 Av du Pr. J-L Viala, 34193 Montpellier Cedex 5, France. Tel.: +33 4 117 59 225; fax: +33 4 117 59 201.
E-mail address: jean-cedric.durand@wanadoo.fr (J.-C. Durand).
URL: http://www.univ-montp1.fr/recherche/unites_de_recherche/laboratoire_de_biologie_sante_et_nanoscience (J.-C. Durand).

0109-5641/$ – see front matter © 2012 Academy of Dental Materials. Published by Elsevier Ltd. All rights reserved.
doi:10.1016/j.dental.2012.02.013

technology, have made zirconia an alternative to traditionally used metal substructures for prosthetic dentistry. The rising interests in esthetics and questionable biocompatibility of competitive restorative systems have accelerated development of zirconia-based restorations [3].

Despite the high stability of the zirconia framework, the long-term success of these restorative materials is determined by the veneering process. The in vivo fracture rate of layering ceramic is 15% after 24 months, 25% after 31 months [3,4] and 8% after 36 months [3]. Yet, no fractures of the zirconia core have been reported. Failure in the layering ceramic is in the form of cone cracking either cohesively within the veneering ceramic (chipping) or adhesively at the core veneer interface (delamination) [4–7]. The location of the interface as a failure origin has been reported previously [8], which suggests that the bond strength between the veneering ceramic and the zirconia framework is a weak point in layered all-ceramic restorations [9,10]. That is none of the zirconia core and veneering ceramics attained the high bond strength values of the metal ceramic combination [3].

The causes of fracture of veneering ceramic are multifactorial, both clinically and technically. Clinically, inadequate framework design with respect to a lack of tooth preparation or inadequate margin taper and volume seems to be decisive issues [3,11]. Technically, the zirconia-veneer bond strength depends on the materials that are used [9]. Well-known factors, such as the surface finish of the core (toughness and roughness) can affect the mechanical retention of layering ceramic. Undesired tensile stress that is generated by a mismatch in the thermal expansion coefficient (TEC) or volumetric shrinkage of the veneer after firing [10,12] and its wetting properties over the core [12], have been reported. Impurities content, grain size, density, and temperature lead to the transformation of the tetragonal into the monoclinic phase of the zirconia core [13] during various manufacturing methods [1,13].

The usual methods for assessment of the interface between layering ceramic and core material are shear bond strength or microtensile bond strength testing [4,8,9,12]. These methods are usually coupled with scanning electron microscopy (SEM) to identify the kind of failure (cohesive or interfacial) or to understand its mechanism [5,7,12,14]. Morphological information is also obtained using optical interferometry (OI) and atomic force microscopy (AFM) [1,15]. Energy dispersive X-ray spectroscopy (EDS) [8] provides elemental composition, and X-ray diffraction (XRD) [15–17] or infrared spectroscopy (IR) [17] measures phase fractions quantitatively. However, each of these techniques has advantages and limitations [1,15]. SEM, even if it can observe the impact of laboratory procedures (temperature factor, humidity) [13] or aging of yttria-stabilized tetragonal zirconia phase (Y-TZP) surface grain pull out [1], cannot detect the first stages of aging and suffers from poor depth resolution [1,16]. The dynamic and mechanism of zirconia transformation evaluated by traditional XRD [17–19] suffers from accuracy during the early stages of the aging process [1] because of the absence of local information [1,20]. This analysis is also limited to the first hundredth of a micron below the surface [15]. AFM is a unique and extremely powerful tool for the investigation of martensitic transformation in zirconia because of its unique lateral and depth resolution and the possible observation of bulk samples [21]. AFM can provide valuable insights on the nucleation and growth processes during the very first stages of zirconia aging, but it remains a surface analysis [1,15].

The effects of sample preparation on material properties must be taken into account. For example, sectioning may change surface observations by inducing microcrack zones that can lead to extensive grain pull out [1], which interferes with measurements [15]. To provide a wide range of material characterization the coupling of experimental techniques is required, such as SEM evaluation with XRD [16,18], OI with XRD [17] or OI with AFM [1].

In 1977, Ishigame, who studied the different phases of zirconia, indicated that Raman scattering is useful for investigation of phase transformation, because the technique reflects the dynamic properties that are associated with the change in crystal structure [22]. Raman spectroscopy is a nondestructive, “non-radiating” analysis technique [23] that allows for collection of quantitative and qualitative information. This technique is based on detection of inelastically scattered photons through the interaction of the sample with monochromatic light. The frequency difference between incident photon and the scattered photon provide information on the chemical nature of the molecule or crystal geometry, responsible for the diffusion. Atomic motions in molecules and crystals are organized into vibrational modes. In crystals these modes are called phonons. Phonon is a quantum-mechanical description of a special type of vibrational motion, in which a lattice uniformly oscillates at the same frequency [24]. Raman spectroscopy helps identify and distinguish the different crystalline phases of zirconia or feldspathic ceramic [23,25,26], on very small and specific sample surface areas [20,26,27], providing enhanced spatial resolution [26–28]. Using Raman spectroscopy, it is possible to determine the chemical nature of a species, to study the distribution of a component (profile), or to determine its degree of crystallinity without any sample preparation. The method allows for monitoring of zirconia phase transformation [20,22,23,28–30] and represents an alternative method for quantification of zirconia transformation [15,26,27,30,31]. Raman spectroscopy has also been used to model the surfaces of silicate or aluminosilicate glasses [28,32,33] as well as in their depth [15,32]. Using a piezo motor XYZ microscope stage, the Raman imaging mode allows for visualization of the distribution and concentration of various compounds (Raman mapping 2 or 3D) [26,28].

The purpose of the present work was to utilize confocal Raman microscopy (CRM) to examine the interface between zirconia and a feldspathic ceramic, an area that is not well known. The allocation of crystalline or amorphous phases was estimated around the zirconia core-veneering ceramic interface. As a coupling technique, the elemental distribution around this interface was estimated using energy dispersive X-ray spectroscopy (EDS).

2. Materials and methods

2.1. *Sample preparation*

The exact procedure for specimen fabrication recommended by the manufacturers was followed. Yttria partially

Please cite this article in press as: Durand J-C, et al. Confocal Raman microscopic analysis of the zirconia/feldspathic ceramic interface. Dent Mater (2012), doi:10.1016/j.dental.2012.02.013

Table 1 – Sintering procedures for the feldspathic ceramic (VM®9) according VITA (VITA Zahnfabrik, Germany) [34].

	Start temp. (°C)	Hold for (min)	Heating time (min)	Rate increase (°C/min)	Approx. temp. (°C)	Hold for (min)	Long-term cooling (°C)	Vacuum holding time (min)
Washbake firing	500	2.00	8.11	55	950	1.00	–	8.11
1st dentin firing	500	6.00	7.27	55	910	1.00	600	7.27

stabilized tetragonal zirconia polycrystalline ceramic (Y-TZP, VITA In-Ceram® YZ, VITA Zahnfabrik, Germany) was used as the framework material. Porously pre-sintered Y-TZP cube blanks suitable for CAD/CAM machines were milled (Cerec® InLab Sirona, Germany) to obtain two blocks (12 mm × 7 mm × 1.5 mm) and were then sintered in a furnace (Vita ZYrcomat, VITA Zahnfabrik, Germany) at a 1530 °C for 2 h. A feldspathic veneering ceramic (VITA VM®9, color shade 3M3) was mixed with a modeling liquid (VITA VM® Modeling Liquid) and was built-up on the zirconia surface. A wash-dentin firing procedure was used for the first stage of ceramic build-up (washbake firing). This stage involves firing of a thin aqueous mixture layer (approximately 50 μm thick) of veneering ceramic to 950 °C [34]. Technical information, such as preheating or temperature rise, is given in Table 1. A furnace was used for baking the layering ceramic (VITA Vacumat® 4000 T, VITA Zahnfabrik, Germany). The second step in layering application was placement of a thicker layer (approximately 2-mm thick) of veneering ceramic that was sintered to 910 °C [34] (1st dentin firing, Table 1). Block No. 1 received only the washbake firing and was preserved in that state. Block No. 2 received two layers of ceramic build-up. To enable an expanded view of the interface, block No. 2 was sectioned perpendicular to the interface using a water-cooled diamond saw (600 μm) (ISOMET® 2000 Precision Saw, Bueher, Germany) and polished (ESCIL manuelle, Chassieu, France) to remove external irregular scratches and defects. The polishing protocol was as follows: pre-polishing with abrasive papers of decreasing grain size (120, 320, 800, and 1200); polishing with a succession of pen discs (FD3, FD1 and FD1N, chronologically. ESCIL, Chassieu, France) that were used with diamond suspensions to 6, 1, and 1/4 μm, respectively; terminal polishing using colloidal silica (POM8. ESCIL, Chassieu, France). The polished specimen was cleaned by soaking in ethanol at 95°. The powdered form of the feldspathic ceramic (VM®9) was also analyzed.

2.2. *Confocal Raman microscopy (CRM)*

A confocal Raman microscope was used (WITec® Alpha 300R, Ulm, Germany), which was composed of a laser source (Nd:YAG 532 nm and 40 mW power), a 20× or 100× objective depending on the experiment (which focused the incident laser spot on the sample surface, then directed the scattered photons to the spectrometer), a rejection filter (holographic «notch» used to separate the signal of interest of the Rayleigh signal), and a monochromator (pinhole to spatially locate the light). A prismatic mirror directed the photons on a holographic grating of 600 grooves/mm (BLZ 500 nm to disperse them according to their wavelength) and a 1024 × 127 CCD multichannel detector that simultaneously collected spatial and spectral information about the sample. The laser spot diameter or lateral resolution (LR), which was improved for confocal study [35], was defined by the relation

$$LR_C = \frac{0.61\lambda}{NA}$$

where λ is the wavelength of the incident radiation and NA is the numerical aperture of the lens. Therefore, with a 100× objective and an NA = 0.9, spatial resolution was approximately 360 nm. The pinhole (50-μm in diameter) acted as a spatial filter to reduce the volume that was analyzed. The depth of field was reduced to ~1 μm at the surface. The depth resolution (DR) is given by Eq. (1) [35], where n is the refractive index of the immersion medium, λ is the laser wavelength, NA is the numerical aperture of the focusing lens, and Δ denotes the so-called nominal depth (distance below the surface).

$$DR = \Delta\left\{\sqrt{\left[\frac{NA^2(n^2-1)}{1-NA^2}+n^2\right]}-n\right\} \quad (1)$$

Reference spectra were acquired on the Y-TZP sintered core and the pre-sintered or sintered veneering ceramic. These unique spectra are represented by averaging ten individual spectra, each achieved with a constant integration time of 1s/spectrum.

A line scan (100× objective) was recorded on the sectioned specimen (No. 2) that perpendicularly crossed the interface from the feldspathic ceramic to Y-TZP. The line scan mode enabled recording of a single spectrum at a predetermined spacing in microns. Subsequently spectra at a depth up to 100 μm (100× objective) was performed on specimen No. 1. That analysis involved acquisition of unique spectra from the surface (washbake firing) toward the core. Spectral analysis was based on the identification of characteristic wavelengths for each component (position and line intensity, full width at half maximum (FWHM)) after spectral deconvolution using a mixed Gaussian–Lorentzian distribution through processing software curves (PeakFit® V4.12, Systat Software, Inc.).

An area of interest, 43 μm × 31 μm on both sides of the interface of specimen No. 2 was selected. Images (150 points per line, 150 lines per image) were recorded with a 0.06 s integration time using a 20× objective. For the basis analysis function (WITec® Project 2.04, Ulm, Germany), selection of the characteristic bands of a given element was established from the first image based on the variation of the intensity of selected bands by integrating the area under the peaks. The second image was reconstructed using the K-Means Cluster Analysis function (WITec® Project 2.04, Ulm, Germany) which allows a cluster analysis of the spectral data set resulting in average spectra, and images indicating the regions where the recorded spectra were allocated to the corresponding cluster [36].

Please cite this article in press as: Durand J-C, et al. Confocal Raman microscopic analysis of the zirconia/feldspathic ceramic interface. Dent Mater (2012), doi:10.1016/j.dental.2012.02.013

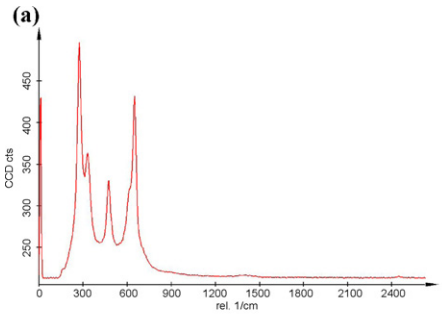

(b)

Frequency (cm^{-1})					Symmetry
Present Study	Values from Literature				
	3Y-TZP [39]	3Y-TZP [30]	3Y-TZP [15]	Pure t-ZrO_2 [38]	
163.2	146	148	142	149	B_{1g}
273.5	260	261	256	269	E_g
331.2	325	320	320	319	B_{1g}
473.3	473	466	466	461	E_g
610.6	613	609		602	A_{1g}
648	641	641	637	648	E_g

Fig. 1 – Raman spectra of sintered Y-TZP (a). Frequency (cm^{-1}) and symmetry of Raman peaks (b). Some experimental Raman literature data of the tetragonal phase on pure zirconia (Pure t-ZrO_2) or partially stabilized zirconia with 3 mol% yttria (3Y-TZP), are listed in Table (b).

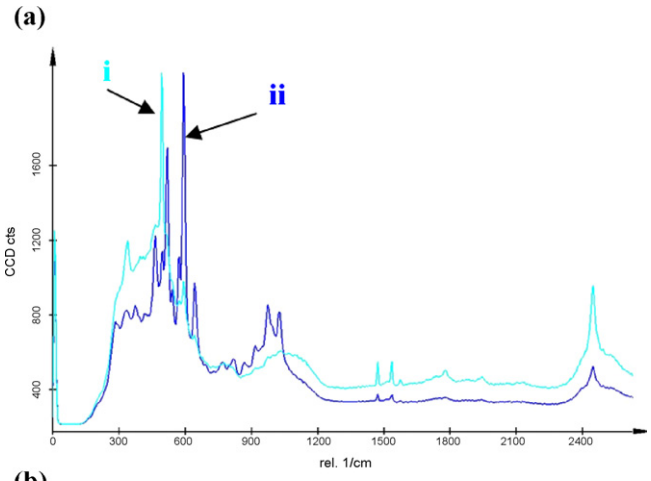

(b)

Raman active modes (cm^{-1}) of VM®9		
	Spectrum i	**Spectrum ii**
Region 300-700	338,396,**495**,589	464,**517**,**592**,645
Region 950-1050	1 broad peak	2 symmetrical peaks 975-1028
Region 1450-1550	2 peaks 1470-1537	2 peaks 1467-1535
Peak > 2400	2447	2446

Fig. 2 – Two main Raman spectra (spectrum i and ii) of feldspathic ceramic (VM®9) (a) and the assignment of wavenumbers (b). Spectrum i identifies a phase close to the glass matrix, and spectrum ii a more crystalline phase. Bold values in Table (b) represent the peaks of highest intensity.

2.3. *Energy dispersive X-ray spectroscopy (EDS)*

Using the same methodology, the elemental composition was performed on the two components, and a line scan was performed of both sides of the interface of specimen No. 2. Analysis of the powdered form of VM®9 was also analyzed (as delivered to the dental laboratory). The line scan was performed over a 10-μm distance with analysis points every micrometers. EDS microanalysis was performed (S-4500 I SEM, Hitachi High Technologies America, Inc., Schaumburg, USA) under the following conditions: high vacuum, 15 kV energy range, and specimens coated with platinum. The lateral resolution was estimated at 1-μm.

3. Results

3.1. *Confocal Raman microscopy: single spectra*

The zirconia core: Fig. 1a shows the Raman active mode of Y-TZP sintered. Crystal phonons were located in a spectral region between 150 and 750 cm^{-1}, according to the data found in the literature of tetragonal phase on pure or partially stabilized zirconia with 3 mol% Y_2O_3 (Fig. 1b). Strong peaks were found at 273, 331, 473 and 648 cm^{-1} with additional weak features at 163 and 610 cm^{-1}. These Raman frequencies of vibration correspond to the six Raman active zone center modes (symmetries) of tetragonal zirconia: $A_{1g} + 2B_{1g} + 3Eg$ (Fig. 1b). Compared to the pure ZrO_2 tetragonal structure, all peaks, except at 648 cm^{-1}, showed a shift toward longer wavelengths from 4 to 14 cm^{-1} (Fig. 1b).

Spectra of the feldspathic veneering ceramic (spectrum i and ii of Fig. 2a) demonstrated the two main Raman active modes. Both spectra showed broadly similar curve, which was characterized by a region of high intensity between ~300 and 700 cm^{-1}, a region more or less sharp between ~900 and 1000 cm^{-1}, and consistent peaks at ~1450, 1550 and 2450 cm^{-1}. The region from 300 to 700 cm^{-1} was the focus of the majority of strong peaks. In the spectrum i, high intensity peaks were centered at 338, 396, 495 and 589 cm^{-1} (Fig. 2b). In the spectrum ii, the vibrations were more numerous and localized. High intensity peaks were centered at 464, 517, 592 and 645 cm^{-1} (Fig. 2b). The area near 1000 cm^{-1} showed a broad band in spectrum i rather than two distinct peaks at 975 and 1030 cm^{-1} in spectrum ii.

3.2. *Confocal Raman microscopy: line scans*

Fig. 3a displays line scans across the interface between zirconia and feldspathic ceramic in specimen No. 2. The unique spectra were acquired every micrometer. As the optical interface was approached, the peak intensity attributed to feldspathic ceramic gradually decreased and correlated with an increase in peaks characteristic of Y-TZP. Therefore, the interface was isolated on three successive spectra as the main peaks of the two materials point this out in the figure. The Raman spectra of the VM®9 were similar to the spectrum i in

Please cite this article in press as: Durand J-C, et al. Confocal Raman microscopic analysis of the zirconia/feldspathic ceramic interface. Dent Mater (2012), doi:10.1016/j.dental.2012.02.013

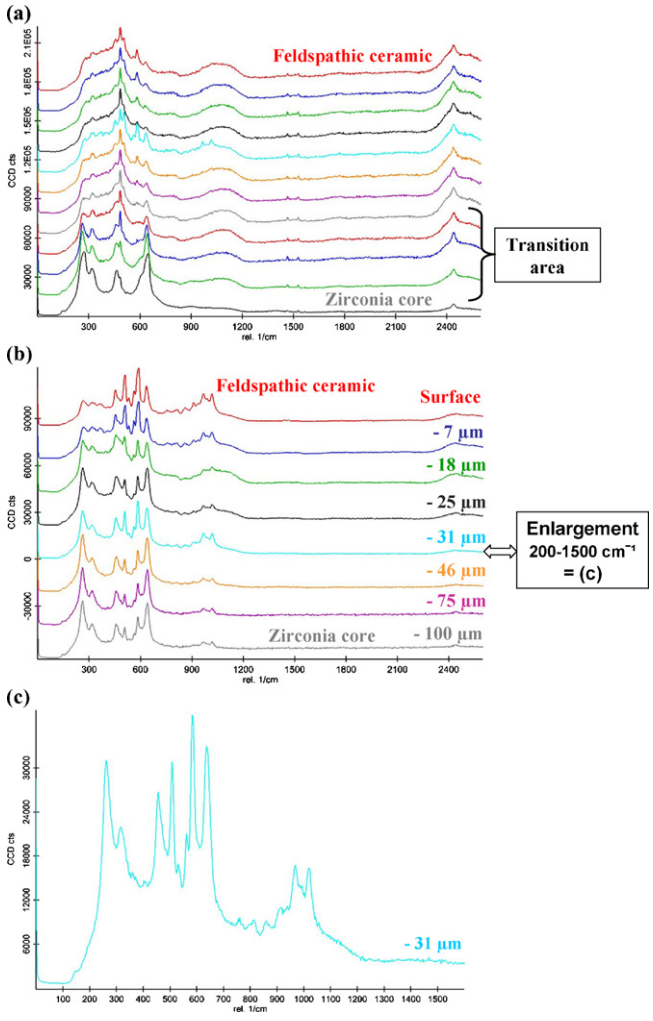

Fig. 3 – Raman line scans of the sectioned specimen (a) and in depth of thin-washed, unsectioned specimen (b). (c) represents an enlargement of the 31-µm deep spectrum (from 200 to 1500 cm^{-1}), identifying the main peaks of VM®9 and Y-TZP.

Fig. 2a, with a dominant and symmetric peak at 495 cm^{-1} and a broad band that was centered around 1000 cm^{-1}.

Fig. 3b and c shows the results of spectral depth profiling up to 100-µm deep on specimen No. 1, which only had a thin feldspathic ceramic layer applied (washbake firing). Despite its small thickness, the surface was irregular. So, of the 100 unique spectra that were recorded at every 1 µm of depth, only 8 were selected for display, and are displayed as a cascade graph: on surface, then at 7, 18, 25, 31, 46, 75 and 100 µm deep. The first spectrum corresponds with the surface spectrum of VM®9 (spectrum ii Fig. 2a). Between 18 and 31-µm deep, the Raman peaks of interest in VM®9 (517, 592 cm^{-1} and the doublet at 975–1028 cm^{-1}) were correlated with a gradual increase in the peaks of Y-TZP (~275, 474 and 650 cm^{-1}). The last 50 µm of depth contained the two main peaks of VM®9 and were associated with the characteristic peaks of the Raman active mode of Y-TZP. There was a large decrease in the intensity of major components of feldspathic ceramic at depths greater than from 50 µm.

3.3. *Confocal Raman microscopy: Raman imaging*

Fig. 4 shows a 43 µm × 31 µm area selected from both sides of the interface of specimen No. 2 that is characteristic of the distribution of a given element in the analyzed area. The selection of bands of interest on VM®9 (centered at 338, 464, 495, 527, 592, and 1000 cm^{-1}) provide an image reconstruction based on variations in the intensity of these bands by integrating the area under the peaks. A clear delineation is made between the veneering ceramic and the Y-TZP in black, according to the optical image of the two components. In VM®9, the distribution of different crystalline phases was observed, which were dominated by a spectrum (spectrum 1a) similar to spectrum i of Fig. 2a. The lighter portions of the reconstructed image correspond to the most ordered phases (spectrum 1b), as a 5-µm diameter area well defined and localized against the zirconia (spectrum 1b). On the other side of the interface, Y-TZP had a very homogeneous structural phase (spectrum 3). Finally, a transition layer at the interface (spectrum 2), with a moderate intensity, was characterized by having peaks of interest that were common to both materials, and was measured as only a few micrometers thick.

A scan of the same area, treated this time by K-Means Cluster Analysis function, resulted in the Raman map of Fig. 5, which allowed for assignment of phase contribution and the selection of specific spectral regions. The image is simplified, compared to Fig. 4 as evidenced by the representation of VM®9. However, it has the advantage to more precisely qualify and quantify a specific region of the interface (spectrum 2), seen as a unique spectrum. This spectrum includes elements of both feldspathic ceramic and Y-TZP and represents an interdiffusion zone, with an estimated thickness of 2 µm. VM®9 has two major crystalline phases, which resulted in spectra 1a and 1b. The spectrum of the dominant phase (spectrum 1a) is identical to spectrum i in Fig. 2a. Spectrum 1b is similar to spectrum ii in Fig. 2a and is located against the interdiffusion zone (spectrum 2).

3.4. *Energy dispersive X-ray spectroscopy: elemental analysis*

The elemental chemical analysis for all products is presented in Table 2. The values in parentheses correspond to the composition prior to the removal of the carbon (C) contribution. This contribution will be discussed later. The analysis revealed a typical chemical structure of Y-TZP with a zirconia concentration of more than 58 wt% and an yttrium concentration of 4 wt%. A major component was represented by oxygen (O) up to 33 wt%. This analysis also revealed traces of silicon (Si), aluminum (Al), potassium (K), sodium (Na) and calcium (Ca). The presence of carbon in the data was surprising with a concentration in our specimen of almost 10 wt%.

The elemental composition analysis of VM®9 included high concentrations of oxygen and silicon at ~58 and 23 wt%, respectively, after subtracting the carbon. In its powder form, i.e., pre-sintered state as delivered to the dental laboratory, O and Si were the greatest component, with less contribution

Please cite this article in press as: Durand J-C, et al. Confocal Raman microscopic analysis of the zirconia/feldspathic ceramic interface. Dent Mater (2012), doi:10.1016/j.dental.2012.02.013

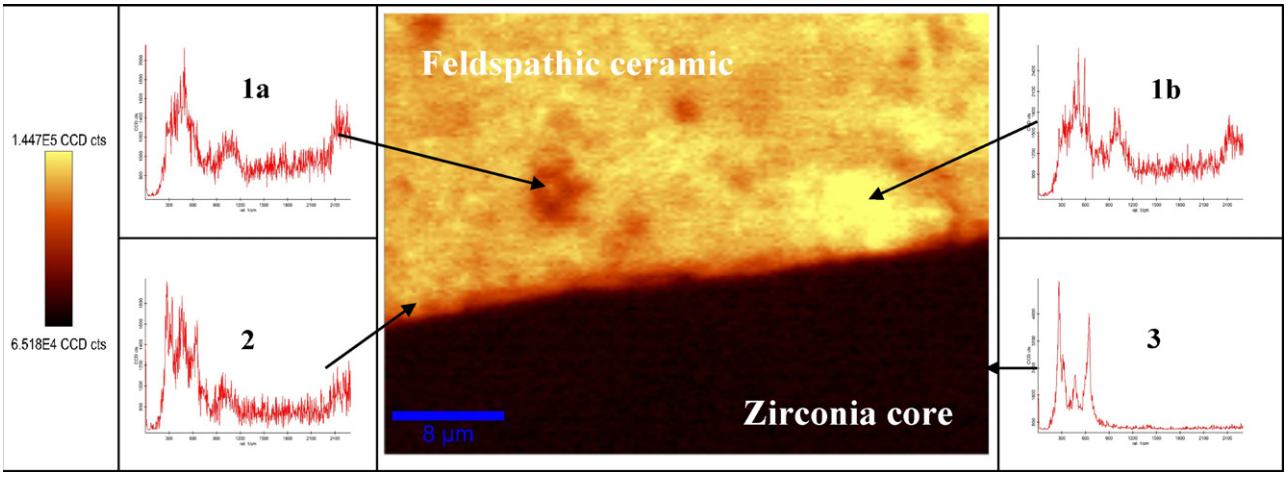

Fig. 4 – Raman microanalysis using the selection of the peaks of interest in the feldspathic ceramic. Spectra corresponding to different crystalline phases are presented in the lateral columns: Feldspathic ceramic (1a = glass matrix, 1b = crystalline phase), interdiffusion area (2), zirconia core (3).

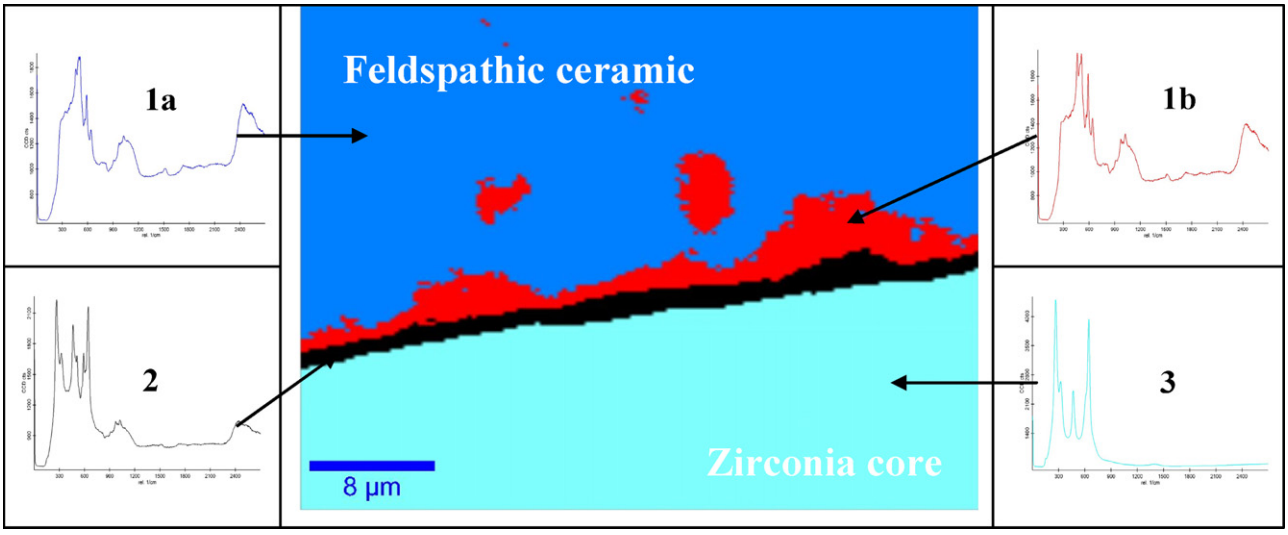

Fig. 5 – Raman microanalysis of the feldspathic ceramic/zirconia interface using K-Means Cluster Analysis function. Representative spectra from the four specific regions are presented in the lateral columns: Feldspathic ceramic (1a = glass matrix, 1b = crystalline phase), interdiffusion area (2), zirconia core (3).

from Al, K, Na, Zr and Ca (Table 2). In this powder, white crystals appear on the SEM image (Fig. 6) and correspond to zirconia crystals. On the sintered, sectioned specimen No. 2, the relative ranking of components remained unchanged and had almost similar values. Carbon was present between 24 and 29 wt%.

Fig. 7 shows the detailed elemental distribution around the interface between zirconia and VM®9 (along the arrow). Only the evolution of Zr and Si concentrations is followed. A decrease in Zr in the core to feldspathic ceramic was correlated with a decrease in Si in feldspathic ceramic to the core. A mutual diffusion or interdiffusion of Zr and Si occurred in

Table 2 – EDS analysis: elemental composition (wt%) of zirconia core (Y-TZP) and feldspathic ceramic (VM®9). Values in parentheses correspond to the composition prior to the removal of the C contribution.

Ceramic	Element								
	C	O	Na	Al	Si	K	Ca	Y	Zr
VM®9 Powder state	0.0 (28.8)	58.5 (47.9)	3.5 (2.0)	6.4 (3.6)	24.0 (13.3)	6.0 (3.4)	0.9 (0.5)	0.0 (0.0)	0.7 (0.4)
VM®9 Sintered	0.0 (24.5)	58.4 (44.1)	3.3 (2.5)	6.1 (4.6)	23.3 (17.6)	5.8 (4.4)	1.2 (0.9)	0.0 (0.0)	2.0 (1.5)
Y-TZP Sintered	0.0 (9.6)	32.8 (29.7)	0.4 (0.4)	0.9 (0.8)	2.3 (2.1)	0.8 (0.7)	0.1 (0.1)	4.0 (3.6)	58.6 (53.0)

Please cite this article in press as: Durand J-C, et al. Confocal Raman microscopic analysis of the zirconia/feldspathic ceramic interface. Dent Mater (2012), doi:10.1016/j.dental.2012.02.013

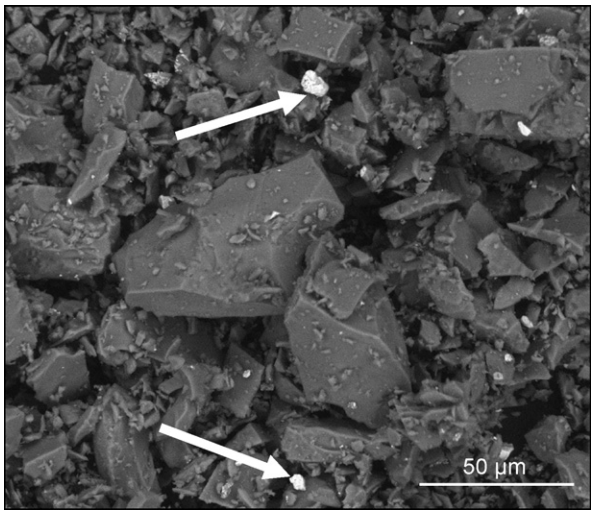

Fig. 6 – SEM observation of the powdered feldspathic ceramic (VM®9). White crystals (white arrows) correspond to zirconia crystals.

a layer with a thickness of approximately 2 μm. There was a marked decrease in Zr to the crossing of the optical interface. In comparison, the Si curve bends less strongly with a decline that appears more gradually and occurs over a greater distance.

4. Discussion

VITA In-Ceram® YZ is a metastable tetragonal zirconia polycrystal (Y-TZP) that is obtained by addition of 2–8 mol% Y_2O_3 [37]. Zirconia has three allotropes. The transformation from tetragonal (*t*) into the monoclinic (*m*) or cubic (*c*) form occurs under high localized stress [20], a slow $t \rightarrow m$ transformation occurs in a humid environment at a relatively low temperature (low temperature degradation) [2,17]. The spectral region between 150 and 750 cm^{-1} contains the strong ZrO_2-related Raman modes [35]. In the ZrO_2 tetragonal structure, the six atoms in the primitive cell are localized in the following special positions: $4d(C_{2v})$ for oxygen (this site corresponds to a tetrahedral site centered on Zr atoms) and $2a(D_{2d})$ for zirconium [38]. The symmetry for the six Raman active zone center modes is given in Fig. 1b. Each of the three main phases (*m*, *t*, *c*) exhibits a specific spectral signature, because phase transformation involves changes in the lengths of Zr–O bonds and in the bond angles accompanied with a volume change [22,38]. Also, these spectra mainly arise due to the polarizability that is associated with the oxygen ion vacancies [39]. Spectra of the Raman active mode of Y-TZP are seen in Fig. 1a and are similar to results of others on a specimen of tetragonal zirconia polycrystal containing 3 mol% yttria [35]. All of the six peaks are mainly characteristic of the *t*-ZrO_2 polycrystal [38–41]. However, the main regions of broad bands that occur at ~273, 473, and 648 cm^{-1} (Fig. 1) are due to tetragonal or cubic phases. At room temperature, Y-TZP has a majority of tetragonal phase (~80 wt%) that is completed by a fraction of cubic phase (~20 wt%) [39,42]. In the present study, as in that

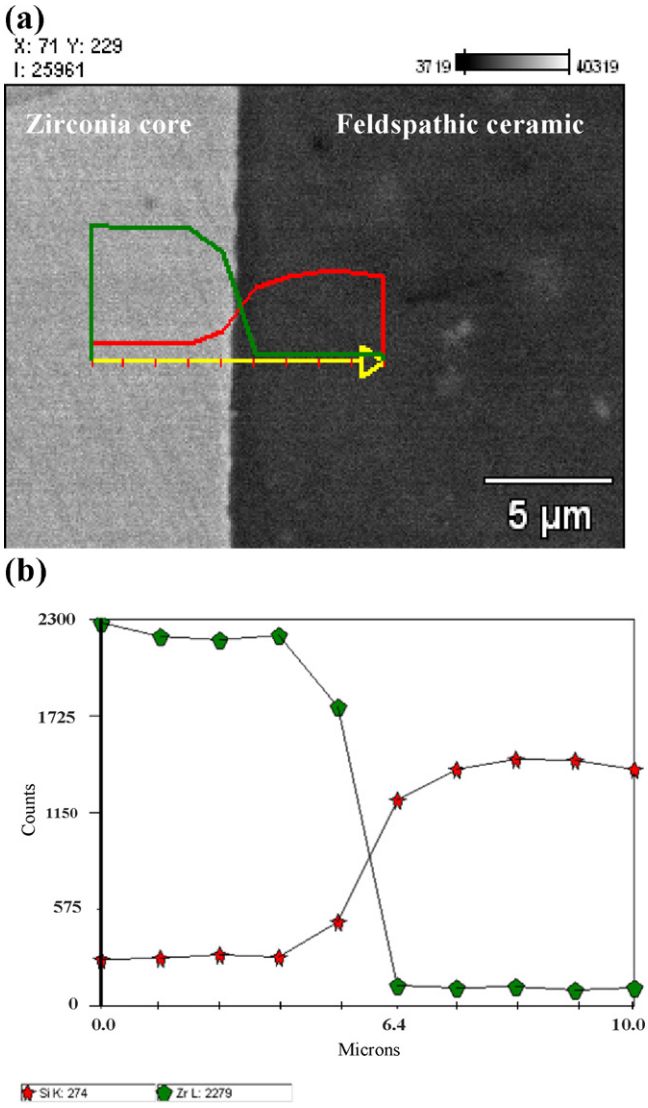

Fig. 7 – Results of elemental analysis across the feldspathic ceramic/zirconia interface by tracking the presence of Zr and Si, using the sectioned specimen. SEM image (a) with superposition of the line scan graph analysis (b).

another [16], the procedures used to obtain specimens did not result in detectable $t \rightarrow m$ transformations on the material.

In the table portion of Fig. 1b, a shift in Raman vibrations is seen toward higher wavelengths, compared to undoped *t*-ZrO_2. This shift depends on many factors, such as crystal size [25], the choice and concentration of doping oxides (stabilizers) [27,31], temperature and water vapor [43,44]. Stabilizers generate a decrease in the internal strain that forms as a result of the distortion of the cubic fluorite structure [31]. Shifts in the Raman bands to higher wavenumbers are produced by stabilizer cations with a smaller radius than Zr^{4+} [27]. Consequently, the factors leading to this stabilization are solute cation size, the number of oxygen vacancies, and the crystal structure of the alloying oxide [31]. Intrinsic defects, impurities, and water vapor are additional factors responsible for grain growth and density at the grain boundaries and cause structural changes, which explain the spectral variations.

Please cite this article in press as: Durand J-C, et al. Confocal Raman microscopic analysis of the zirconia/feldspathic ceramic interface. Dent Mater (2012), doi:10.1016/j.dental.2012.02.013

VM®9 is a feldspathic ceramic consisting of a vitreous phase (75–85% of volume) and a more ordered crystalline phase. According to industry data, after firing, the material is characterized by a very fine and uniform distribution of leucite crystals within the vitreous phase, which reduces major stress cracks [34]. The two main Raman spectra of VM®9 (Fig. 2) are broadly superimposable and are mainly indicative of silica glass [29,45]. In the feldspathic ceramic, the large band of silica glass (between 300 and 700 cm^{-1}) was replaced by a succession of symmetrical high intensity peaks that corresponded to the inclusion of different phases of crystallization in the glass [32]. The sharpness suggests localized vibrations from a well-ordered crystal lattice. A large band, or a shift to lower wavenumbers, is associated with a decrease in network crystallinity [32]. The glass network is represented by Si—O—Si bending. Peaks at ~917, 975 and 1030 cm^{-1} correspond to the symmetric Si—O stretching of a silicate tetrahedron with 3, 2 and 1 non-bridging oxygens, respectively [32,33]. A densification process is identified by a decrease in Si—O—Si bond angles within the network of the SiO_4 tetrahedral [29]. The crystal lattice is less ordered in the presence of broad band (spectrum i Fig. 2). The peak at 2447 cm^{-1} that was found in both spectra corresponds to residual bicarbonate in the glass [32].

The analysis is complicated because many of the crystalline silicates also respond in these regions, which could be in any of these forms [32]. However, some assignments are not mutually exclusive. For example, the band at 975 cm^{-1} could also respond to a symmetric Si—OH stretch, and the 592 cm^{-1} vibration could also respond to either Si—O^- stretching or to Si—O—Si bending [32]. The Raman active mode of crystal leucite ($K(Si_2Al)O_6$) consists of a doublet of low intensity at 156 and 183 cm^{-1} (not found in our analysis) and two peaks of high intensity at 497 and 529 cm^{-1} [46].

In summary, the main characteristics of Raman active mode of leucite glass ceramic can be compared with aluminosilicate glasses [33]. The main metal cations (Al, K) embedded in the glass matrix (SiO_2) are responsible for changing the network properties [33], in a more crystalline spectrum with more and well-defined peaks. Spectrum i (Fig. 2) characterizes a phase that is close to the glass matrix, and spectrum ii (Fig. 2) characterizes the more crystalline phase. Allocation of these different phases in sintered feldspathic ceramic is the source of many different Raman spectra.

The line scan mode tracked the intensity of the characteristic bands of the two different materials that were present on both sides of the interface in sectioned specimen (Fig. 3a) or in depth of thin-washed, unsectioned specimen (Fig. 3b and c). In both cases, line scans identified an interdiffusion process, by the presence in the same spectra of peaks associated with zirconia or feldspathic ceramic. The main components of feldspathic ceramic, in addition to silica, can be found in the zirconia. The interdiffusion layer was estimated at ~3 μm in sectioned specimen and at 10 μm or more in unsectioned specimen. Origin of this difference should probably be answered in depth profiling resolution. The depth resolution depends upon two factors: the volume of the laser focus and how Raman photons generated within this volume are recycled back into the spectrometer via the confocal aperture [47]. Depth resolution improves as NA increases. But depth resolution determined only by the objective numerical aperture, magnification and the pinhole size, is an incorrect assumption if we do not take account of how deeply one focuses below the sample surface [47], as expressed by Eq. (1). The depth resolution includes a significant contribution from a comparatively large excitation volume, so called out-of-focus areas, for which the change of ray path profile due to spherical aberration and refraction must be considered [35]. The larger the pinhole aperture, the wider and deeper the material probed [15]. Because minor phases may become undetectable due to the dilution effect of the sampling volume [35], these results must be treated with caution. Using an oil-immersion objective (to reduce the refractive index discontinuity at the sample surface) and maximize NA, could minimize spherical aberration and the out-of-focus response, respectively [48]. Authors have shown that the affecting sampling depth, defined as the zone from which 99% of the signal information comes, extends to several tens of micrometers, and may be minimized by choosing a low wavelength and a high numerical aperture [35]. Under these instrumental parameters, data in sectioned specimen (favoring lateral resolution) identify a gradient closer to the reality. Moreover, these results (2-μm thick) are similar to those of EDS analysis. The progress in construction of confocal Raman microscopes has significantly improved the spatial resolution [35]. However, due to the inevitable effects of refraction and spherical aberration, the best spatial resolution usually will be attained by mechanical preparation of a cross-section [49]. In addition, a study assessing the impact of build-up procedures on zirconia found that, in the presence of liquid, the monoclinic content from the surface is far greater than that which results from the cutting, grinding, and polishing of zirconia [18].

It has been mentioned [8] that some veneer elements, such as silicon, sodium, aluminum and potassium, can diffuse into the zirconia layer, gradually decreasing in concentration to a depth of 8–10 μm. Only slight diffusion of Zr and Si in a transition layer less than 10 μm has been found using an EDS line analysis [16]. Interdiffusion, i.e., the movement of atoms in different homogeneous environments, is made possible due to defects in the crystalline solid. One would also expect that the grain boundaries are the site of much of the spread, which are then combined with a reduction in yttrium [9].

Raman imaging, which uses the same principle as line scan, is used to collect a Raman spectrum at regular intervals to observe the distribution of elements on a given surface. Unlike the second image which allowed a cluster analysis of the spectral data, in Fig. 4, the characteristics of feldspathic ceramic provide more information on the distribution of different crystalline phases in the VM®9, feldspathic material. This distribution was generally consistent over the selected area, but presented a dominance of an amorphous phase, i.e., the glass matrix. The presence of a highly crystalline area 5-μm in diameter can be attributed to a possible contamination of the specimen with the cross-sectioning procedure. In both cases (Figs. 4 and 5), a transition zone is apparent, correlated by line scans analyses. This transition area is the zone of interdiffusion, which is more easily visualized and quantified using the K-Means Cluster function in Fig. 5. The interdiffusion zone

Please cite this article in press as: Durand J-C, et al. Confocal Raman microscopic analysis of the zirconia/feldspathic ceramic interface. Dent Mater (2012), doi:10.1016/j.dental.2012.02.013

was estimated at a 2-μm thick maximum according to data from the spectroscopy line scan (Fig. 3a).

The elemental analysis conducted on the sintered specimen confirmed a zirconia framework doped with yttrium (Table 2). According to the manufacturer [3,34], VITA In-Ceram® YZ is composed of at least 91% zirconium oxide (ZrO_2), 5% yttrium oxide (Y_2O_3), 3% hafnium oxide (HfO_2) a small amount (<1%) of aluminum oxide (Al_2O_3), and silicon oxide (SiO_2). The main oxides found in the present analysis are in the same order of ranking. The dispersion of a small amount of Al_2O_3 particles contributes to delay in the tetragonal-to-monoclinic transformation in air, a phenomenon also caused by humid aging conditions [43].

VITA VM®9 is a feldspathic ceramic composed of SiO_2 (60–64 wt%), Al_2O_3 (13–15%), K_2O (7–10%), Na_2O (4–6%) and B_2O_3 (3–5%) [3]. The analysis of elements found in the present study (Table 2) confirmed this general formulation. According to VITA, VM®9 is a ceramic veneer that is designed for layering onto ZrO_2 partially stabilized with yttrium and is characterized by a very fine distribution of leucite crystals in the glass matrix. The presence of zirconium in the powder (Fig. 6) improves the mechanical properties (as does leucite) and lowers the TEC of the as-prepared ceramics [50] (opposite of this case, unlike the leucite). The fine homogeneous structure depends on several factors with one being the percentage of aluminum to control the crystallization kinetics [51]. Another factor is related to leucite. The most homogeneous glass ceramic is one with the highest relative leucite content [52]. A high concentration of leucite is the origin of compressive stress in the latter by the creation of a difference in TEC between tetragonal leucite and the glass matrix. However, a high content of leucite is automatically linked to a high TEC of the whole ceramic [52]. Ceramics that are designed to cover a zirconia core typically have a slightly lower TEC, which is designed to minimize residual stresses in both layers [3,4,12] and decrease delamination failures [5]. Therefore, the VM®9 has a TEC (from 25 to 500 °C) = $9.0 - 9.2 \times 10^{-6}\,K^{-1}$ as opposed to $10.5 \times 10^{-6}\,K^{-1}$ for In-Ceram® YZ [34]. This finding should explain why the concentrations of Si, Al and K are lower in the ceramics designed for use with a ZrO_2 core than in conventional ceramics [53].

The EDS analysis revealed an abnormal carbon concentration in both the VM®9 (24–29 wt%) and the Y-TZP (>9 wt%). There is no conclusive answer from this finding, but is it hypothesized that contamination by the crucible sintering or melting base did not seem to be the cause in the powder stage. For the same reason, contamination from cross-sectioning and polishing is not a sufficient reason; this was confirmed by the analysis of a specimen not cut (not shown in Table 2). However, if one refers to similar analyses by EDS, it is observed that some authors have removed the contribution of carbon from their analysis to eliminate the bias of procedural section [54]. Others [53] found a carbon content above 50 wt% without explanation. The K line X-ray carbon is easily absorbed only from the surface of the specimen. Significant carbon background signals and hydrocarbon interfere with the quantitative analysis and can be responsible for a fast growing C peak [55]. Nevertheless, the latter explanation does not seem sufficient to explain these high concentrations. Final hypothesis would be that the carbon concentration comes from organic additives used as binders for green forming of ceramics materials, despite sintering [56,57]. Molding of ceramics [56] as wet chemical processing in order to avoid hard agglomerates of Y-TZP [57], may lead to excess carbon residue on the surface. This hypothesis requires further investigations.

The EDS line scan analysis (Fig. 7) showed an interdiffusion process, as suggested previously [8,16]. The line scan spacing was set by the lateral resolution in micrometers. A decrease in the concentration of Si was correlated with a decrease in Zr (Fig. 7). The graph overlay on the SEM image shows that the optical interface defined a 50% loss (or gain) in Si concentration against a 70% loss (or 30% gain) for Zr. The zirconium curve declines sharply in feldspathic ceramic, but the curve of silicon is more gradual. Material composition variation and differences in the sintering temperatures (1530 °C for Y-TZP vs. 950 °C for VM®9) could distinguish features between these two curves. Under the conditions of this study, the elemental transition layer that defined the interdiffusion zone was estimated at 2 μm in thickness as opposed to 10 μm found in another study [16]. However, authors of that study indicated that, due to the low lateral resolution in their experimental conditions (2–3 μm), this zone was smaller than 10 μm.

5. Conclusions

We chose confocal Raman microscopy for its ability to investigate the chemical and morphological changes in ceramic materials because of its ease of implementation and higher resolution. This technique was applied to the evaluation of the interface between a zirconia core and veneering ceramic with or without preparation (cross-section procedure) of the specimen.

Within the limitations of this study, confocal Raman microscopy highlighted an interdiffusion process with an estimated elemental transition layer of a maximum of 2 μm in thickness. Depth profiling with confocal Raman microscopy involves the choice of instrumental parameters favoring depth resolution. No phase transformation ($t \rightarrow m$) was observed in the zirconia.

However, the zirconia-feldspathic ceramic relationship is not well known. It would be interesting to compare the analytical capabilities of the confocal Raman microscopy monitoring of chemical and morphological changes of the interface according to different process stages, such as a liner and temperature differences.

Acknowledgments

The dental laboratory, “Laboratoire dts” in Montpellier, who provided the sintered specimens, is gratefully acknowledged. Mr. Bertrand Rebiere from IEM (The European Membrane Institute – UMR5635, Montpellier, France), is acknowledged for performing the SEM/EDS analyses.

REFERENCES

[1] Chevalier J. What future for zirconia as a biomaterial? Biomater 2006;27:535–43.

[2] Kelly JR, Denry I. Stabilised zirconia as a structural ceramic: an overview. Dent Mater 2008;24:289–98.
[3] Guess PC, Kuliš A, Witkowski S, Wolkewitz M, Zhang Y, Strub JR. Shear bond strengths between different zirconia cores and veneering ceramics and their susceptibility to thermocycling. Dent Mater 2008;24:1556–67.
[4] Özkurt Z, Kazazoglu E, Ünal A. *In vitro* evaluation of shear bond strength of veneering ceramics to zirconia. Dent Mater J 2010;29:138–46.
[5] Aboushelib MN, de Jager N, Kleverlaan CJ, Feilzer AJ. Effect of loading method on the fracture mechanics of two layered all-ceramic restorative systems. Dent Mater 2007;23:952–9.
[6] Studart AR, Filser F, Kocher P, Lüthy H, Gauckler LJ. Mechanical and fracture behaviour of veneer-framework composites for all-ceramic dental bridges. Dent Mater 2007;23:115–23.
[7] Taskonak B, Yan J, Mecholsky Jr JJ, Sertgöz A, Koçak A. Fractographic analyses of zirconia-based fixed partial dentures. Dent Mater 2008;24:1077–82.
[8] Aboushelib MN, Kleverlaan CJ, Feilzer AJ. Microtensile bond strength of different components of core veneered all-ceramic restorations. Part II: zirconia veneering ceramics. Dent Mater 2006;22:857–63.
[9] Aboushelib NM, Kleverlaan CJ, Feilzer AJ. Effect of zirconia type on its bond strength with different veneer ceramics. J Prosthodont 2008;17:401–8.
[10] Fahmy NZ. Bond strength, microhardness, and core/veneer interface quality of an all-ceramic system. J Prosthodont 2010;19:95–102.
[11] Manicone PF, Iommetti PR, Raffaelli L. An overview of zirconia ceramics: basic properties and clinical applications. J Dent 2007;35:819–26.
[12] Aboushelib MN, de Jager N, Kleverlaan CJ, Feilzer AJ. Microtensile bond strength of different components of core veneered all-ceramic restorations. Dent Mater 2005;21:984–91.
[13] Tholey MJ, Swain MV, Thiel N. SEM observations of porcelain Y-TZP interface. Dent Mater 2009;25:857–62.
[14] Scherrer SS, Quinn GD, Quinn JB. Fractographic failure analysis of a Procera® AllCeram crown using stereo and scanning electron microscopy. Dent Mater 2008;24:1107–13.
[15] Wulfman C, Sadoun M, Lamy de la Chapelle M. Interest of Raman spectroscopy for the study of dental material: the zirconia material example. IRBM 2010;31:257–62.
[16] Kawai Y, Uo M, Watari F. Microstructure evaluation of the interface between dental zirconia ceramics and veneering porcelain. Nano Biomed 2010;2(1):31–6.
[17] Chevalier J, Cales B, Drouin J-M. Low-temperature aging of Y-TZP ceramics. J Am Ceram Soc 1999;82:2150–4.
[18] Tholey MJ, Berthold C, Swain MV, Thiel N. XRD^2 micro-diffraction analysis of the interface between Y-TZP and veneering porcelain: role of application methods. Dent Mater 2010;26:545–52.
[19] Kansal I, Tulyaganov DU, Goel A, Pascual MJ, Ferreira JMF. Structural analysis and thermal behavior of diopside–fluorapatite–wollastonite-based glasses and glass–ceramics. Acta Biomater 2010;6:4380–8.
[20] Pittayachawan P, McDonald A, Young A, Knowles JC. Flexural strength, fatigue life, and stress-induced phase transformation study of Y-TZP dental ceramic. J Biomed Mater Res B Appl Biomater 2009;88:366–77.
[21] Deville S, Chevalier J, El Attaoui H. Atomic force microscopy study and qualitative analysis of martensite relief in zirconia. J Am Ceram Soc 2005;88:1261–7.
[22] Ishigame M, Sakurai T. Temperature dependence of the Raman spectra of ZrO_2. J Am Ceram Soc 1977;60:367–9.
[23] Witke K, Österle W, Skopp A, Woydt M. Raman microprobe spectroscopy and transmission electron microscopy of thermal sprayed ZrO_2 coatings before and after rub testing of outer air seals. J Raman Spectrosc 2001;32:1008–14.
[24] Merlin R, Pinczuk A, Weber WH. Overview of phonon Raman scattering in solids. In: Weber WH, Merlin R, editors. Raman scattering in materials science. Berlin Heildeberg: Springer-Verlag; 2000. p. 1–34.
[25] Djurado E, Bouvier P, Lucazeau G. Crystallite size effect on the tetragonal-monoclinic transition of undoped nanocrystalline zirconia studied by XRD and Raman Spectrometry. J Solid State Chem 2000;149:399–407.
[26] Mayoral MC, Andrés JM, Bona MT, Higuera V, Belzunce FJ. Yttria stabilized zirconia corrosion destabilization followed by Raman mapping. Surf Coat Technol 2008;202: 5210–6.
[27] Muñoz Tabares JA, Anglada MJ. Quantitative analysis of monoclinic phase in 3Y-TZP by Raman spectroscopy. J Am Ceram Soc 2010;93:1790–5.
[28] Pezzotti G, Sakakura S. Study of the toughening mechanisms in bone and biomimetic hydroxyapatite materials using Raman microprobe spectroscopy. J Biomed Mater Res A 2003;65:229–36.
[29] Kailer A, Nickel KG, Gogotsi YG. Raman microspectroscopy of nanocrystalline and amorphous phases in hardness indentations. J Raman Spectrosc 1999;30:939–46.
[30] Baklanova NI, Kolesov BA, Zima TM. Raman study of yttria-stabilized zirconia interfacial coatings on Nicalon™ fiber. J Eur Ceram Soc 2007;27:165–71.
[31] Kim D-J, Jang J-W, Lee H-L. Effect of tetravalent dopants on Raman spectra of tetragonal zirconia. J Am Ceram Soc 1997;80:1453–61.
[32] Jestel NL, Morris MD, O'Brien WJ. Depth-resolved Raman microprobe examination of a commercial dental porcelain exposed to a simulated oral environment. Dent Mater 1998;14:375–82.
[33] Musić S, Živko-Babić J, Mehulić K, Ristić M, Popović S, Furić K. Microstructure of Lucite glass–ceramics for dental use. Mater Lett 1996;26:195–9.
[34] Vita VM®9 working instructions. http://www.vita-zahnfabrik.com/resourcesvita/shop/en/en_3050430.pdf; 2011.
[35] Presser V, Keuper M, Berthold C, Nickel KG. Experimental determination of the Raman sampling depth in zirconia ceramics. Appl Spectrosc 2009;63:1288–92.
[36] Tan P-N, Steinbach M, Kumar V. Cluster analysis: basic concepts and algorithms. In: Tan P-N, Steinbach M, Kumar V, editors. Introduction to data mining. New-York: Addison-Wesley; 2006. p. 487–568.
[37] Kisi EH, Howard CJ. Crystal structures of zirconia phases and their inter-relation. Key Eng Mater 1998;153:1–36.
[38] Bouvier P, Lucazeau G. Raman spectra and vibrational analysis of nanometric tetragonal zirconia under high pressure. J Phys Chem Solids 2000;61:569–78.
[39] Ghosh A, Suri AK, Pandey M, Thomas S, Rama Mohan TR, Rao BT. Nanocrystalline zirconia–yttria system – a Raman study. Mater Lett 2006;60:1170–3.
[40] Bouvier P, Gupta HC, Lucazeau G. Zone center phonon frequencies in tetragonal zirconia: lattice dynamical study and new assignment proposition. J Phys Chem Solids 2001;62:873–9.
[41] Sekulić A, Furić K, Stubičar M. Raman study of phase transitions in pure and alloyed zirconia induced by ball-milling and laser beam. J Mol Struct 1997;410:275–9.
[42] Matsui K, Horikoshi H, Ohmichi N, Ohgai M, Yoshida H, Ikuhara Y. Cubic-formation and grain-growth mechanisms in tetragonal zirconia polycrystal. J Am Ceram Soc 2003;86:1401–8.
[43] Djurado E, Dessemond L, Roux C. Phase stability of nanostructured tetragonal zirconia polycrystals versus

Please cite this article in press as: Durand J-C, et al. Confocal Raman microscopic analysis of the zirconia/feldspathic ceramic interface. Dent Mater (2012), doi:10.1016/j.dental.2012.02.013

temperature and water vapour. Solid State Ionics 2000;136:1249–54.
[44] Casellas D, Cumbrera FL, Sanchez-Bajo F, Forsling W, Llanes L, Anglada M. On the transformation toughening of Y-ZrO_2 ceramics with mixed Y-TZP/PSZ microstuctures. J Eur Ceram Soc 2001;21:765–77.
[45] Raman spectrum of silica glass SiO_2. Handbook of Raman spectra; 2011. http://www.ens-lyon.fr/LST/Raman/spectrum.php?nom=silica glass.
[46] Raman spectrum of leucite $K(Si_2Al)O_6$. RRUFF database: Raman, X-ray, infrared and chemistry; 2011. http://rruff.info/leucite/display=default/R040107.
[47] Everall N. Depth profiling with confocal Raman microscopy, part I. Spectroscopy 2004;19(10):22–7.
[48] Everall NJ. Confocal Raman microscopy: common errors and artefacts. Analyst 2010;135:2512–22.
[49] Everall N. Depth profiling with confocal Raman microscopy, part II. Spectroscopy 2004;19(11):16–25.
[50] Kang M, Liao X, Yin G, Sun X, Yin X, Xie L, et al. Synthesis and properties of dental zirconia–leucite composites. Bull Mater Sci 2010;33:713–7.
[51] Aboushelib MN, Kleverlaan CJ, Feilzer AJ. Microtensile bond strength of different components of core veneered all-ceramic restaurations. Part 3: double veneer technique. J Prosthodont 2008;17:9–13.
[52] Assmann S, Ermrich M, Kunzmann K. Determination of quantitative leucite content in pressable ceramics compared to conventional dental porcelains. J Mater Sci Mater Med 2000;12:833–5.
[53] Chaiyabutr Y, McGowan S, Phillips KM, Kois JC, Giordano RA. The effect of hydrofluoric acid surface treatment and bond strength of a zirconia veneering ceramic. J Prosthet Dent 2008;100:194–202.
[54] Hooshmand T, Daw R, Van Noort R, Short RD. XPS analysis of the surface of leucite-reinforced feldspathic ceramics. Dent Mater 2001;17:1–6.
[55] Rolland P, Carlino VL, Vane R. Improved Carbon analysis with evactron plasma cleaning. Paper presented at Microscopy and Microanalysis 2004; 2004 Aug 1-5; Savannah, USA.
[56] Masia S, Calvert PD, Rhine WE, Bowen HK. Effect of oxides on binder burnout during ceramics processing. J Mater Sci 1989;24:1907–12.
[57] Shojai F, Pettersson A, Mäntylä TA, Rosenholm J. Detection of carbon residue on the surface of 3Y-ZrO_2 powder and its effect on the rheology of the slip. Ceram Int 2000;26:133–9.

Please cite this article in press as: Durand J-C, et al. Confocal Raman microscopic analysis of the zirconia/feldspathic ceramic interface. Dent Mater (2012), doi:10.1016/j.dental.2012.02.013

DENTAL MATERIALS 28 (2012) e229–e238

Available online at www.sciencedirect.com

SciVerse ScienceDirect

journal homepage: www.intl.elsevierhealth.com/journals/dema

Comparative mechanical behavior of dentin enamel and dentin ceramic junctions assessed by speckle interferometry (SI)

Michel Fages[a,*], *Pierre Slangen*[b], *Jacques Raynal*[a], *Stephane Corn*[b], *Kinga Turzo*[c], *Jacques Margerit*[a], *Frédéric J. Cuisinier*[a]

[a] *EA4203, Department of Biologic Sciences, University of Montpellier I, Montpellier, France*
[b] *Ecole des Mines d'Alès, I.L.O.A., Alès, France*
[c] *Department of Prosthodontic and Oral Biology, University of Szeged Dental School, Szeged, Hungary*

ARTICLE INFO

Article history:
Received 23 October 2011
Received in revised form 3 May 2012
Accepted 18 May 2012

Keywords:
Dentin enamel junction (DEJ)
Dentin ceramic junction (DCJ)
Speckle interferometry (SI)
Tooth crown
Ceramic crown

ABSTRACT

Objective. The dentin–enamel junction (DEJ) plays a crucial role in dental biomechanics; however, little is known about its structure and mechanical behavior. Nevertheless, natural teeth are a necessary model for prosthetic crowns. The mechanical behavior of the natural DEJ and the dentin ceramic junction (DCJ) manufactured with a CAD-CAM system are compared.
Methods. The reference samples undergo no modification, while the experimental samples were drilled to receive a cemented feldspathic ceramic crown. Longitudinally cut samples were used to achieve a planar object observation and to look "inside" the tooth. A complete apparatus enabling the study of the compressive mechanical behavior of the involved tooth by a non-contact laser speckle interferometry (SI) was developed to allow nanometric displacements to be tracked during the compression test.
Results. It is observed that the DEJ acted as a critical zone accommodating the movement between dentin and enamel. A smooth transition occurs between dentin and enamel. In the modeled prosthetic, the same kind of accommodation effects also occurs, but with a steeper transition slope between dentin and ceramic.
Significance. On the natural tooth, the stress accommodation arises from a differential behavior between enamel and dentin from the DEJ. In the ceramic crown, the cemented dentin–ceramic junction should play this role. This study demonstrates the possible realization of prosthetic crown reconstructions approaching biomechanical behaviors.

1. Introduction

The dentin–enamel junction (DEJ) in teeth is the zone between two distinct calcified tissues with very different biomechanical properties: enamel and dentin [1]. Enamel is hard and brittle and envelops the softer dentin. The enamel and dentin work together during the many load cycles experienced by the tooth over its lifetime. Generally, interfaces between materials with dissimilar elastic and mechanical properties represent "weak links" in a structure; however, the DEJ acts to successfully transfer applied loads (e.g., masticatory or impact) from the enamel to the dentin and inhibits enamel cracks from propagating into the dentin and causing tooth fracture [2,3].

* *Corresponding author at*: 11 Avenue Celestin Arnaud, 34110 La Peyrade, France. Tel.: +33 6 84 85 57 15; fax: +33 4 67 48 60 92.
E-mail address: mifages@wanadoo.fr (M. Fages).
0109-5641/$ – see front matter
http://dx.doi.org/10.1016/j.dental.2012.05.006

The DEJ appears as a discrete line when visualized microscopically and is thought to represent the original position of the basement membrane of the ameloblasts and odontoblasts where they coincide in the embryological tooth bud [4]. In human enamel and dentin, fatigue damage is the end result of extreme loads and is frequently associated with pathology or extensive wear. The fracture-resistant properties of the DEJ are believed to originate from a gradual change in microstructure and in the properties of dentin and enamel rather than from the abrupt transition between the two dissimilar materials [5,6]. Wang and Weiner suggested that the DEJ is one of the working sites of the tooth during mastication [7]. Imbeni et al. [1] believe that collagen fibrils perpendicular to the interface constitute the key reinforcing mechanism at the DEJ, thus explaining why so few cracking events cause delamination when they impinge on the DEJ. Zaslansky et al. [8,9] highlighted the importance of the DEJ as the binding interface between enamel and dentin. They have shown that adjacent to the DEJ is a 200–300 mm-thick zone of dentin of a much lower stiffness (compression elastic modulus) than the bulk of the dentin in the tooth.

Restorations that are all ceramic require proper adhesive bonding on the dentin to achieve their required life expectancy. All-ceramic restorations are made with feldspathic or zirconia ceramics. The strongest ceramics have a fracture toughness of at least 3.0 MPa $m^{1/2}$ [10], which is relatively close to the enamel fracture toughness of 1.3 MPa $m^{1/2}$, in a direction perpendicular to the enamel rods [8]. Nevertheless, fractures of the ceramic part of all-ceramic crowns are difficult to prevent, and crack growth is a significant problem [11]. This phenomenon can be explained by the absence of a stress accommodation zone. The natural stress accommodation zone of 200–300 μm-thick dentin has a much lower stiffness than the bulk of the dentin core [8].

Bonding agents must be selected very carefully because they determine not only the adhesion but also the ultimate strength of full-ceramic crowns [12–14]; therefore, it is important to compare the mechanical behavior of natural teeth and of the all-ceramic crown cemented on dentin. Instead of "cement joint", we will use the term "dentin–ceramic junction" (DCJ).

We applied compressive forces representative of those occurring in the oral cavity on natural teeth and all-ceramic crowns, and we determine the relative movement of enamel and dentin, or ceramic crown and dentin, respectively.

2. Materials and methods

2.1. Natural teeth

Intact lower first premolars free of caries were stored in physiological serum after having been extracted as part of the routine orthodontic treatment of young healthy adolescent patients (aged < 18). Five sets of two samples each (one natural tooth and one prosthetic tooth) were amassed. Right and left premolars from the same patient were used. One was kept intact, and the other was prepared to receive the prosthetic crown.

2.2. Prosthetic crowns

We employed the Cerec 3D® (Sirona Dental System®, Bensheim, Germany) CAD/CAM (computer aided design/computer aided manufacturing) unit to manufacture each prosthetic crown as a clone of the opposite tooth using the reproduction capability of the Cerec® software V2.80. This CAD/CAM system is composed of two distinct units: the optical imprint recording also allowing the CAD, and the milling unit using the CAD data to manufacture the sample out of a ceramic block. The software was set to give a dento-prosthetic spacing of 100 μm and a peripheral joint of 40 μm for a total thickness of 800 μm. Optical imprints, of the prepared tooth and of the opposite tooth, were recorded, and the Cerec MC® machine milled the prosthetic crowns [15]. The whole cloning process is presented in Fig. 1.

The Vita MarkII® (Vita Zahnfabrik, Bad Säckingen, Switzerland) ceramic blocks of albite-enriched feldspathic ceramic were used. Their abrasion coefficient is close to that of natural dental enamel. After milling, the extrados were glazed (Azkent®, Vita Zahnfabrik, Bad Säckingen, Switzerland).

The crowns were cemented onto the prepared teeth using Relyx Unicem® adhesive cement (3MESPE Dental Division, St. Paul, MN, USA) following the standard clinical protocol of illumination of each side of the crown for 4 s at 3000 mW/cm^2 with a Swissmaster Light® lamp (E.M.S., Nyons, Switzerland).

2.3. Specimen preparation

After extraction, the teeth were disinfected and stored in physiological serum with traces of chloroform. The teeth were longitudinally cut in the vestibular–lingual orientation, and one of the two resulting parts was removed with a diamond disc. Longitudinal cuts have been used to allow planar observation and to appreciate the different behaviors inside the tooth of the natural DEJ and of the DCJ interfaces. The tooth was then glued into the sample holder with a layer of Araldite® (Hunstman Advanced Materials, The Woodlands, Texas, USA). The sample holders have been cast in chromium cobalt using the imprint of a root. The mechanical stability of the specimen holders was validated by a speckle interferometry (SI) experiment.

2.4. Loading system

The compression test device fulfills the high sensitivity of speckle interferometry and copes with the rigid body motions of the whole system. The sample tooth cemented in the sample holder was placed under the force transducer (Model 31, Honeywell International, Morriston, NJ, USA). This mid-range precision miniature load cell is slowly translated vertically by the motor (M-235®, PI. Karlsruhe, Germany). The system can generate a force-driven displacement (C-862 Mercury PI, Karlsruhe, Germany) or simply a user's displacement. The compression apparatus communicates with the computer through a NI USB-6251 port (National Instruments, Austin, TX, USA) and is interfaced with an in-house LabView program. The entire mechanical system was bolted onto the holographic table top (Newport, Irvine, CA, USA). Very small displacement steps, as small as 1.6 nm, can theoretically be achieved. The

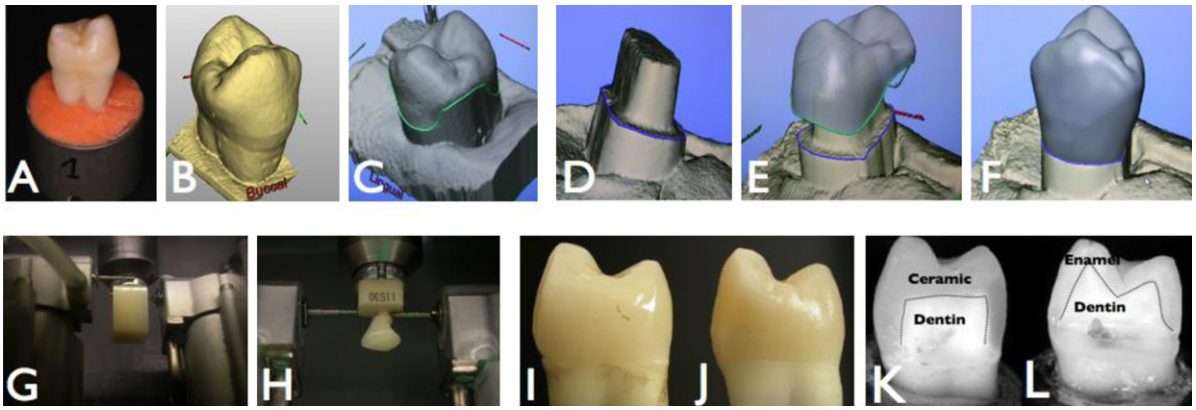

Fig. 1 – Cloning process: the intact natural crown sample (A), optical print (B), shaping (C), optical print of the second tooth prepared to receive the prosthetic clone (D), adaptation of the shaping on the tooth prepared (E), CAD finished, CAM ready (F), ceramic block in the milling unit (G), the prosthetic clone milled (H), the prosthetic clone cemented on the tooth prepared (I), the natural tooth (J), vertical cuts (K), prosthetic clone (L) natural tooth.

force can be applied to the tooth directly with the force transducer or through a relay rod. Force has always been applied to the same part of the lingual cusp. Preliminary testing by SI showed good performances of the mechanical set-up and no spurious displacements.

2.5. *SI apparatus*

The optical set-up was previously presented in detail [16]. The frequency-doubled YAG laser emits 50 mW at 532 nm wavelength in the green range. The laser beam is then injected in a COTS (commercially off-the-shelf) system (Canadian Instruments, Nottingham, UK) offering injection, variable intensity coupling in the output fibers, and phase shifting.

There are two input fibers: one for injection and one for detection of the reflected signal at the output fiber interfaces. Parts of the output fibers are bared and wrapped around piezoelectric transducers. The phase shift is applied on either or both of the two output fibers by applying a voltage at the PZT and thus generating a tiny extension of the fiber. The system is protected from thermal and mechanical effects by a plastic box and is easily breadboardable. Phase shifts were calibrated using common procedures [16].

A sensitive optical fiber in-plane interferometer has been designed with sensitivity vector Sv. Horizontal sensitivity is achieved. Two symmetrical beams produce an interference signal on the whole object and then illuminate the samples. The objects are optically rough-rendered by white powder. An XC70 CCD camera (Sony, Tokyo, Japan) records the sample surface under loading forces. The images are then stored in live memory or on the computer's hard disk.

The image processing was performed using the appropriate software in LabView, and the results are presented as vector maps or false color maps. Isodisplacement maps can be visualized in real time during the loading of the sample. The system can handle areas ranging from 5 mm × 5 mm to 1 m × 1 m when using the appropriate type of laser and loading system. The measurement uncertainty is approximately 50 nm, which is common for interferometric measurement in a controlled environment. The displacement resolution is approximately 10 nm, while the spatial resolution is directly linked to the magnification of the object scene on the image sensor (1280 × 900 pixels).

A "4-buckets" phase shifting algorithm leads to phase variations during the compression test [17]. During the test, the initial phase state was memory-resident and real-time subtracted from the current state. Sometimes the reference state was also refreshed because for some loading steps, the number of fringes can be too high, and the resulting noise would interfere with the interpretation of the resulting fringes. Interferograms show the in-plane displacements from phase shifting speckle interferometry. Highest quality images were stored on the hard disk and overlaid with upper jaw position and load value (N).

2.6. *Typical experiments*

Specimens were white powdered using Eutest 3 Developer Castolin Eutectic powder (Castolin, Lausanne, Switzerland) to generate a uniform diffusing surface and to avoid different modulations between dentin and enamel or ceramic and dentin. The same loads were applied to the natural tooth and the prosthetic crown samples to allow comparisons of their respective compressive behaviors.

The starting load was approximately 0 N. The compression was increased stepwise, performing discrete displacements of the transducer tip (one step is approximately 1.6 nm of Y-displacement). Therefore, a greater number of steps corresponds to a higher compression. The sample can be loaded or unloaded. The loading range applied to the different samples was between 5 N and 120 N. The CCD camera records at the sample surface the interferences of the two illumination beams coming from the two output optical fibers. Live fringes are displayed between a reference state and the current load state. Between minimal and maximal loading, different phase maps are recorded and stored in the memory.

The mechanical deformations are computed from the displacement maps generated from the phase difference maps.

Speckle interferometry is a relative displacement measurement. The maximum range between two successive

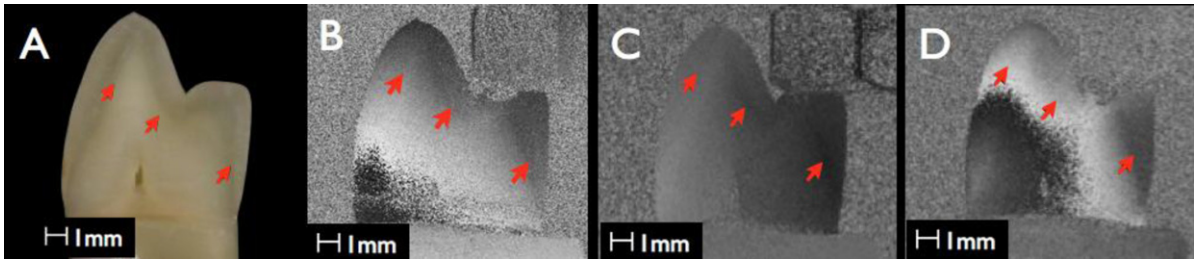

Fig. 2 – Natural tooth sample under different loads. (A) White light images. (B) Screenshot no. 04: force: 35.5 N, ΔF: 35.5 N (new ref: 0). (C) Screenshot no. 13: force: 40.23 N, ΔF: 0.16 N (new ref: 40.39). (D) Screenshot no. 24: force: 82.54 N, ΔF: 13.96 N (new ref: 96.5).

measurements is approximately 20 μm. In our experiments, we need to record smaller steps as some mechanical noise appears. Therefore, new displacement references (zero displacement reset) are recorded during the test.

2.7. *Displacement calculations*

Different operation modes of SI are commonly used, e.g., subtraction-mode, time-averaged SI, and double-pulsed SI [16]. In this work, we focus on subtraction-mode SI, or more specifically, on phase-shifting SI, which is mainly used for static deformation measurements.

Combining the primary interference pattern phase changes between the recordings yields new secondary interference fringes (also called correlation fringes).

The variable φ_s denotes the start phase (also called speckle phase) at the initial state of the object. The variable $\Delta\varphi$ represents the phase change between two states.

These speckle interferograms can be subtracted and lead to the following equation for the secondary interference fringe pattern, assuming perfect spatial correlation between the two primary speckle patterns:

$$I_1 - I_2 = 2\sqrt{I_r I_o}(\cos(\varphi_s + \Delta\varphi) - \cos(\varphi_s))$$

Currently, noise limits the accuracy of intensity subtraction SI to approximately 15 nm. Regarding the in-plane sensitivity of the setup, the angle of the impinging beam θ is approximately 30° and determines the correspondence between the phase gray level variation and the in-plane displacement u_x.

In our interferometer, the wavelength of the laser is 532 nm, and its relationship with the in-plane displacement is given by the following equation:

$$u_x = \frac{\lambda}{4\pi \sin\theta}\varphi_x$$

The resulting variation of one gray level of phase u_x is approximately 2.08 nm.

3. Results

Five sets of two samples each (natural tooth and prosthetic crown) were produced. The experimental protocol was tested and validated with four of them. Presented results correspond solely to the fifth sample (for natural tooth and prosthetic clone).

The interferometric images distinctly show the behavior of the samples and confirm the quality of the mechanical apparatus and the integrity of the dedicated sample holder (Figs. 2 and 3).

A natural tooth is presented in Fig. 2. Figure captions also present the screenshot number (or image number), the force applied to the sample, the force difference from the reference state, and force from the reference state (or phase reset).

Fig. 2A displays the sample under white light before painting. Fig. 2B–D is SI images recorded at different compression levels and present typical fringes. Fringes occur when the displacement induces an optical phase of 360–0°. The displacement in the *X* direction is computed from the optical phase.

In Fig. 2B–D, different continuous gray lines demarcate the DEJ (red arrows) corresponding to the image taken in white

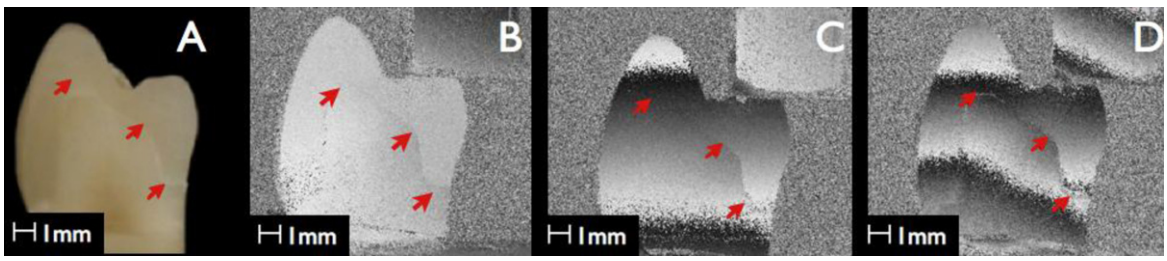

Fig. 3 – Prosthetic crown sample under different loads. (A) White light images. (B) Screenshot no. 08: force 36.78 N, ΔF: 2.57 N (new ref: 41.01 N). (C) Screenshot no. 15: force 77.56 N, ΔF: 5.29 N (new ref: 82.85 N). (D) Screenshot no. 33: force 64.09 N, ΔF: 18.76 N (new ref: 41.01 N).

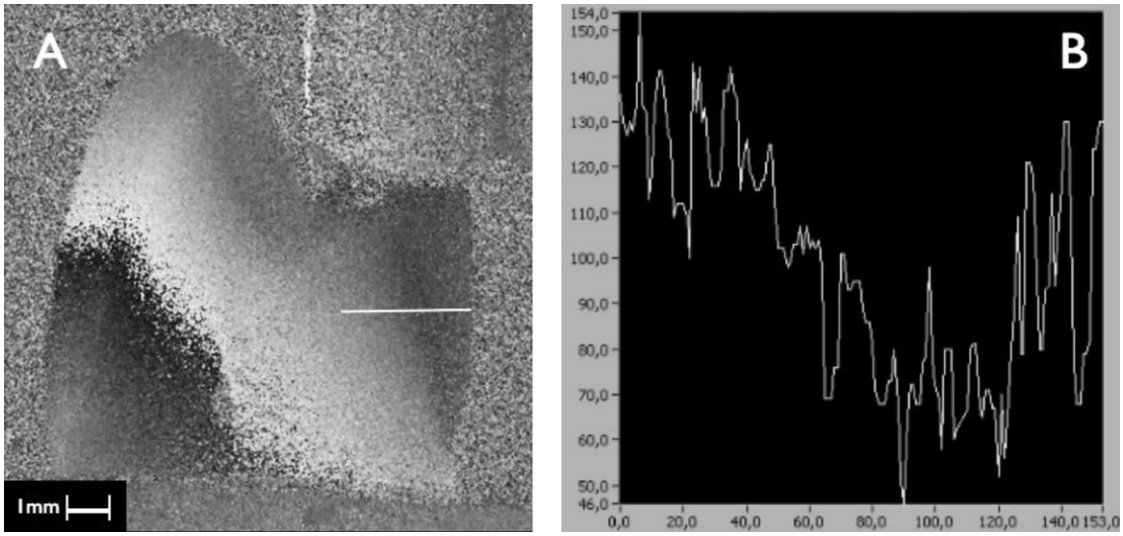

Fig. 4 – Natural tooth behavior at a load of 38.65 N, $\Delta F = 1.74$ N, new ref: 40.39 N. (A) SI image: the single white line corresponds to the region of interest (ROI) used for the calculation of displacement. (B) Displacement curve along the white line, displacements in nm versus position in pixels. Step is about 43 nm.

light (2A). The DEJ is clearly visible when the applied force reaches 35.5 N. The DEJ is always more visible in front of the loading point.

Fig. 3A presents a prosthetic crown sample under white light before painting, and Fig. 3B–D are recorded at different compression levels and present typical fringes at different loads.

The DCJ appears from 38 N and is clearly visible in Fig. 3B–D (red arrows). For the prosthetic crowns, it appears as a continuous gray line corresponding to the image taken in white light (Fig. 3A).

The SI images displayed in Fig. 2B–D show that the natural enamel cap moves independently from the dentin. This difference is clearly delimited by a line corresponding to the anatomical location of the dentin–enamel junction (DEJ). For the prosthetic crown, in the SI images (Fig. 3B–D) the same kind of shift occurs at the cement junction of the ceramic crown with the dentin. The DEJ is less well marked than the DCJ due to the smaller associated displacements. Large variations in intensity (Fig. 3C and D) correspond to fringes resulting from rigid body motion (in plane rotation projected onto the sensitivity vector).

The highest loading values enabling the distinction of the interface zone were 117.4 N for the prosthetic crown and 82.5 N for the natural tooth. Beyond 120 N, all samples behaved like rigid bodies. Around 200 N, some samples were destroyed due to fractures of the brittle materials. From all of the screenshots, different images were chosen for use in computing the displacement maps.

In Fig. 4A, from left to right, we denote the transition between light gray and dark gray corresponding to the region between the dentin and the enamel. One horizontal white line has been defined as the region of interest (ROI). In Fig. 4B, the curve represents the displacement change in nanometers versus the position along the white straight line shown in Fig. 4A. The relative displacement between the dentin and the enamel is 52 nm for loads between 38.6 N and 40.4 N ($\Delta F = 1.8$ N).

In Fig. 4B, the gray level are rising at the end of the curve as it is close to the right edge of the tooth, it is clearly visible on the native image with higher magnification. This is generated by the smooth inplane tilt of the palatine cuspid following the upper displacement of the upper jaw rod from the mechanical testing as the force decreases from 40.39 N to 38.65 N.

In Fig. 5A, in front of the cusp subjected to the load, the delineation made by the DEJ is visible, and the gray levels differ because of a different accommodation.

To calculate the displacement value, six red equal parallel lines were defined perpendicularly across the DEJ. The red lines are separated by 1 pixel one to the other, and so appear as a bold red line on the figures. The displacement is the average value of the six-stacked profiles. In Fig. 5B, the black curve is the mean value fitting of the blue curve values along the six paths, and the blue curve is one of the six displacement curves. The mean relative displacement between the dentin and the enamel is about 20 nm for loads between 39.21 N and 40.39 N ($\Delta F = 1.18$ N).

The same analytical process was applied for the prosthetic crowns (Figs. 6–8).

In Fig. 6A, one horizontal black line was defined as the region of interest, as the technical noise was less prominent than for the natural tooth. The area of interest is located in a fringe in front of the stress zone from left to right. We denote the transition between light gray and dark gray corresponding to the region between the dentin and the ceramic cap. In Fig. 6B, the curve represents the displacement change in nanometers versus the position along the white straight line shown in Fig. 6A. The relative displacement between the dentin and the ceramic cap is 43 nm for loads between 82.8 N and 76.3 N ($\Delta F = 6.5$ N).

In Fig. 7, to evaluate the displacement values, six equal parallel straight paths have been defined in the region of interest

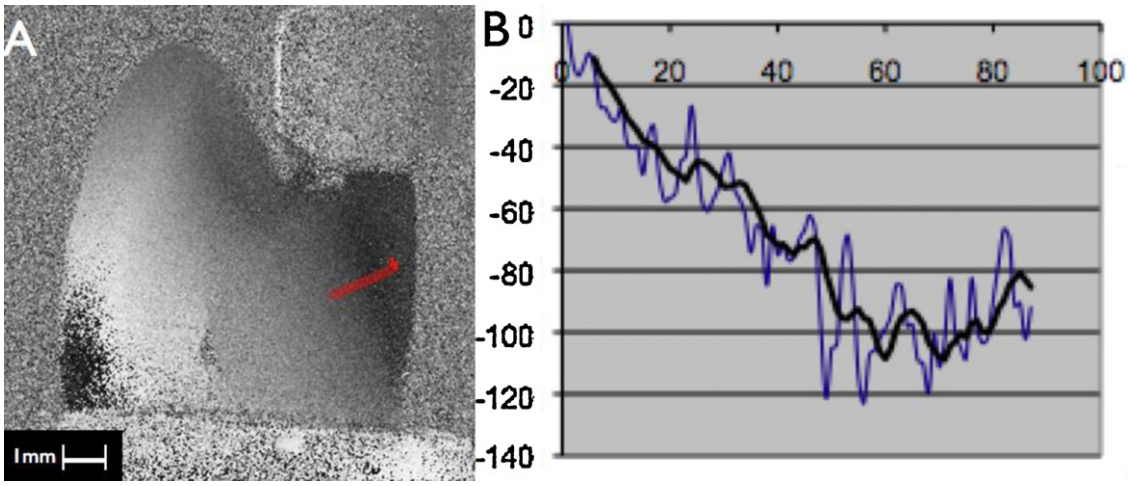

Fig. 5 – Natural tooth behavior at a load of 39.21 N, $\Delta F = 1.18$ N, new ref: 40.39 N. (A) SI image: six red equal parallel lines, 1 pixel separated, are defined across the DEJ. (B) Displacement curves: blue curve: displacement values along one of the six red lines. Black bold curve is the mean value fitting of the 6 blue curves. (For interpretation of the references to color in this figure legend, the reader is referred to the web version of the article.)

across the DCJ in the palatine zone in front of the loading point (Fig. 7A). The six red lines are drawn perpendicularly to the DCJ to accurately measure the displacement variation across the DCJ. This is much appropriate than the single horizontal black line for Fig. 6 as the red lines enable the real comparison from one side to the other perpendicular to the DCJ.

In Fig. 7B, the displacement is displayed as the average value of the six stacked profiles. The black curve is the median value fitting of the blue curve values. In this case, the relative displacement is approximately 95 nm for loads between 82.8 N and 72.8 N ($\Delta F = 10$ N). It shows clearly the effect of the DCJ acting as an accommodation area for the applied displacement, but with a sharper slope than the natural DEJ.

The SI image in Fig. 8 was selected to represent the characteristic isodisplacement map of the discontinuity zone located in front of the loading point for a ceramic crown. A colored and zoomed image is also presented. The fringe shift in the region of interest clearly delineates a mechanical interface between the ceramic and the dentin, which are separated by the cement.

Fig. 8 presents the characteristic fringes obtained for a huge load difference (30.07 N) and the important noise occurring due to some speckle decorrelation effect. Results from Fig. 8 show it is mandatory to make step references enabling smaller displacement load and thus very low decorrelation noise.

Fig. 9 shows the natural tooth with the same charge than prosthetic tooth (Fig. 8) and allows to compare DEJ and DCJ.

4. Discussion

The importance of the DEJ as an interface binding the enamel and dentin surfaces has long been recognized (Tylman [2]). Our understanding of the role and the location of the DEJ has

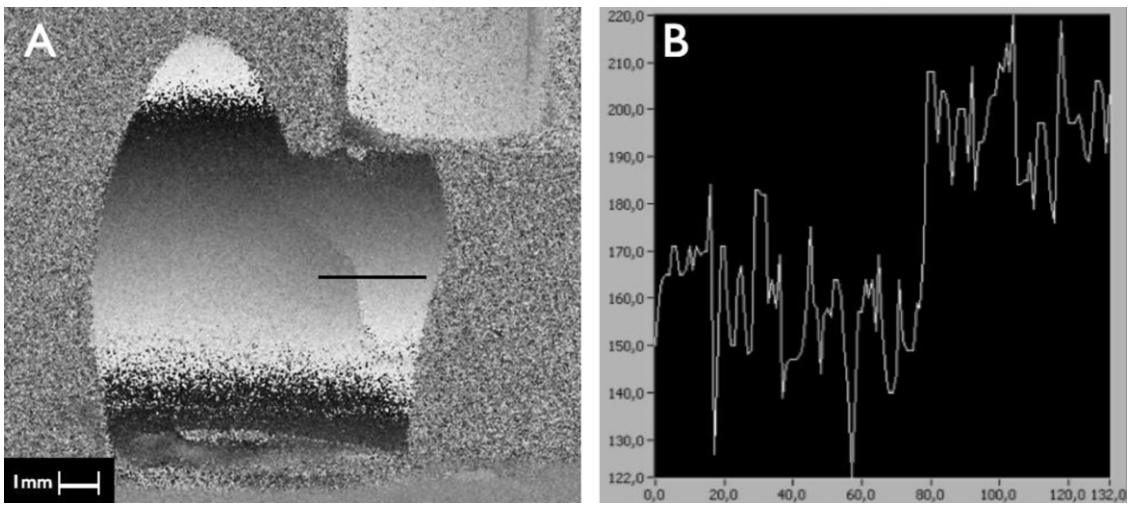

Fig. 6 – Prosthetic crown behavior at a load of 76.34 N, $\Delta F = 6.51$ N, new ref: 82.85 N. (A) SI image: a single black line corresponds to the region of interest (ROI) used for displacement calculation. (B) Displacement curve along the black line, displacements in nm versus position in pixels. Step is about 43 nm.

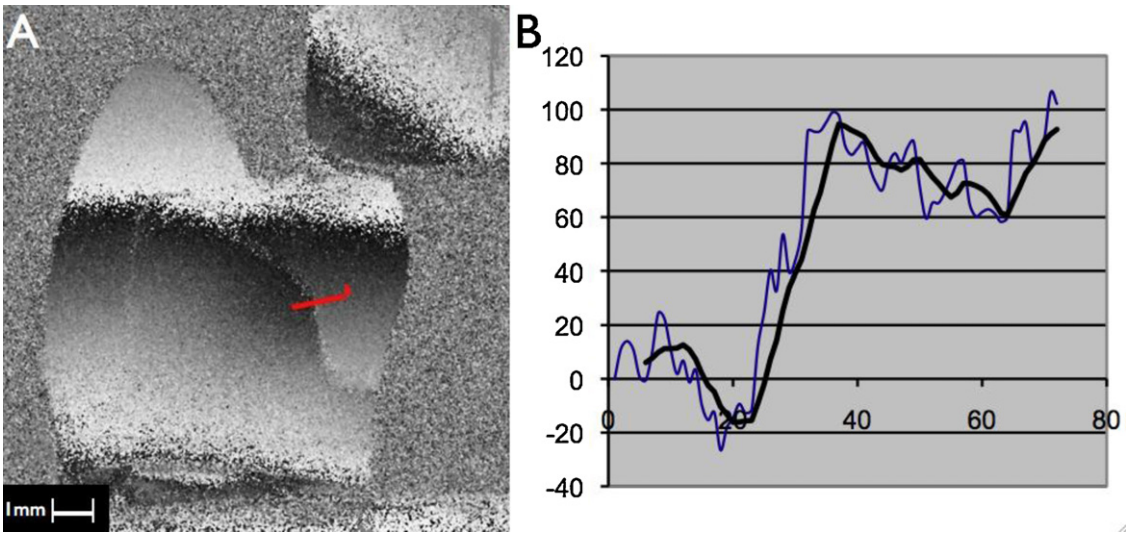

Fig. 7 – Prosthetic crown behavior under a load of 72.85 N, ΔF = 10 N, new ref: 82.85 N. (A) SI image: six red equal parallel lines, 1 pixel separated, are defined across the DEJ. (B) Displacement curves: blue curve: displacement values along one of the six red lines. Black bold curve is the mean value fitting of the 6 blue curves. The displacement is approximately 95 nm. (For interpretation of the references to color in this figure legend, the reader is referred to the web version of the article.)

evolved with ongoing research. The unique mechanical properties of this zone were first recognized from micro-hardness profiles (Craig et al. [18,19]). Wang and Weiner [7] measured the strain across this zone when a compressive load was applied and suggested that this is an important working part of the tooth during mastication. An asymmetry between enamel and dentin was noted previously (Wood et al. [20]) but was not quantified. Bechtle et al. explained the phenomenon of crack arrest at the DEJ using the elastic modulus mismatch between the dentin and the enamel [21].

It was found (Zaslansky [9]) using SI that a compressive load applied to the tip of the main cusp of a human premolar caused the entire enamel cap to move essentially as a stiff body, tilting toward the buccal surface.

Recently, Barak et al. [22] highlighted the importance of enamel in a whole-tooth demonstration through a finite element model study and validated their findings by a metrology method. Chattah et al. [23] showed that the enamel cap in a minipig animal model is capable of deforming and rotating at loads as low as 16 N. Zaslansky et al. [9] showed that the enamel cap of an isolated human premolar did not deform or rotate at loads lower than 80 N. Human enamel is stiffer than that of the minipig, and the cusps do not deform or crack until high loads are reached. However, in both cases, the aim was to preserve the functionality of the grinding surfaces over long

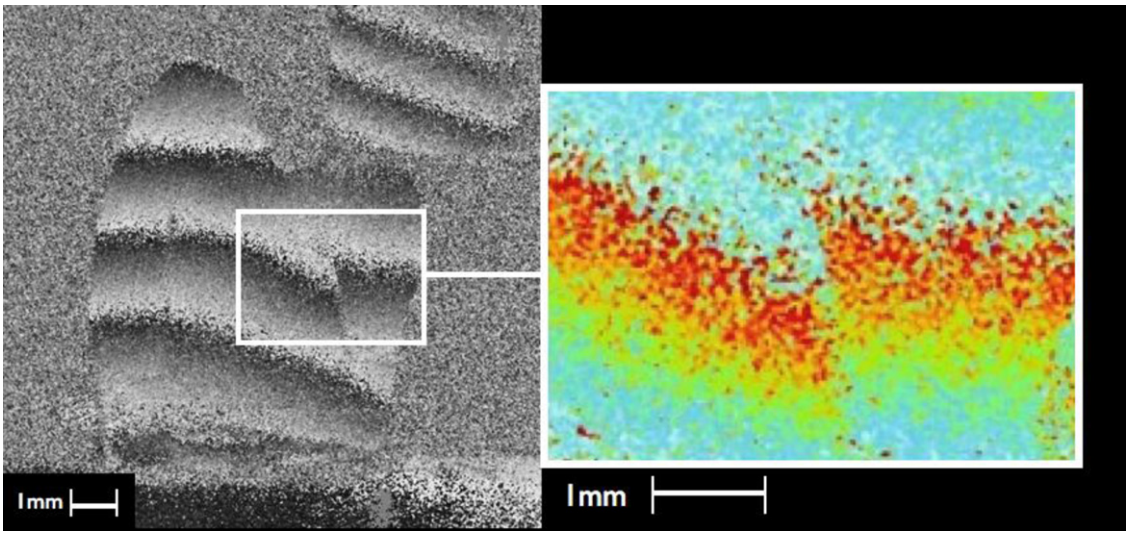

Fig. 8 – SI image sample "prosthetic crown" and displacements shown in a contour colored map. Behavior for a load of 52.78 N, ΔF = 30.07 N, new ref: 82.85 N.

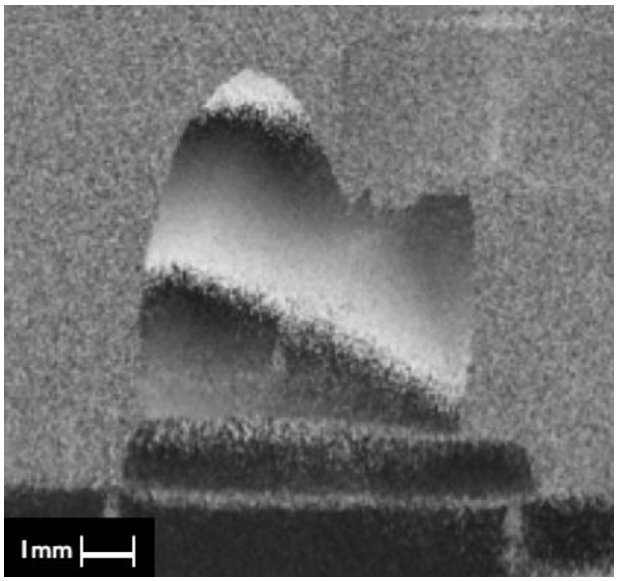

Fig. 9 – SI image sample "natural tooth". Behavior for a load of 52.3 N, $\Delta F = 6.5$ N, new ref: 58.8 N.

periods of time. The use of these opposing strategies to achieve the same end has been attributed to phylogenetic differences in masticatory function. [24,25]. The minipig molar is capable of deforming and rotating at low loads, and the intrinsic reaction of the crown to eccentric loading is complemented and even enhanced by the structures supporting the tooth [23].

In our study, we considered the half-cut crown because this configuration has the major advantage of observing the in-plane behavior of the DEJ and the DCJ in and doing so from either far from or close to the loading zone. Zaslansky worked with parallelepiped cuts from premolars [9], while Chattah et al. [23–25] studied whole teeth. On SI images, the interfaces appear distinctly along their entire lengths, thus showing their complete loading (from 35.5 N for the DEJ on the natural tooth and from 36 N for the prosthetic crown). The first interpretation confirms that the enamel bulk and the ceramic cap will move slightly under loading as rigid bodies. However, the mechanical response is different for the same applied loading force, and the displacement is larger for ceramic than for enamel. Thus in Fig. 8, at a load of 52.7 N, the SI image clearly shows a relative displacement between enamel and dentin. In Fig. 9, at a similar load (52.3 N), the image identifies the DEJ and the differing behaviors of the enamel and dentin. However, it does not show a relative displacement as high as in Fig. 8. This displacement is confirmed in SI pictures in Figs. 6 and 7, with values of 83 nm and 95 nm, respectively. This behavior demonstrates the accommodation strength of the DCJ and confirms its protective role for the ceramic caps.

Moreover, we emphasize that the displacement of the crown, whether enamel or ceramic, is different if the measurement area is far from or close to the loading zone. In each case, the larger displacement is located opposite to the load. The gray levels maps also show a displacement of the opposite cuspid but of smaller magnitude.

For the natural tooth, Zaslansky writes, "the asymmetry in stiffness between the buccal and lingual sides may therefore have a profound significance in determining how exactly the enamel cap responds to load during mastication". This asymmetric nature of the structure may also contribute to the distribution of loads that are not applied along the long axis of the tooth. The possible asymmetry in stiffness between the buccal and lingual sides of the tooth points to a basic property of tooth function, presumably related to the precise manner in which stress is distributed during mastication.

Conversely, for the prosthetic crown, the cement joint thickness will be the same everywhere (100 μm), except in the zone of the cervical joint, where it is approximately 40 μm. The displacement of the ceramic cap will be a function of the thickness of the cement and its elastic modulus [26]. The behavior of the samples appears to be rational. Above a certain load (117.4 N for the prosthetic crown and 82.6 N for the natural tooth), the SI images show that the DEJ and the DCJ cannot be observed. When the interfaces in both settings can no longer accommodate the loading stress, the teeth begin to act as whole rigid objects, and higher loading forces generate cracks and fractures of the samples.

Our work tends to confirm both Zaslansky's and Weiner's studies: the DEJ zone is an important part of the tooth structure. Moreover, we have demonstrated a comparable behavior for the DCJ. We believe these zones are crucial for the stress resistance of the crown structure, whether natural or prosthetic. For monobloc vitreous ceramic prosthetic crowns, load resistance is a result of the cementing process [27,28].

The soft DEJ interface is actually a graded structure, and much remains to be understood about the manner in which the whole tooth behaves under load. Figs. 6 and 7 show that the DCJ presents a graded behavior but with a sharper slope than the DEJ. An interesting use of dento-prosthetic spacing could be to select the cement joint thickness based upon the cement elastic modulus. This would refine attempts to mimic the physiological behavior of the natural tooth [29], according to the biomimetic concept [30]. This seems already very important as several authors have investigated the effect of differences in the resin-cement elastic modulus on stress-transmission to several composite or ceramic reconstructions [31,32]. Other authors have studied the influence of different bonding agents under stress on the internal and marginal adaptation of composite or ceramic reconstructions [33].

The biomimetic principle through the use of reconstruction ceramics that have wear coefficients close to that of natural enamel resulting from cements with an elastic modulus similar to that of the natural DEJ, we can expect the construction of real biomimetic prosthetic teeth in the near future.

5. Conclusion

Speckle interferometry is highly recommended for performing displacement measurements for dental biomechanics. The SI approach allows for the measurement of the mechanical properties of biological structures and other biomaterials that are a few hundred microns thick. The strain accommodation capacity of the tooth is derived from the differential displacement between the enamel and the dentin. The dentin–enamel junction acts as an interface until a certain maximal loading. Beyond this threshold, the loading accommodation property

disappears, and the tooth then behaves as a rigid body. We demonstrate a similar behavior for the prosthetic crown tooth. In this case, the enamel is replaced by the ceramic crown and the dentin–enamel junction by the dentin–cement junction. These behaviors indicate the interface role of the DEJ and the DCJ in the capacity of teeth to accommodate the stresses of their physiological functions or even of their parafunctions. For the cement characteristics and the cement thickness used in this paper, the accommodation effect of the DCJ is less marked than that of the DEJ. Future study will deal with the effect of the cement characteristics and the cement thickness by applying SI for samples having different cements and different thickness of cement joint, thanks to the CAD/CAM system. The limits of SI measurement are the sensitivity to rigid body motion and decorrelation noise affecting the spatial resolution. This can be enhanced by using smaller pixel sensors with higher photographic magnification.

REFERENCES

[1] Imbeni V, Kruzic JJ, Marshall GW, Marshall SJ, Ritchie RO. The dentin–enamel junction and the fracture of human teeth. Nature Materials 2005;4:229–32.

[2] Tylman SD. The dentino-enamel junction. Journal of Dental Research 1928;8:615–22.

[3] Habelitz S, Marshall SJ, Marshall GW, Balooch M. The functional width of the dentino-enamel junction determined by AFM-based nanoscratching. Journal of Structural Biology 2001;135:244–301.

[4] Lin CP, Douglas WH. Structure-property relations and crack resistance at the bovine dentin–enamel junction. Journal of Dental Research 1994;73:1072–8.

[5] Meyer JM, Bodier-Houlle P, Cuisinier FJG, Lesot H, Ruch JV. Initial aspects of mineralization at the dentino-enamel junction in embryonic mouse incisor in vivo and in vitro: a TEM comparative study. In Vitro Cellular and Developmental Biology-Animal 1999;35(March (3)):159–68.

[6] Marshall GW, Balooch M, Gallagher RR, Gansky SA, Marshall SJ. Mechanical properties of the dentin–enamel junction: AFM studies of nano hardness, elastic modulus and fracture. Journal of Biomedical Materials Research 2001;54:87–95.

[7] Wang R, Weiner S. Strain–structure relations in human teeth using Moiré fringes. Journal of Biomechanics 1998;31:135–41.

[8] Zaslansky P, Shahar R, Barak MM, Friesem A, Weiner S. Tooth and bone deformation: structure and material properties by ESPI. Proceedings of SPIE 2006;6341.

[9] Zaslansky P, Friesem AA, Weiner S. Structure and mechanical properties of the soft zone separating bulk dentin and enamel in crowns of human teeth: insight into tooth function. Journal of Structural Biology 2006;153(February (2)):188–99 [Epub. 2005 December 9].

[10] Bieniek KW, Marx R. The mechanical loading capacity of new all-ceramic crown and bridge materials. Schweizer Monatsschrift fur Zahnmedizin 1994;104(3):284–9.

[11] Gonzaga CC, Cesar PF, Miranda Jr WG, Yoshimura HN. Slow crack growth and reliability of dental ceramics. Dental Materials 2011;27(April (4)):394–406 [Epub. 2010 December 24].

[12] Addison O, Sodhi A, Fleming GJ. Seating load parameters impact on dental ceramic reinforcement conferred by cementation with resin-cements. Dental Materials 2010;26(September (9)):915–21.

[13] Attia A, Kern M. Influence of cyclic loading and luting agents on the fracture load of two all-ceramic crown systems. The Journal of Prosthetic Dentistry 2004;92(December (6)):551–6.

[14] Guarda GB, Gonçalves LS, Correr AB, Moraes RR, Sinhoreti MA, Correr-Sobrinho L. Luting glass ceramic restorations using a self-adhesive resin cement under different dentin conditions. Journal of Applied Oral Science 2010;18(June (3)):244–8.

[15] Fasbinder DJ. The Cerec system: 25 years of chairside CAD/CAM dentistry. Journal of the American Dietetic Association 2010;141(June (Suppl. 2)):3S–4S.

[16] Slangen P, De Veuster C, Renotte Y, Berwart L, Lion Y. Computer-aided interferometric measurements of drift and phase shifter calibration for DSPI (digital speckle pattern interferometry). Optical Engineering 1995;34(12): 3526–30.

[17] Creath K. Phase-measurement interferometry techniques. In: Progress in optics XXVI. Elsevier Science Publisher B.V.; 1988 [Chapter 5] p. 349–393.

[18] Craig R, Peyton FA. The micro-hardness of enamel and dentin. Journal of Dental Research 1958;37:661–8.

[19] Craig R, Gehring P, et al. Relation of structure to the microhardness of human dentin. Journal of Dental Research 1959;38:624–30.

[20] Wood JD, Wang RZ, et al. Mapping of tooth deformation caused by moisture change using Moiré interferometry. Dental Materials 2003;19:159–66.

[21] Bechtle S, Fett T, Rizzi G, Habelitz S, Klocke A, Schneider GA. Crack arrest within teeth at the dentinoenamel junction caused by elastic modulus mismatch. Biomaterials 2010;31(May (14)):4238–47 [Epub. 2010 February 18].

[22] Barak MM, Geiger S, Chattah NLT, Shahar R, Weiner S. Enamel dictates whole tooth deformation: a finite element model study validated by a metrology method. Journal of Structural Biology 2009;168:511–20.

[23] Chattah LT, Shahar R, Weiner S. Design strategy of minipig molars using electronic speckle interferometry: comparison of deformation under load between the tooth mandible complex and isolated tooth. Advanced Materials 2009;21:413–8.

[24] Strait DS, Richmond BG, Spencer MA, Ross CF, Dechow PC, Wood BA. Masticatory biomechanics and its relevance to early hominid phylogeny: an examination of palatal thickness using finité-elements analysis. Journal of Human Evolution 2007;52(May (5)):585–99.

[25] Chattah NL, Kupcik K, Shahar R, Hublin JJ, Weiner S. Structure-function relation of primate lower incisor: a study of the déformation of Macaca dentition using electronic speckle pattern interferometry (ESPI). Journal of Anatomy 2011;218(1):87–95.

[26] Nakamura T, Wakabayashi K, Kinuta S, Nishida H, Miyamae M, Yatani H. Mechanical properties of new self-adhesive resin-based cement. Journal of Prosthodontic Research 2010;54(April (2)):59–64 [Epub. 2009 October 30].

[27] Attia A, Abdelaziz KM, Freitag S, Kern M. Fracture load of composite and feldspathic all ceramic CAD/CAM crowns. Journal of Prosthetic Dentistry 2006;95(February (2)): 117–23.

[28] Attia A, Kern M. Fracture strength of all ceramic crowns luted using two bonding methods. Journal of Prosthetic Dentistry 2004;91(March (3)):247–52.

[29] Urabe I, Nakajima S, Sano H, Tagami J. Physical properties of the dentin–enamel junction region. American Journal of Dentistry 2000;13(June (3)):129–35.

[30] Magne P, Belser U. Understanding the intact tooth and the biomimetic principle. In: Magne, Belser, editors. Bonded porcelain restorations in the anterior dentition: a biomimetic approach. Chicago: Quintessence Publishing Co.; 2002. p. 23–55.

[31] Ausiello P, Rengo S, Davidson CL, Watts DC. Stress distributions in adhesively cemented ceramic and resin-composite class II inlay restorations: a 3D-FEA study. Dental Materials 2004;20(November (9)):862–72.
[32] Burke FJ, Watts DC. Effect of differing resin luting systems on fracture resistance of teeth restored with dentin-bonded crowns. Quintessence International 1998;29(January (1)):21–7.
[33] Dietschi D, Moor L. Evaluation of the marginal and internal adaptation of different ceramic and composite inlay systems after an in vitro fatigue test. Journal of Adhesive Dentistry 1999;1(1):41–56.

19400

CAD/CAM: a “tailor made” methodology for assessing the mechanical behavior of complete ceramic crowns

ABSTRACT

Statement of the problem. Rupture tests of materials are only worthwhile when they are accurate, reproducible and simulate a clinical setting. There is no normalized reference method for assessing the mechanical behavior of complete ceramic dental crowns. Computer-assisted design and manufacturing enable the manufacturing of samples and sample holders that are identical.

Purpose. This study proposes a method for assessing the mechanical behavior of complete ceramic crowns. Computer-assisted design and manufacturing systems were used to manufacture a series of samples and sample holders that are perfectly appropriate for dental prosthetic tests.

Material and Methods. Five series of six different shapes of dental preparations were designed and manufactured in aluminum supports using computer-aided design and manufacturing methods. Glass-reinforced ceramic caps were duplicated using dental computer-assisted design and computer-assisted manufacturing and optical imprints were cemented on the aluminum supports following a standard protocol. Using a mechanical press, samples were exposed to a compressive load in the occlusal direction until rupture. The compressive displacement response of the samples and the measure of their stiffness and strength were monitored. Then, loading force curves were plotted, and mean rupture forces for each series were calculated.

Results. The results for each series and comparisons of the series revealed the reproducibility and the scientific potential of the developed experimental methodology.

Conclusion. By preventing most of the operator-dependent variations, this method provides a new approach for evaluating the mechanical properties of fixed dental prostheses. The quality of this protocol is reflected by the low standard deviations of the series and should be highly suitable for dental prosthetic tests.

Clinical implications. This method has the following two main advantages: it allows for testing of the behavior of materials and enables selection of shapes of support that are well suited for the clinical setting. This provides a new perspective for the analysis and validation of dental support preparations that are appropriate for ceramic materials used for the restorations and the resin used for luting crowns on teeth.

INTRODUCTION

All-ceramic systems are suitable for a wide range of clinical indications in almost all areas of fixed restorative dentistry (1,2). However, complete glass-ceramic crowns are vulnerable to fracture during their normal function (3,4). One of the major problems is their potential fracture due to occlusal forces in the posterior area (5,6). A systematic review has indicated an urgent need for a comprehensive classification system for clinical prosthesis failures, technical complications and biological complications (7). Dynamic loading of all-ceramic materials is indispensable for assessing the clinical performance of all-ceramic molar crowns (6). However, traditional tests of ceramic crowns create a state of stress and damage in ways that differ greatly from those observed clinically, emphasizing the need for an effective in-vitro testing protocol (8,9).

In fixed prosthetics, the set-up must consist of two parts: an infrastructure, representing the tooth with a standardized preparation, and a superstructure, representing the prosthetic element. The two elements are assembled using an adhesive luting system (10). Then the sample is generally cemented into a sample holder (11,12).

To create the infrastructure, several methods were employed. It is possible to prepare human teeth or parts of animal teeth (bovine) manually (13,14). It is also possible to prepare a natural or synthetic dental crown and then use epoxy resin (15), or a prefabricated standard wax model to construct several replications of the prepared tooth (16) (17), or in other ways (18) (19). Naturally hydrated teeth most closely resemble the actual clinical setting (14); however, it is impossible to manually obtain several samples that are identical and calibrated because the various manual procedures are too operator dependent (20). Some authors have proposed using

"CAD/CAM" (Computer Aided Design and Computer Aided Manufacturing) technology to evaluate the main and interacting effects of a set of clinical variables, on the maximal principal stress (MPS) within the core of an anatomically correct veneer-core-cement-tooth model (21). Others have imported the average dimensions of prepared teeth into the CAD software (22). The aim of this study is to propose a new 'tailor-made' methodology for assessing the mechanical behavior of ceramic samples. The proposed method uses CAD/CAM properties to improve reproducibility and reduce experimental variations (23). Therefore, we developed a method to create samples using only the CAD/CAM systems. This method can be applied for any type of tooth preparation.

First, CAD is used to create the infrastructure. The software enables the creation of a 3D model with high precision and in accordance with clinical requirements (16,24,25). For example, it is possible to input the dimensions of a standardized preparation, as well as the angulations of its axial walls and the size and form of its shoulder. It is also possible to modify geometrical parameters to study their effects on the mechanical properties of the prosthesis.

Once the design is completed, the infrastructure is milled with an industrial automated machining system, and the CAM stage is initiated.

The superstructure is a monolithic ceramic cap, which is created with the dental CAD/CAM technology from an optical print of the infrastructure (26) and subsequently milled in a ceramic block (27). The ceramic samples (superstructures) with identical external geometries are cemented onto the infrastructure using adhesives. Therefore, the whole set-up (infrastructure and superstructure) is created entirely by the CAD/CAM system, thereby ensuring precision and infinite reproducibility.

To validate our set-up, different series of samples were exposed to axial compressive loading

until rupture and their mechanical responses were recorded and analyzed. The experimental variations were determined within each series and between the different series.

The purpose of this study was to validate a method for assessing the mechanical behavior of reproducible complete ceramic crowns obtained with the CAD-CAM system. The hypothesis was that the results show only little difference inside each series. The null hypothesis was that no significant difference would be found among the different series of specimens used in this study.

MATERIALS AND METHODS

Infrastructure

CAD

CAD: The Catia V5 software (Dassault Systems, Vélizy-Villacoublay, France) was used to design the infrastructures.

The CAD system is used to design a geometric form based on the fixed prosthetic principles **(19,20)** using the following seven parameters:

D1: total diameter.

D2: preparation diameter.

HI: occluso-cervical dimension.

LI: width of the shoulder.

TOC: total occlusal convergence.

SA: shoulder angulations.

COF: radius of curvature of the occlusal .

Six different specimens were constructed based on the above parameters, with variations in the following critical parameters: TOC, SA, COF.

TOC: 7° or 21°.

SA: 45° or 90°.

COF: 1.9 mm, 13 mm, 0 mm (0 mm corresponds to a flat occlusal face)

The specimens are named according to their characteristics:

S1: $7^{TOC}45^{SA}19^{COF}$

S2: $21^{TOC}45^{SA}13^{COF}$

S3: $7^{TOC}90^{SA}19^{COF}$

S4: $21^{TOC}90^{SA}13^{COF}$

S5: $7^{TOC}90^{SA}0^{COF}$

S6: $7^{TOC}45^{SA}0^{COF}$

The goal was not to reproduce an identically prepared tooth, but to individualize the elements of the preparation, which affected the mechanical response of the ceramics. The height and diameter of the infrastructure were determined in order to obtain volumes close to reality (in this case a lower premolar). They do not reflect a strict clinical reality but are the outcome of different measures that will allow a discussion of the method**.**

Table I shows the different values for each infrastructure, and figure 1 shows the different 3D models obtained using the CAD software.

CAM

We used a 5-axis DMU40 milling machine (Deckel Maho Gildemeister, Bielefeld Germany). The DMU-40 machine assures an accuracy of 2 μm.

The infrastructure was milled from aluminum barrels (Al 6060). Although Kelly

recommended the use of epoxy resin for the infrastructures (15), reproducibility has been enhanced with 6060 aluminum-milled infrastructures (although it is stiffer than epoxy resin). For each shape, 5 identical samples were milled into aluminum bars. This is an acceptable number for operating results to establish significant statistical values**.** The bars were 2 cm diameter and 1.5 cm in height. The infrastructure had a height of 9 mm, and the part of the barrel that was not milled was used as a sample holder, which is why there was no interface between the sample holder and the infrastructure (figure 2).

Superstructure

Superstructures were produced with a Cerec AC CAD/CAM system. (Sirona Dental System, Bensheim, Germany).

CAD:

The optical imprints were produced with a blue cam intraoral camera. Models of the superstructures were created with the 2.80 CAD/CAM software. Optical imprints of each of the infrastructures were recorded. The software was set to yield a dental-prosthetic spacing of 100 µm and a peripheral joint of 40 µm for a total thickness of 800 µm. The maximum thickness on the occlusal face was 1.5 mm, resulting in a flat surface of 4 mm^2.

CAM:

Superstructures were manufactured using the MC-XL milling unit.

The caps were milled from Vita MarkII ceramic blocks (Vita Zahnfabrik, Bad Sackingen, Germany). One optical imprint was taken for each shape. Five superstructures were milled from the same optical print. A total of 30 (5 times 6) ceramics caps were milled. There was no

significant difference between the dimensions of the superstructures. For this study, the resulting samples were not glazed or polished.

Specimen (infrastructure + superstructure)

To increase the ceramic surface area, the superstructures were etched on their internal surface with 5% hydrofluoric acid gel for 1 min. The superstructure was cemented to the infrastructure with Relyx-Unicem cement (3M ESPE Dental Division, St. Paul, Minn) and subsequently cured using a Swiss Master Light curing unit ((E.M.S., Nyons, Switzerland) following the standard clinical protocol of illumination (4 s at 3000 mW/cm^2 per face). Each series was numbered, and each sample within the series was numbered separately.

Mechanical testing systems

Compression tests were performed with the mechanical testing system Dartec (TestRessources Inc., Shakopee, Minn.), which was driven by the Tematest software (Tema Concept, Chanteloup les Vignes, France) using regulated loading speeds. We used the load cell TC4 transducer (Nordic Transducer, Hadsund, Denmark), which consists of a 500 daN maximum load and is coupled with an LVDT (Linear Variable Differential Transformer) displacement sensor with a 1 mm range (L10R transducer, RDP Electrosense, Pottstown,Pa).

Mechanical measurements

The samples were positioned between the jaws of the testing press (figure 3). A 10 N preload was applied to the sample prior to the test. Then, sequential loading was performed to measure specific mechanical values (stiffness, strength). Thus, successive loading (+300 N) and

unloading (-100 N) cycles were performed, while the LVDT sensor monitored the compressive displacement response of the sample. As soon as rupture occurred, the press was stopped. During the test, the force and displacement were continuously recorded and the rupture force values were noted.

RESULTS

A summary of all results is shown in tables II and III and in figures 4 and 5. None of the results were rejected.

Table II provides the values of the ultimate loading forces in kN for each sample and displays the mean value of the ultimate force, the standard deviation and the dispersion. The dispersion is the ratio of the standard deviation and the mean and is expressed as a percentage. The lowest mean rupture force was 1.048 kN ($21^{TOC}45^{SA}13^{COF}$) and the highest was 1.902 kN ($7^{TOC}45^{SA}0^{COF}$), which is approximately 80% higher.

Ultimate force values were used to distinguish two groups of results: [1.04-1.3 kN] for series $7^{TOC}45^{SA}19^{COF}$, $21^{TOC}45^{SA}13^{COF}$, $7^{TOC}90^{SA}19^{COF}$ and [1.7-1.9 kN] for series $21^{TOC}90^{SA}13^{COF}$, $7^{TOC}90^{SA}0^{COF}$, $7^{TOC}45^{SA}0^{COF}$. Each group was associated with geometric features.

Series $21^{TOC}90^{SA}13^{COF}$, $7^{TOC}90^{SA}0^{COF}$, $7^{TOC}45^{SA}0^{COF}$ presented a higher dispersion than series $7^{TOC}45^{SA}19^{COF}$, $21^{TOC}45^{SA}13^{COF}$, $7^{TOC}90^{SA}19^{COF}$. However, the standard deviations observed for each series were low, and the dispersion remained below 18% at all times. The mean dispersion was 11.5%, which indicated good reproducibility for the rupture mechanics.

Figure 4 shows the force-displacement (loading force in kN vs compressive displacements in mm) curves of the samples. For each of the figures, 5 curves corresponding to the five samples

are shown. Force-displacement curves exhibit the mechanical response of the samples. The force increased with displacement until rupture of the samples occurred. For each series, the measured curves showed a similar shape for all the samples within the series. However, series $21^{TOC}90^{SA}13^{COF}$, $7^{TOC}90^{SA}0^{COF}$ and $7^{TOC}45^{SA}0^{COF}$ exhibited a change of slope at high force levels. In contrast, series $7^{TOC}45^{SA}19^{COF}$, $21^{TOC}45^{SA}13^{COF}$, $7^{TOC}90^{SA}19^{COF}$ exhibited progressive damage before rupture occurred. As a result, the curves in figures 4 ($21^{TOC}90^{SA}13^{COF}$, $7^{TOC}90^{SA}0^{COF}$, $7^{TOC}45^{SA}0^{COF}$) have a higher rupture force as well as a higher dispersion than the curves in figures 4 ($7^{TOC}45^{SA}19^{COF}$, $21^{TOC}45^{SA}13^{COF}$, $7^{TOC}90^{SA}19^{COF}$).

To present the responses to stress exhibited by the samples, the evolution of apparent stiffness (kN/mm) for different loading force levels was calculated (table III and fig 5).

The apparent stiffness increased with increasing loading force. All samples showed an increase in stiffness by approximately 50%. In all the series, a similar degree of stiffness evolved in the same way (figure 5) for the different load levels. For series, $21^{TOC}45^{SA}13^{COF}$ rupture occurred before 1 kN was reached.

Table II shows that standard deviations and dispersion values increased with increasing load levels but remained moderate overall. The series $21^{TOC}90^{SA}13^{COF}$, $7^{TOC}90^{SA}0^{COF}$, $7^{TOC}45^{SA}0^{COF}$ are again distinguished by slightly higher stiffness values associated with greater dispersions. The apparent stiffness decreased at the end of the test. In contrast, series $7^{TOC}45^{SA}19^{COF}$, $21^{TOC}45^{SA}13^{COF}$, $7^{TOC}90^{SA}19^{COF}$ are characterized by a sudden brittle fracture. An extreme value of the stiffness is obtained at approximately 25 kN/mm and at values greater than 1 kN for series.$7^{TOC}90^{SA}0^{COF}$.

DISCUSSION

The first hypothesis was supported by our results, and the null hypothesis was rejected. A larger number of samples would have resulted in a more refined data set.

Although not every operation was "operator-dependent" in this study, bonding is a manipulation in which the operator can introduce variations. This operation would require standardization. It was also possible to make more shapes to complete the study.

The results show similar fracture force values for the five samples within each of the 6 series. The lowest and highest dispersions were 4% (series$21^{TOC}45^{SA}13^{COF}$) and 18% (series$7^{TOC}90^{SA}0^{COF}$), respectively. It is interesting that such a low dispersion was obtained with a total of 30 samples (5 samples per series) and that none had to be rejected.

Six different shapes were designed by varying the following three parameters: the total occlusal convergence (T.O.C), the occlusal face curve (C.O.F.) and the shoulder angulations (S.A). For series $21^{TOC}45^{SA}13^{COF}$ and $7^{TOC}45^{SA}0^{COF}$, these three parameters (T.O.C., C.O.F. and S.A.) were different. As a result, the mean force for rupture was 1.048 kN for series $21^{TOC}45^{SA}13^{COF}$ and 1.902 kN for series $7^{TOC}45^{SA}0^{COF}$, which represents an 81% difference. In contrast, we only made one change between series $7^{TOC}45^{SA}19^{COF}$ and $21^{TOC}45^{SA}13^{COF}$ (TOC). The resulting difference was approximately 20% (1.255 kN for series $7^{TOC}45^{SA}19^{COF}$ and 1.048 N for series $21^{TOC}45^{SA}13^{COF}$). It is possible to perform these assessments for all the series and determine the factors or combination of factors that lead to the observed results. This analysis identifies the specific role of each factor and its effect on the mechanical response. The standard deviation is 0.057 for series $7^{TOC}45^{SA}19^{COF}$ and 0.099 for series $21^{TOC}45^{SA}13^{COF}$. The dispersions are 4% and 9%, respectively, which are very good for fracture mechanics results.

However, there is an association between the dispersion and the load level as indicated by the increase in the stiffness with increasing loading force, as shown in table III and figure 5.

The mean stiffness was approximately 60%, with a mean dispersion of 10% (Table III). These results are satisfactory because the percentage of dispersion is much lower than the percentage of stiffness, and they suggest that the glue junctions would be the same for all samples. This is likely due to a change in the elastic response of the structure. The shape does not influence the apparent stiffness. In fact, all the series showed an evolution in stiffness regardless of the shape of the sample. The increase in the stiffness could be due to glue compaction or an increase in the contact area between the ceramic and the aluminum infrastructures during the loading cycles. As a result, the stack of elements (infrastructure/glue/superstructure) must be considered a laminated composite. The difference between 15 kN/mm and 25 kN/mm (the most extreme distance from the results) corresponds to a difference of approximately 27 μm in the compressive displacement. This value of compaction may correspond to the progressive plasticization of the adhesive during testing and the progressive positioning of the tooth on its support. This phenomenon is intrinsic to the composite effect of our assembly, and could explain the similar evolution of the apparent stiffness of the entire series. In addition, it explains the interest surrounding the CAD/CAM construction and confirms that this method is efficient for creating all types of models to obtain results with a minimum dispersion, which is due to the reduction of operator-dependent steps and the suppression of the material dependence of the conventional prosthetic chain. The infrastructures may be created manually (18), with a milling machine (19) or from a prefabricated standard wax model. The use of CAD has several advantages because the measurements are very accurate and make it possible to create a model with a geometric shape or clinical shape depending on the study. Most importantly, it is possible to vary the geometrical parameters individually to evaluate their effects on mechanical properties. The results exhibit differences because of different geometries. CAM allows precise

production of as many samples as necessary. Furthermore, the optical imprint used to produce the ceramic cups is devoid of all the inconveniences of the traditional prints (20). An added benefit is that the infrastructures and the sample holders were milled as one unit. Previous studies used natural teeth or a model glued to a metal or resin sample holder as a sample (11,12); however, the interface and its behavior could affected the results.

It is interesting to note that several studies used 10 samples and obtained results with much higher standard deviations and dispersions. Those results are satisfactory when considering that some important studies commonly propose results with a dispersion of more than 30%.

However, to obtain samples with a limited set of controllable design parameters, the modulus of elasticity of the dentin and the periodontal-ligament was deliberately omitted. The infrastructure is not a material having the same modulus of elasticity as dentin, as Kelly reported (15). Therefore, the nature of the study is strictly comparative of materials that are subject to certain constraints on media and not specific physiological responses of the dental organ.

However, based on the quality of the results this method can be used for additional studies with finite elements. The protocol for reconstructing teeth with monolithic complete ceramic crowns is the subject of a paper that will be published soon.

CONCLUSION

Dispersion is an important factor in the design of experiments (DOE). Variations due to the experimental procedure must be minimized as much as possible. Based on the results of this study we conclude that monitored mechanical tests based on CAD/CAM-designed samples are satisfactory. This method has the following two main advantages: it tests the behavior of materials, and it enables the production of shapes of support that are well suited for the clinical setting. This study provides a new view regarding the analysis and validation of dental support

preparations, which is appropriate for the materials used during restorations and bonding. Additional analyses based on finite element modeling will help extrapolate the results obtained in natural teeth and validate the shapes of preparations that are the most appropriate for all-ceramic restorations. In future studies, it will be possible to focus on the effects of different shapes on the behavior of the ceramic cups. Because it prevents most of the operator-dependent tasks, CAD-CAM is an ideal way of producing samples for reproducible mechanical tests in the fixed-prosthesis field. This new approach shows great promise and could be implemented for the study of reconstruction materials, interfaces and the geometry of preparations.

REFERENCES

1. Keough BE, Kay HB, Sager RD, Keen E. Clinical performance of scientifically designed, hot isostatic-pressed (HIP'd) zirconia cores in a bilayered all-ceramic system. Compend Contin Educ Dent. 2011 Jul-Aug; 32(6): 58-68.

2. El-Mowafy O, Brochu JF. Longevity and clinical performance of IPS-Empress ceramic restorations--a literature review. J Can Dent Assoc. 2002 Apr; 68(4): 233-7.

3. Guess PC, Zavanelli RA, Silva NR, Bonfante EA, Coelho PG, Thompson VP. Monolithic CAD/CAM lithium disilicate versus veneered Y-TZP crowns: comparison of failure modes and reliability after fatigue. Int J. Prosthodont. 2010 Sep-Oct; 23(5): 434-42.

4. Zahran M, El-Mowafy O, Tam L, Watson PA, Finer Y.Fracture strength and fatigue resistance of all-ceramic molar crowns manufactured with CAD/CAM technology. J. Prosthodont. 2008 Jul; 17(5): 370-7.

5. Magne P, Dietschi D, Holz J. Esthetic restorations for posterior teeth: practical and clinical considerations. Int J Periodontics Restorative Dent. 1996 Apr; 16(2): 104-19.

6. Heintze SD, Cavalleri A, Zellweger G, Büchler A, Zappini G. Fracture frequency of all-ceramic crowns during dynamic loading in a chewing simulator using different loading and luting protocols. Dent Mater. 2008 Oct; 24(10): 1352-61.

7. Anusavice KJ, Kakar K, Ferree N.Which mechanical and physical testing methods are relevant for predicting the clinical performance of ceramic-based dental prostheses? Clin Oral Implants Res. 2008 Mar; 19(3): 326-8.

8. Kelly JR.Clinically relevant approach to failure testing of all-ceramic restorations. J Prosthet Dent. 1999 Jun; 81(6): 652-61.

9. Kelly JR, Rungruanganunt P, Hunter B, Vailati F.Development of a clinically validated bulk failure test for ceramic crowns. J Prosthet Dent. 2010 Oct;104(4):228-38.

10. Ghazy M, El-Mowafy O and Roperto R. Microleakage of porcelain and composite machined crowns cemented with self-adhesive or conventional resin cement. J Prosthodont, 2010; 19:523-530.

11. Kelly JR, Hunter B, Brenyo MR, et al; Simulating clinicalfailure duringin vitro-testing of all ceramic crowns. J Dent Res 1998;77 (Special Issue B): 778 (Abstract 1175)

12. Soares PV, Santos-Filho PC, Gomide HA, Araujo CA, Martins LR, Soares CJ.Influence of restorative technique on the biomechanical behavior of endodontically treated maxillary premolars. Part II: strain measurement and stress distribution.J Prosthet Dent. 2008 Feb;99(2):114-22.

13. FAbdelaziz KM, Freitag S, Kern M ; Fracture load of composite resin and feldspathic all-ceramic CAD/CAM crowns.. J Prosthet Dent. 2006 Feb; 95(2): Attia 117-23A,

14. Borges GA, Caldas D, Taskonak B, Yan J, Sobrinho LC, de Oliveira WJ. Fracture loads of all-ceramic crowns under wet and dry fatigue conditions.

15. Kelly JR, Rungruanganunt P, Hunter B, Vailati F. Development of a clinically validated bulk failure test for ceramic crowns.J Prosthet Dent. 2010 Oct;104(4):228-38.

16. Schilinburg HT, Hobo S, Whitsett LD, Jacobi R, Brackett SE. Fundamentals of Fixed. Prosthodontics. Quintessence Books, Chicago, 1997; 11-72.

17. Heintze SD, Cavalleri A, Zellweger G, Büchler A, Zappini G Fracture frequency of all-ceramic crowns during dynamic loading in a chewing simulator using different loading and luting protocols. Dent Mater. 2008 Oct; 24(10):1352-61. Epub 2008 Apr 22.

18. Min-Ho Kim, Jae-Ho Yang, Sun-Hyung Lee, Hun-Young Chung, Ik-Tae Chang. In vitro study of compressive fracture strength ofEmpress 2 crowns cemented with various luting agents; J Korean Acad Prosthodont : Volume 39, Number 3, 2001 ; 260-272

19. Magne P, Schlichting LH, Maia HP, Baratieri LN.In vitro fatigue resistance of CAD/CAM composite resin and ceramic posterior occlusal veneers. J Prosthet Dent. 2010 Sep;104(3):149-57.

20 Christensen GJ. Improving the quality of fixed prosthodontic services. J Am Dent Assoc. 2000 Nov; 131(11):1631-2

21. Rafferty BT, Bonfante EA, Janal MN, Silva NR, Rekow ED, Thompson VP, Coelho PG. Biomechanical evaluation of an anatomically correct all-ceramic tooth-crown system configuration: core layer multivariate analysis incorporating clinically relevant variables. J Biomech Eng. 2010 May; 132(5):051001.(impact factor 1.6)

22. Rafferty BT, Janal MN, Zavanelli RA, Silva NR, Rekow ED, Thompson VP, Coelho PG.Design features of a three-dimensional molar crown and related maximum principal stress. A

finite element model study. Dent Mater. 2010 Feb;26(2):156-63. Epub 2009 Oct 25.

23 Beuer F, Schweiger J, Edelhoff D.Digital dentistry: an overview of recent developments for CAD/CAM generated restorations. Br Dent J. 2008 May 10; 204(9):505-11.

24Andersson M, Carlsson L, Persson M, Bergman B.Accuracy of machine milling and spark erosion with a CAD/CAM system. J Prosthet Dent. 1996 Aug; 76(2):187-93.

25 Charles J. Goodacre, DDS, MSD,aWayne V. Campagni, DMD,band Steven A. Aquilino, DDS, MSc School of Dentistry, Loma Linda University, Loma Linda, Calif., and College of Dentistry, University of Iowa, Iowa City, Iowa Tooth preparations for complete crowns: An art form based on scientific principles. The Journal of Prosthetic Dentistry. Avril 2011. Vol 85 N°4, 363-376

26. Lorenzoni FC, Martins LM, Silva NR, Coelho PG, Guess PC, Bonfante EA, Thompson VP, Bonfante G. Fatigue life and failure modes of crowns systems with a modified framework design.) J Dent. 2010 Aug; 38(8): 626-34.

27. Mehl A, Ender A, Moremann W,Th Attin : Accuracy testing of a new intra-oral Camera. International Journal of Computerized Dentistry 2009; vol 12, N°1,11-28.

28. Schneider W. No compromises the new CEREC MC XL and inLab MC XL milling machines. Int J Comput Dent. 2007 Jan; 10(1): 119-26.

TABLES

Table I. dimensional specifications of the infrastructure.

	Series 1 $7^{TOC}45^{SA}19^{COF}$	**Series 2** $21^{TOC}45^{SA}13^{COF}$	**Series 3** $7^{TOC}90^{SA}19^{COF}$	**Series 4** $21^{TOC}90^{SA}13^{COF}$	**Series 5** $7^{TOC}90^{SA}0^{COF}$	**Series 6** $7^{TOC}45^{SA}0^{COF}$
D1 (mm)	6	6	6	6	6	6
D2(mm)	4.2	4.2	4.2	4.2	4.2	4.2
H1 (mm)	9	9	9	9	9	9
L1 (mm)	0.9	0.9	0.9	0.9	0.9	0.9
TOC (°)	7	21	7	21	7	7
SA (°)	45	45	90	90	90	45
COF (mm)	1.9	1.3	1.9	1.3	0	0

Table II. Rupture force values of complete ceramic caps during the mechanical test (kN, kiloNewton).

	Series 1 $7^{TOC}45^{SA}19^{COF}$	Series 2 $21^{TOC}45^{SA}13^{COF}$	Series 3 $7^{TOC}90^{SA}19^{COF}$	Series 4 $21^{TOC}90^{SA}13^{COF}$	Series 5 $7^{TOC}90^{SA}0^{COF}$	Series 6 $7^{TOC}45^{SA}0^{COF}$
Mean (kN)	1.255	1.048	1.314	1.744	1.884	1.902
Standard deviation	0.057	0.099	0.150	0.256	0.344	0.252
Dispersion (%)	4	9	11	14	18	13

Table III. Apparent stiffness of every sample vs loading force for all series and all samples. (kN, kiloNewton)

	load (kN)	series 1	series 2	series 3	series 4	series 5	series 6
Mean	-0.1	14.92	13.11	14.29	14.10	14.26	15.96
	-0.4	20.42	18.14	19.21	20.45	18.79	20.46
	-0.7	21.93	20.13	19.99	20.02	22.26	23.73
	-1	22.82		22.60	22.87	24.91	22.36
Standard Deviation.	-0.1	1.08	0.73	0.77	2.38	1.09	2.35
	-0.4	2.30	0.63	1.67	2.18	0.93	1.77
	-0.7	1.48	1.65	1.69	1.02	3.04	4.32
	-1	2.16		1.76	3.80	2.28	5.55
Dispersion (%)	-0.1	7.3	5.6	5.4	16.8	7.6	14.7
	-0.4	11.3	3.5	8.7	10.7	4.9	8.6
	-0.7	6.7	8.2	8.4	5.1	13.7	18.2
	-1	9.5		7.8	16.6	9.2	24.8

FIGURES:

Fig. 1. 1.1 Characteristics of the infrastructure characteristics. 1.6: the different designs

Fig. 2. Aluminum-milled infrastructures

Fig. 3. Sample positioned between the jaws of the testing machine

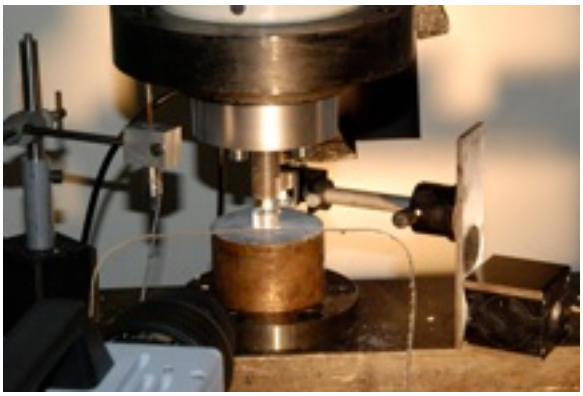

Fig. 4. Force-displacement curves (force in kN)

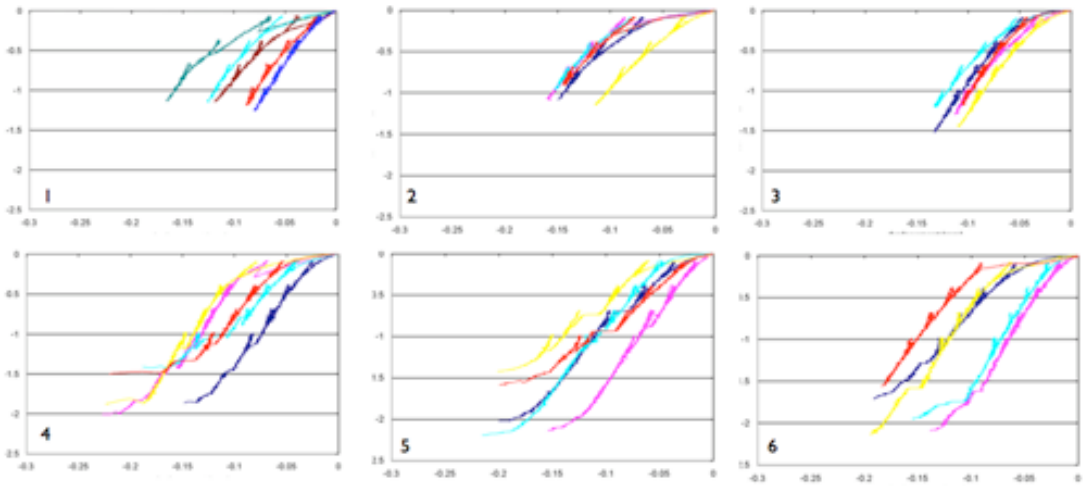

Fig. 5. Apparent stiffness